NASA
Lyndon B. Johnson Space Center
Space & Life Sciences Branch
Houston, Texas 77058

FINAL REPORT

THIN-SECTIONING AND ANALYSIS OF FINE-GRAINED METEORITIC MATERIALS

Contract No. NAS 9-17749

Date: 5 June 1992

MA Number: 15750

Copy 6 of 7

mccrone associates, inc.
850 PASQUINELLI DRIVE • WESTMONT, ILLINOIS 60559

TABLE OF CONTENTS

Final Report

NASA Contract No. NAS 9-17749

I. Introduction

This report summarizes the research efforts performed at McCrone Associates, Inc. under the above contract since the inception of the contract on January 2, 1987 through April 30, 1992.

The analytical research efforts performed during this 64 month period were based upon the four tasks detailed in our proposal of July 30, 1986 and subsequent proposals as the contract was amended and extended. The original Statement of Work is included as Appendix I.

The four specific tasks proposed were contingent upon the availability of particulate extraterrestrial materials from specific sources (e.g., Long Duration Exposure Facility, and Greenland and Antarctica micrometeorites). Since some samples were not available within the anticipated timetable, alternative tasks were proposed within subsequent Progress Reports (dated March 30, 1990 and March 28, 1991) and completed. Reprints of abstracts and papers documenting results of the proposed tasks are attached.

The overall theme of the work was the identification of the sources and formation/aggregation mechanisms of the various classes of interplanetary dust particles (IDPs) and to clarify the relationship between IDPs and conventional meteorites. IDPs are believed to be derived from a much broader range of parent bodies than conventional meteorites. Some of these parent bodies (e.g., comets) have escaped the post accretional processing that has affected the parent bodies of

meteorites. Therefore, IDPs are likely to preserve a record of early solar system and possibly presolar grain forming reactions. Using analytical electron microscopy (AEM) and more recently micro-infrared (IR) microspectroscopy to examine ultramicrotomed thin sections, we have addressed the questions of IDP formation mechanisms, sources, and their relationship to conventional meteorites. The following sections describe specific findings resulting from these studies.

II. Automated AEM Study of Hydrated "Layer Silicate" IDPs

The "layer silicate" (LS) chondritic IDPs are of interest because they bear a superficial resemblance to the fine-grained matrices of C1 and CM carbonaceous chondrites. Like C1 and CM chondrites, LS IDPs (1) have bulk compositions that are chondritic (solar), (2) contain matrix layer silicates and carbonates, and (3) are low porosity, compact objects. Due to this possible relationship, it may be possible to relate LS IDPs directly to an asteroidal source. The determination of the sources or parent body environments of IDPs are fundamental goals of interplanetary dust research. Until this study, there had been no systematic study of a large group aimed at clarifying the relationship between LS IDPs, and C1 and CM chondrites. Eight LS IDPs were thin-sectioned by ultramicrotomy, and analyzed by automated AEM. Thin sections of Murchison (CM) and Orgieul (C1) were prepared and analyzed in the same manner. The results of this study are detailed in Appendix II, Paper 1. They are summarized as follows:

1) The LS IDPs are a mineralogically diverse group of objects, with no two particles resembling one another.

2) Despite their similar bulk compositions, most LS IDPs are mineralogically unlike C1 and CM chondrites.

3) The degree of aqueous alteration varies widely from one IDP to another but is generally less well developed than in the matrices of C1 and CM chondrites.

4) Phases that are associated with advanced aqueous alteration in C1 and/or CM chondrites are notably absent in the eight LS IDPs. These include vein sulfates and vein carbonates, and ordered mixed layer structures (e.g., serpentine/tochilinite).

The above findings were unexpected, particularly the mineralogical diversity and limited aqueous alteration among the IDPs. Although most of them are mineralogically unlike Murchison or Orgieul, it is clear that they have been subjected to in-situ aqueous alteration similar to those processes which occurred in the fine-grained matrices of C1 and CM chondrites. The wide diversity in mineralogy and variability in degree of aqueous alteration suggests that they may be derived from a variety of asteroidal parent bodies rather than a single object. Such a hypothesis is not inconsistent with the notion that, if asteroidal IDPs are indeed represented in the stratosphere, we would see a broad sampling of the cumulative surface area of the asteroids. Perhaps, some of the IDPs, particularly those that were found to have suffered very limited aqueous alteration, are derived from the outer P and D asteroids that are not represented among conventional meteorites.

III. An Interplanetary Dust Particle Linked Directly to Type CM Meteorites and an Asteroidal Origin (Appendix II, Paper 2)

As stated in Section II, the hydrated layer silicate subset of chondritic IDPs are similar to the fine-grained matrices of C1 and CM meteorites in that they are (relatively) low porosity objects containing fine-grained layer lattice silicates and sometimes Fe-Mg carbonates. These textural and mineralogical similarities have been cited as evidence that "layer silicate" IDPs, like C1 and CM meteorites, are derived from asteroids.

The first direct evidence for an asteroidal origin for at least one "layer silicate" IDP was provided by IDP RB12A44 (Appendix II, Paper 2). This IDP was found as a grouping of five 10 to 12 μm fragments of a larger 30 μm IDP that broke up upon collection. In this section the observed textures indicated that RB12A44 is an unusual IDP. The fine grained matrix contains serpentine (rather than smectite) and serpentine/tochilinite intergrowths (also known as PCP). Tochilinite has been found in only one other class of meteoritic materials, type CM carbonaceous chondrites. The bulk composition, texture, and mineralogy of RB12A44 establish it as a type CM carbonaceous chondrite, but solar flare tracks indicate that it was exposed in space as an IDP rather than a piece of a conventional type CM meteorite.

The finding of tochilinite establishes the first direct petrogenetic link between an IDP and a class of meteorites and implies a common asteroidal origin for this IDP and CM meteorites. It also focuses attention on the entire subset of "layer-silicate" IDPs as a diverse sampling of hydrous asteroids.

IV. Chondritic Micrometeorites from Greenland and Antarctica Ices (Appendix II, Paper 3)

During the past few years, extraterrestrial dust grains have been collected from Greenland and Antarctica ices. These collections are unique in that they contain an abundance of grains >100 μm. Although most grains >100 μm should have been heated above 1000°C during atmospheric entry, the Greenland samples contain an unusually large number of what appear to be unmelted chondritic particles. The mass distribution of these particles is similar to that of the micrometeorite flux at 1 AU suggesting that most are micrometeorites and not simply ablation products of larger meteorites (Maurette et al., 1987). Measurements which are difficult if not impossible to perform on 5-25 μm stratospheric IDPs may now be possible with these new larger micrometeorites providing they are as pristine as IDPs.

A key issue concerning the Greenland and Antarctica micrometeorites is, therefore, the degree to which they have been modified by pulse heating during atmospheric entry or by subsequent alteration on the Earth's surface. It has been suggested that highly porous micrometeorites analogous to stratospheric IDPs can be found among the Greenland particles, but this has yet to be verified by detailed microanalysis. Some Greenland micrometeorites have apparently been altered by bacterial activity but the Antarctica samples are thought to have suffered negligible terrestrial alteration (pers. comm. M. Maurette). Although most particles >100 μm should be almost melted during atmospheric entry, Maurette et al., suggest an efficient cooling mechanism to explain the abundance of apparently unmelted 50-300 μm chondritic micrometeorites in their collection.

We performed a study of Antarctica and Greenland micrometeorites in collaboration with Maurette and co-workers in France. Our analytical procedures included thin-sectioning and automated AEM analyses. We also performed SEM analyses of individual micrometeorites on substrates for determination of morphology and bulk composition, and automated analyses of polished thick flats of fields of micrometeorites. The goals of this study were (1) to investigate the mineralogy of particles from Greenland and Antarctica whose bulk compositions are approximately chondritic; (2) to assess the degree to which atmospheric entry heating may have modified this mineralogy; this involves searching for solar flare tracks (as yet not found) and textures or morphological features that might indicate strong heating; and, (3) evaluation of their relationship to stratospheric IDPs and chondritic meteorites using comparison of mineralogy and petrography in thin-sections.

V. Nanometer Scale Mineralogy and Petrography of the Fine-Grained Matrices of Anhydrous IDPs (Appendix II, Paper 4)

The matrices of some anhydrous IDPs, particularly pyroxene-rich particles, contain discrete aggregates of nanometer-scale mineral grains embedded in a non-crystalline matrix. These aggregates have been described as "granular clusters" and (albeit inappropriately) as "tar balls". Understanding the mineralogy of such aggregates is important, not only because they may be unique to IDPs, but because their IR spectral transmission characteristics resemble those of comets and possibly certain interstellar objects. During the past four years a series of abstracts have reported progress in this area. A variety of electron beam imaging and spectroscopic methods have been employed,

including lattice fringe imaging, electron microdiffraction, brightfield/darkfield imaging, energy dispersive x-ray analysis, and electron energy-loss spectroscopy.

The aggregates contain both crystalline mineral grains (5-50 nm diameter) and non-crystalline matrices. Since the grains are crystalline, electron microdiffraction can be used to determine their (crystal) structures. Most of the grains yield patterns that index in terms of alpha-iron, and x-ray energy-dispersive analyses showing that they contain major Fe and minor Ni. These data establish that kamacite (FeNi alloy) is the major crystalline component of the aggregates. This result is surprising because reduced iron is relatively uncommon among the coarser grained components of anhydrous IDPs. Other nanometer-sized mineral grains include pyrrhotite, magnetite, and clinoenstatite.

The non-crystalline matrices of the aggregates were studied using electron energy loss near edge structure (ELNES), an electron beam technique capable of probing the local crystallographic (and electronic) environments of atoms. Mg-K, Si-K, O-K, and Fe-L core scattering edges have been obtained from aggregates and compared with Mg-K and Si-K edges from both crystalline (olivine, pyroxene) and non-crystalline silicates (glass). Such comparisons strongly suggest that most of the Mg and Si in the aggregates are concentrated in non-crystalline silicates (i.e., glass) rather than crystalline silicates (e.g., olivine and pyroxene). Examination of the O-K edge indicates that both silicate oxygen (in glass) and oxide oxygen (in Fe_3O_4) are present in the aggregates (Appendix II, Paper 4). In principle, the Fe-L edge can distinguish Fe^0 from Fe^{n+}. However, determination of the oxidation state(s) of Fe in the aggregates is complicated by the fact that Fe resides in multiple oxidation states in silicates, sulfides, metal, and oxides.

This study is in the process of being written up as a full technical paper.

VI. Interplanetary Dust Analogs for Silicate Infrared Emission from Comets (Appendix II, Paper 5)

Infrared (IR) spectroscopy provides a method by which properties of dust particles in the laboratory can be compared directly with those of dust in space. The dominant feature in IDP IR spectra is a strong band around 10 μm representing the Si-O stretch mode of silicates. Similarly, IR spectra from comets (and other astrophysical objects) exhibit a prominent feature between 8 and 12 μm, which is also believed to be due to silicate grains. The nature of the grains responsible for this "silicate feature" in astronomical spectra have been the object of numerous investigations.

The first study of the IR properties of IDPs was made by Sandford and Walker (1985). Using the shape of the 10 μm silicate feature they classified chondritic IDPs into three classes ("olivine", "pyroxene", and "layer silicate") after the minerals that provide the best match for the observed spectral features.

In principle, it should be possible to recognize cometary IDPs by their "comet-like" silicate IR emission at approximately 10 μm. However, Sandford and Walker found that none of the IR classes of IDPs matches comets. A reasonable comet match can be obtained simply by combining spectra from each of the three classes but, since an increasing amount of evidence suggests each IR class of IDPs are derived from significantly different parent body environments, it is unlikely that all three classes of IDP are cometary.

Using a micro-FTIR spectrophotometer with optics configured specifically for analysis on a micrometer scale, we obtained IR spectra from electron transparent thin sections of IDPs mounted on TEM grids (Appendix II, Paper 5). This approach offers the advantage of collecting IR data from thin sections whose silicate mineralogy has been rigorously evaluated in the AEM. The 10 μm "silicate feature" of each thin section is then evaluated in terms of the relative abundances of silicates determined from the AEM studies. The relationship between an IDPs silicate mineralogy and its IR silicate emission can then be used to investigate the likely mineralogy of dust grains responsible for silicate IR emission from comets.

Thin sections of eight chondritic IDPs were studied. Most of the IDPs do not provide a good match to comets, in accordance with the earlier findings of Sandford and Walker. "Pyroxene", olivine" and "layer silicate" IDPs typically exhibit narrow and complex band structure around 10 μm, in contrast to comets which exhibit broad band structure around 10 μm with a prominent peak at 11.3 μm. However, two glass-rich chondritic IDPs, W7027A11 and U219C11, exhibit a 10 μm "silicate feature" comparable with those of comets Halley and Bradfield in terms of overall band width and shape as well as the presence of a distinct 11.3 μm "olivine" peak. In addition, the mineralogy of these two IDPs appears to resemble comet grains analyzed by the PIA and PUMA mass spectrometers during the Halley encounters.

This combined AEM/micro-FTIR study has revealed the presence of specific particles among chondritic IDPs collected in the stratosphere whose silicate IR emission characteristics, mineralogy, and petrography are similar to those of comet Halley.

VII. Solar Flare Tracks in IDPs (Appendix II, Paper 6)

The presence of solar flare tracks provides unambiguous proof of the extraterrestrial origins of an IDP and confirms that it was exposed to interplanetary space as a small particle (as opposed to a component of a larger meteorite that broke up during atmospheric entry), and provides an upper temperature limit for heating during atmospheric entry. However, the questions of its extraterrestrial source is still in question. Two other issues that can be addressed from studies of tracks are (1) the possibility of distinguishing between the sources of IDPs based on their measured track densities and (2) examination of the structure of latent tracks in solids.

The use of track densities to investigate the sources of specific classes of IDPs depends upon the premise that particles from different sources have undergone different exposure ages in space and hence will exhibit characteristic track densities (Sandford, 1986, Flynn, 1990). However, our efforts have been frustrated by the observation that almost all IDPs examined thus far show essentially the same range of track densities (1-5 X 10^{10} cm^{-2}). We have identified two chondritic IDPs exhibiting a track density of 5 X 10 10^{11} cm^{-2}, (i.e., an order of magnitude higher than previously examined particles). It remains to be determined whether these IDPs are a known class of IDPs or whether they are a new class from a previously unsampled source. In either case, the finding of such high track densities is important, as it demonstrates that IDPs with a range of exposure ages can be collected from the stratosphere, which in turn implies that the interplanetary dust cloud at 1 AU is derived from multiple sources.

The atomic scale structure of latent nuclear tracks in solids remains the object of some discussion (see Dartyge et al., 1981). Solar flare tracks in IDPs provide an opportunity to address this question. In collaboration with K. Thiel (University of Cologne, FRG) we have examined both solar flare tracks in IDPs and tracks implanted in mineral standards during a series of heavy ion irradiations at the UNILAC-accelerator of GSI in Damstadt. Particular attention was given to one of the IDPs exhibiting a track density of 5×10^{11} cm^{-2}, since the tracks exhibit variations in length and diameter that have not been observed before.

IX. Principal Investigator

The Principal Investigator of the research efforts performed under this contract was John P. Bradley. John Bradley acted as the Project Leader with a team of other McCrone Associates' scientists including:

Anna S. Teetsov
Hazel H. Bales
John Gavrilovic
Kent L. Rhodes
Mark S. Germani
Howard J. Humecki

Without a team effort, the many tasks required to complete these research efforts could not have been performed.

Respectfully submitted,

D.A. Brooks

Donald A. Brooks
President

APPENDIX I

Statement of Work

STATEMENT OF WORK

THIN-SECTIONING AND ANALYSIS OF FINE-GRAINED METEORITIC MATERIALS

I. Background

The effort to be performed under this Statement of Work is the production and analysis of thin-sections (500 - 1000 angstrom thickness) of interplanetary dust particles (IDP's) and other meteoritic materials. During the past two years, research performed at McCrone Associates has yielded important new data about IDP's. For example, the discovery of solar flare nuclear tracks unambiguously confirmed the extraterrestrial nature of IDP's, and provides an upper temperature limit for their heating during atmospheric entry. More recently, production of thin-sections of IDP's has enabled textural studies, elucidation of petrographic associations, and an investigation of solar flare track implantation phenomena.

Although results to date have demonstgrated the utility of thin-sectioning, some aspects of the procedure require refinement. In order to produce perfect, defect-free sections, further experimentation is needed with embedding media and diamond cutting edges. Thin-sectioning provides the ability to perform high resolution structural and chemical analyses using analytical transmission electron microscopy, and it is intended that this technique be applied for characterization of sectioned micrometeorites.

II. Technical Requirements

A. Refinement of Micrometeorite Thin-Sectioning Procedure

Although results presented to date demonstrate the utility of thin-sectioning, there are several aspects of the procedure that require further development. For example, hard materials like olivine and pyroxene tend to fragment during sectioning with a diamond knife, a phenomenon referred to as "chatter." There are at least three ways minimize this problem: (1) use of embedding media whose hardness is as close as possible to that of the material being sectioned; (2) use of a sharper diamond knife; and (3) manipulation of the diamond knife angle with respect to the sample. Accordingly, the contractor shall experiment with a number of different epoxies of different hardness to minimize "chatter" during sectioning, and shall evaluate diamond knives (mounted at various angles) for micrometeorite sectioning.

B. Electron-Beam Characterization of Thin-Sections of Micrometeorites

Even in thin-section, micrometeorites are mineralogically

complex structures, and heterogeneity may persist below the 100 angstrom level. Therefore, the contractor shall use analytical scanning transmission electron microscopy (STEM) to characterize the thin-sections, initially using conventional TEM to further investigate textural and petrographic features of a larger population of micrometeorites. Then using a 20 angstrom diameter nanoprobe, the contractor shall characterize the fine-grained matrices both chemically (via X-ray energy dispersive spectroscopy) and structurally (via high resolution lattice fringe imaging, selected area and convergent beam micro-diffraction).

C. Investigation of Solar Flare Nuclear Tracks in Sectioned Micrometeorites

The presence or absence of tracks in micrometeorites is of fundamental importance because it confirms the recent exposure of a particle to interplanetary space. To date, four of five anhydrous particles sectioned by the contractor show track densities on the order of 10^{10} to 10^{11} cm^{2}. However, of six hydrated particles sectioned so far, none of them appear to have implanted tracks. Taken at face value, these observations imply that the hydrous subset of chondritic micrometeorites were not recently exposed to interplanetary space as small particles. However, because there may be an alternative explanation, the contractor shall thin-section additional micrometeorites in an attempt to resolve this question.

D. Thin-Sectioning of Fine-Grained Matrices from Conventional Meteorites and Other Meteoritic Materials

The contractor shall prepare ultra-thin (less than 1000 angstroms) sections of fine-grained matrix material from the Murchison and Murray meteorites, and shall prepare several 3-5 micron diameter impact particles from Solar Max for ultramicrotome sectioning in an attempt to answer the questions: "How effective is an impact device for non-destructive collection of particles in space?" "What type of meteoritic material does the debris represent (e.g., hydrated or anhydrous interplanetary dust)?"

APPENDIX II

Reprints of Technical Papers

Paper 1 M.S. Germani, J.P. Bradley, D.E. Brownlee, "Automated thin-film analyses of hydrated interplanetary dust particles in the analytical electron microscopy, "Earth and Planetary Science Letters, 101, 162-179 (1990).

Paper 2 J.P. Bradley and D.E. Brownlee, "An interplanetary dust particle linked directly to type CM meteorites and an asteroidal origin, Science, 251, 549-552 (1991).

Paper 3 M. Maurette, C. Jouret, Ph. Bonny, J.P. Bradley, M.S. Germani, Y. Kinhn, "Electron microscope studies of carbon-rich grains in a new collection of Antarctica micrometeorites, Lunar and Planetary Science, XX, 638-639 (1989).

Paper 4 J.P. Bradley, "Electron energy-loss spectroscopy of the fine-grained materials of interplanetary dust particles, Meteoritics, 126, 322-323, (1991).

Paper 5 J.P. Bradley, H.J. Humecki and M.S. Germani, "Combined infrared and analytical electron microscope studies of interplanetary dust particles, Astrophysical Journal in press, (August 1992).

Paper 6 K. Thiel, J.P. Bradley, R. Spohr, "Investigation of solar flare tracks in IDPs: Some Recent Results", Nuclear Tracks and Radiation Measurements, 19, 709-716 (1992).

Appendix II, Paper 1

Earth and Planetary Science Letters, 101 (1990) 162–179
Elsevier Science Publishers B.V., Amsterdam

[FB]

Automated thin-film analyses of hydrated interplanetary dust particles in the analytical electron microscope

M.S. Germani [a], J.P. Bradley [a], D.E. Brownlee [b]

[a] *McCrone Associates Inc., Westmont, IL 60559, USA*
[b] *Department of Astronomy, University of Washington, Seattle, WA 98195, USA*

Received May 18, 1990; revised version accepted July 30, 1990

ABSTRACT

An automated 200 keV analytical electron microscope was used to obtain elemental analyses from over 4000 points on ultramicrotomed thin sections of eight "layer silicate" class interplanetary dust particles (IDPs). Each analysis yielded major and minor element abundances from a volume approaching that of a cylinder 50 nm in diameter. Multi-element cluster analysis was employed to identify mineral phases and their relative abundances in the thin sections. Petrographic characteristics were determined using brightfield and darkfield imaging, lattice fringe imaging and electron diffraction. Three of the particles contained smectite (1.0–1.2 nm basal spacing) and two contained serpentine (0.7 nm basal spacing). The mineralogy of three of the eight IDPs appears to have been modified by heating, possibly during atmospheric entry. The point count analyses and Mg-Si-Fe ternary diagrams show that one of the serpentine-containing IDPs is similar to CI and CM chondritic meteorites, but the fine-scale heterogeneity among the other seven is distinct from these meteorites, which are more uniform on a 50 nm scale. The IDPs exhibit evidence of aqueous processing, but they have typically experienced only short range, submicrometer scale alteration. In comparison, CI and CM chondrites are compositionally more uniform, presumably as a result of more extensive aqueous alteration. The hydrated "layer silicate" IDPs may provide a broad sampling of the asteroid belt, including samples of the outer P and D asteroid classes.

1. Introduction

Chondritic interplanetary dust particles (IDPs) are fine-grained aggregates of mineral grains, glass and carbonaceous material, whose elemental compositions generally agree with those of CI/CM carbonaceous chondrites [1,2]. They are collected from the stratosphere as individual 5–50 μm particles. Two principal groups of chondritic IDPs have been recognized using infrared (IR) spectroscopy and electron microscopy [3–5]. One group consists exclusively of *anhydrous* mineral phases, while the other group contains *hydrated* layer silicates as well as anhydrous phases. The anhydrous group can be subdivided into "pyroxene" and "olivine" classes, and the hydrated group into "smectite" and "serpentine" classes, after the most prominent crystalline silicates within their matrices [4–6]. The extraterrestrial origins of chondritic IDPs have been confirmed by measurement of solar noble gases, hydrogen isotopic anomalies and high densities of fossil solar flare tracks [2,7]. The presence of tracks also indicates the degree to which an IDP was pulse heated during atmospheric entry. Most "pyroxene" and "layer silicate" IDPs survive atmospheric entry with minimal heating, but the "olivine" class may contain a higher proportion of IDPs whose properties have been modified by heating [8].

Comets and asteroids are the major sources of interplanetary dust in the inner solar system [7,8]. The high porosities, fragile microstructures, and mineralogy of "pyroxene" IDPs have been interpreted in terms of a cometary origin [9], while similarities between "smectite" and "serpentine" IDPs and the fine-grained matrices of CI/CM carbonaceous chondrites have been cited as evidence for an asteroidal origin [1,10,11]. However, no chondritic dust class has yet been linked unambiguously to one source or the other. In principle, particles generated anywhere within the solar system outside of 1 AU can eventually reach Earth-

0012-821X/90/$03.50

crossing orbits as they spiral in towards the Sun under the influence of Poynting–Robertson drag [7,8]. Therefore, IDPs are an important source of extraterrestrial materials because they sample a much wider range of parent bodies than conventional meteorites, which originate primarily from a limited number of asteroids [12].

A fundamental goal of interplanetary dust research is to determine which IDPs are cometary and which are asteroidal. Among chondritic IDPs, the "smectite" and "serpentine" layer silicate (LS) IDPs are the best candidates for (generic) parent-body identification because of their similarity to the matrices of CI and CM carbonaceous chondrites. Hydrated chondritic materials are usually low-porosity fine-grained objects that are systematically depleted in Ca and Mg relative to solar abundances [1,13]. Studies of individual LS IDPs have shown that like CI/CM carbonaceous chondrites, their matrix layer silicates appear to have formed *in situ* during parent-body aqueous alteration [5,11,14]. However, there has been no systematic study of a larger group of LS IDPs targeted specifically towards investigation of the relationship between LS IDPs and CI/CM carbonaceous chondrites and the source(s) of LS IDPs.

This paper presents the results of a study of thin sections of eight LS IDPs and the fine-grained matrices of two carbonaceous chondrites. The purposes of the study were to clarify the relationship between LS IDPs and CI/CM chondrites and, if possible, to identify the source(s) of LS IDPs. Several hundred X-ray energy-dispersive spectra were collected from each thin section using an automated (200 keV) analytical electron microscope (AEM). A total of 4153 individual analyses were collected from the IDPs, 2826 from Murchison (CM) matrix and 1532 from Orgueil (CI) matrix. Petrographic properties of the thin sections were investigated manually in the AEM using brightfield/darkfield imaging, lattice fringe imaging and electron diffraction.

2. Experimental procedures

2.1. IDP collection and preparation

All of the studied particles were recovered from the stratosphere at 18–20 km altitude by U-2 and RB-57 aircraft. Details of the airborne collection procedure are described by Sandford [7]. The particles were individually hand picked from the collection "flags" and washed with solvents to remove silicone oil, the collection substrate used on the "flags". Six of them were mounted in epoxy or acrylic resin for thin sectioning using an ultramicrotome equipped with a diamond knife (a complete description of this procedure is presented elsewhere [5]). The remaining two had first been prepared for other types of microanalysis. The first, "Butterfly" (R21-M4-8A), had originally been mounted as crushed fragments of a 10×12 μm sized particle onto a gold substrate for D/H isotopic measurements in the ion microprobe [15,16]. Two of the ion-probed fragments were subsequently recovered from the gold substrate by replication and mounted together in epoxy for thin sectioning. The second, U230A34, was first mounted in Araldite and examined as a polished thick-flat section in the electron microprobe. After microprobe examination the particle was ultramicrotomed while still embedded in the Araldite. Multiple thin sections of all eight IDPs were cut and transferred to carbon support substrates on 3 mm copper TEM grids. Section thickness was usually about 80 nm although some sections as thin as 50 nm or less were produced.

2.2. Data acquisition and reduction

A 200 keV AEM equipped with digital beam control and an X-ray energy-dispersive spectrometer were used for this study. The electron beam was digitally rastered on a two-dimensional grid over each thin section and a video thresholding procedure was used to distinguish epoxy and the carbon substrate from meteoritic material [4]. Figure 1 shows ultramicrotomed thin sections of an LS IDP, most of which exhibit low porosity in thin-section (in contrast to anhydrous IDPs which are usually highly porous [1,5].) Between 300 and 900 data points were analyzed from each thin section. The electron probe spot could be imaged directly in the AEM operating in conventional (CTEM) mode but not in scanning (STEM) mode used for automated analyses. Therefore, the STEM spot size was measured indirectly by the following procedure. First, a premeasured (≈ 10 nm) 200 keV CTEM probe was positioned at points on a thin (≈ 80 nm) glass film (Fig. 2, upper 3 spots) to confirm that the resulting beam damage accu-

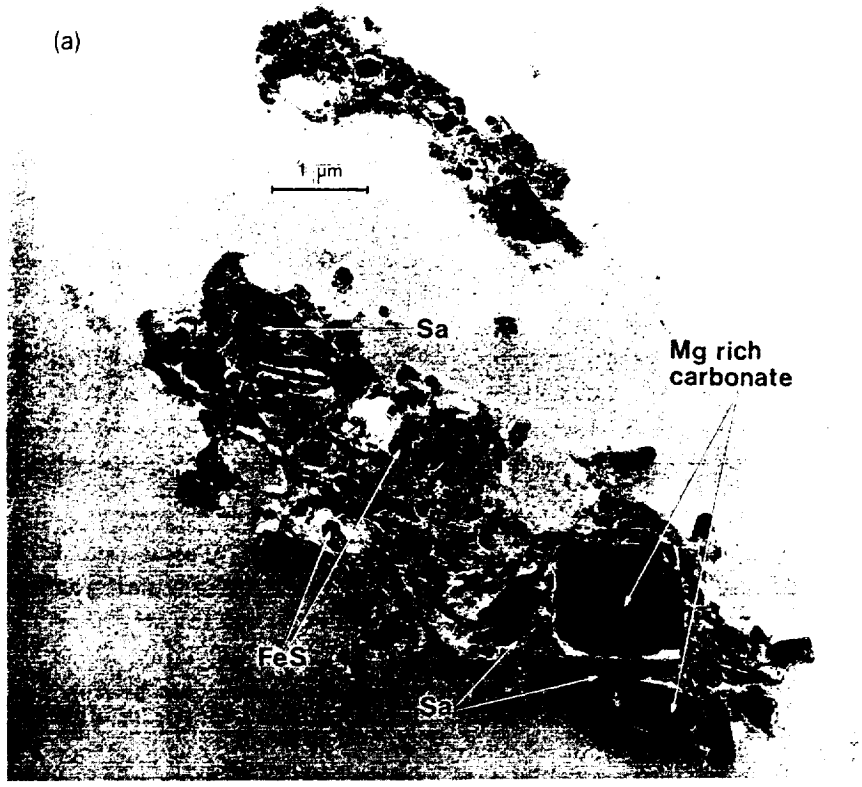
(a)
1 μm
Sa
Mg rich
carbonate
FeS
Sa

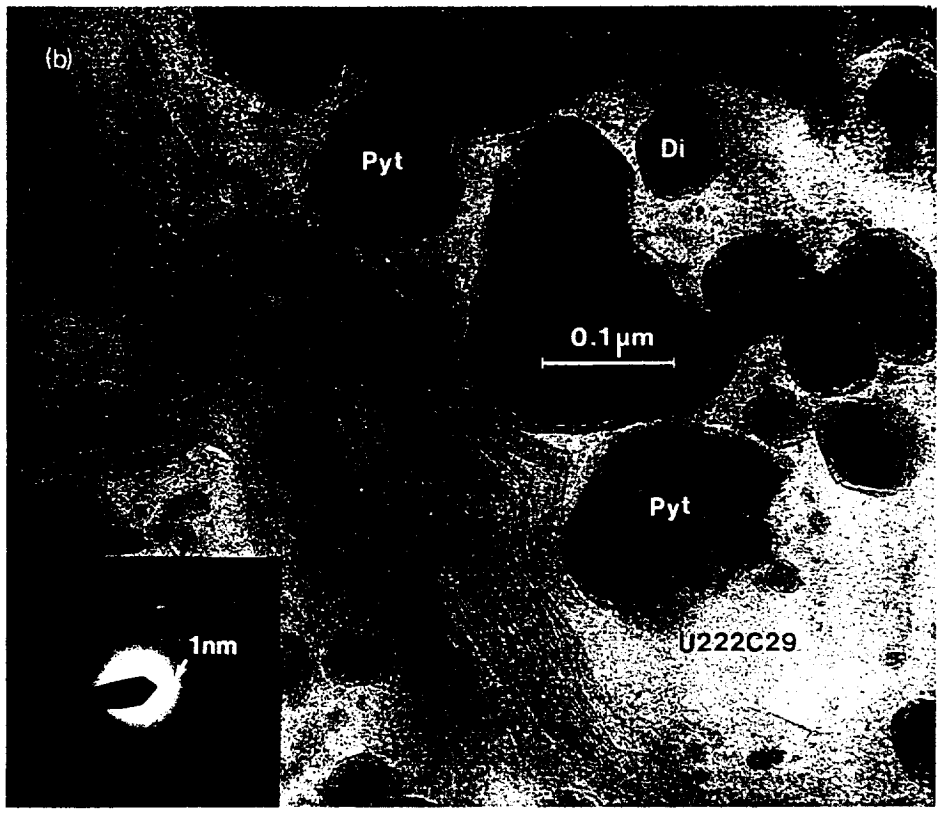
(b)
Pyt
Di
0.1μm
Pyt
1nm
U222C29

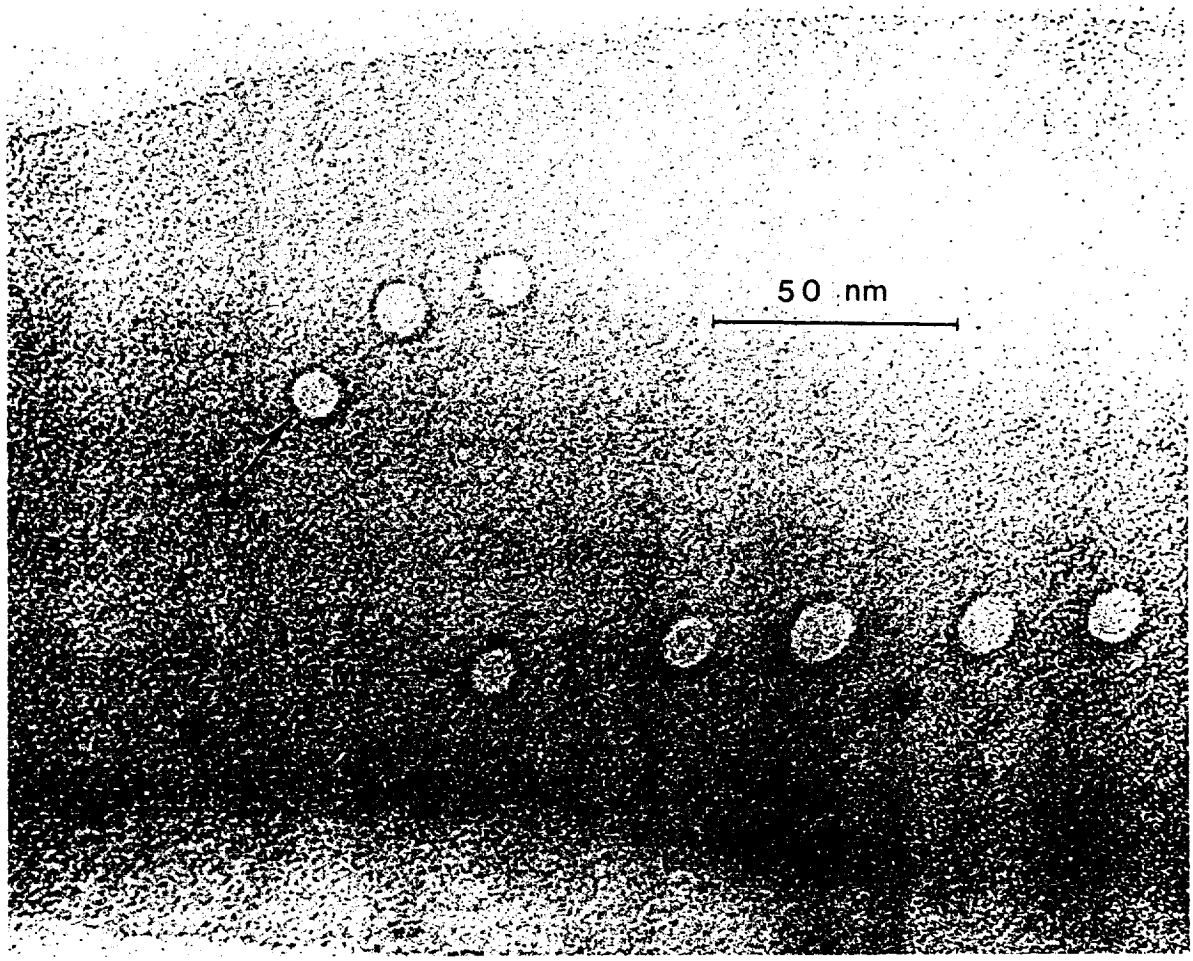

Fig. 2. Brightfield micrograph of a feldspathic glass (≈ 80 nm thick) containing spots caused by electron beam damage. These spots enable determination of the shape and diameter of the electron probe beam used for automated analyses.

rately reflected the size and shape of the electron probe. Then in STEM mode the probe was positioned at multiple points on the same glass (Fig. 2, lower 5 spots), thereby enabling determination of the STEM probe shape and diameter. For the automated analyses the spot diameter was set between 10 and 20 nm, with a probe current between 0.1 and 0.5 nA. Due to the thinness of the sections, beam divergence was small and the analyzed volume was assumed to approach that of a cylinder with diameter and length equal to the electron beam diameter and specimen thickness, respectively [17,18]. X-ray spatial resolution at each data point was estimated to be better than 50 nm [18,19].

The large data sets obtained with high spatial resolution are prerequisites to recognizing fine-scale chemical detail and mineralogical trends because IDPs are typically fine-grained and mineralogically heterogeneous on a scale < 100 nm [2,4,5,9–11]. All sections were maintained at liquid nitrogen temperature to minimize specimen con-

Fig. 1. Brightfield electron micrographs of a thin section (≈ 80 nm thick) of U222C29. (a) Low-magnification image showing a low-porosity matrix dominated by saponite (*Sa*) and euhedral Mg-rich carbonates. (b) High-magnification image showing a typically fibrous saponite (*Sa*) and euhedral matrix grains (including pyrrhotite (*Prt*) and diopside (*Di*)). Rims on these grains are suspected to be an amorphous carbonaceous phase (solar flare tracks were observed in the diopside crystal). The inset, lower left, is a selected-area electron diffraction pattern from the saponite showing a 1.0 nm basal spacing characteristic of smectites.

TABLE 1

Comparison of experimental and actual elemental concentrations in Kakanui hornblende [a]

Element	Experimental [b]	Actual [c]
Mg	13.3 ± 0.6	14.11
Al	15.3 ± 0.9	14.42
Si	35.7 ± 1.0	34.48
K	2.8 ± 0.3	3.11
Ca	12.3 ± 0.6	13.45
Ti	5.3 ± 0.7	4.81
Fe	15.5 ± 1.0	15.52

[a] Specimen thickness, 50 ± 10 nm; accelerating voltage, 200 keV; probe size, 20 nm; probe current, 0.15 nA; X-ray acquisition time, 45 s.
[b] Ten analyses total.
[c] From Mason and Allen [22].

tamination arising from surface migration of volatiles during analysis. After data acquisition each spectrum (containing a threshold number of X-ray counts) was analyzed for Mg, Al, Si, S, Ca, Cr, Mn, Fe and Ni using a Cliff-Lorimer thin-film procedure [20], with K-factors derived from ultramicrotomed mineral standards [21]. The accuracy of this procedure is illustrated in Table 1, which lists point count analyses of a mineral standard (Kakanui hornblende) aquired under the same conditions as those used to analyze the IDPs. Carbon was not measured in this study because of a ubiquitous contribution from epoxy and the carbon support substrate, and the solid-state X-ray detector was not sensitive to elements with atomic numbers $Z < 11$.

The identities and relative abundances of mineral phases were extracted from the quantitative point count data sets using a Microvax II computer and a cluster analysis program EXPLOR [23]. The ease with which mineral identifications were made depended on the average grain size relative to the X-ray spatial resolution of the incident beam. Coarse-grained (> 100 nm) materials tend to cluster tightly about specific mineral compositions, but fine-grained (< 100 nm) materials yield diffuse clusters. Manual examination of fine-grained components using brightfield and darkfield imaging, electron diffraction, and X-ray analysis were therefore critical adjuncts to automated analyses of thin sections. The thin sectioning and automated analysis procedures have already been applied to a group of eight anhydrous IDPs, and the results are presented in a previous paper [4].

3. Results

Figure 3 shows ternary Mg-Si-Fe diagrams of the eight particles studied. Mg-Si-Fe plots are used because these are the major elements in chondritic interplanetary dust, and their relative concentrations reflect the abundances of the important mafic silicates (e.g., smectite, serpentine, pyroxene, olivine). Identification of each particle as an LS IDP was originally made on the basis of the following criteria: (1) observation of basal lattice fringes (Fig. 4) and a chemical composition characteristic of layer silicates (U222C29, W7029J10, U230A34, U230A11A, U230A39); and (2) measurement of $-OH$ and CO_3^{2-} infrared absorption bands characteristic of LS IDPs (R21-M4-8A) 3]). The other two particles (U2022F4, U2022G20) are believed to be LS IDPs that have been modified by strong heating during atmospheric entry (see section 4.1).

The distribution of data points in Fig. 3 is in most cases confined to a broad but continuous region of each plot, resulting from the predominance of a fine-grained matrix of layer silicates and/or glassy materials whose compositions can include silica-rich material as well as smectite or serpentine. Buried within the data sets are clusters of data points arising from "accessory" phases dispersed throughout the matrices of each IDP. Some of these clusters, particularly Mg-rich carbonates, can be observed directly (cf. Figs. 3a, and d), since their (Mg-rich) compositions do not overlap those of the matrices. However, in most cases multi-element cluster analysis is required to identify specific mineral compositions within the data sets (Fig. 5, Table 2). Details of the mineralogy of each of the eight IDPs as determined by automated analysis and manual characterization are summarised below.

3.1. U222C29

The ternary plot for this IDP (Fig. 3a) exhibits three distinct features. First, there are many low-Fe silicates. Second, the positions of most data points can be explained by a mixture of Mg silicate, a high-Si phase, and a high-Fe phase. Third, except for a cluster of high-Mg (carbonate) grains, there

are no data points with an Mg/Si ratio > 0.5. U222C29 is a low-porosity particle whose most distinctive features are large, euhedral Mg carbonates, some of which were almost a micrometer in size (Fig. 1a). These grains are in a matrix of fibrous (or platey) layer silicate that exhibits a 1.0 nm basal spacing (Fig. 1b, inset) and a composition consistent with saponite. A variety

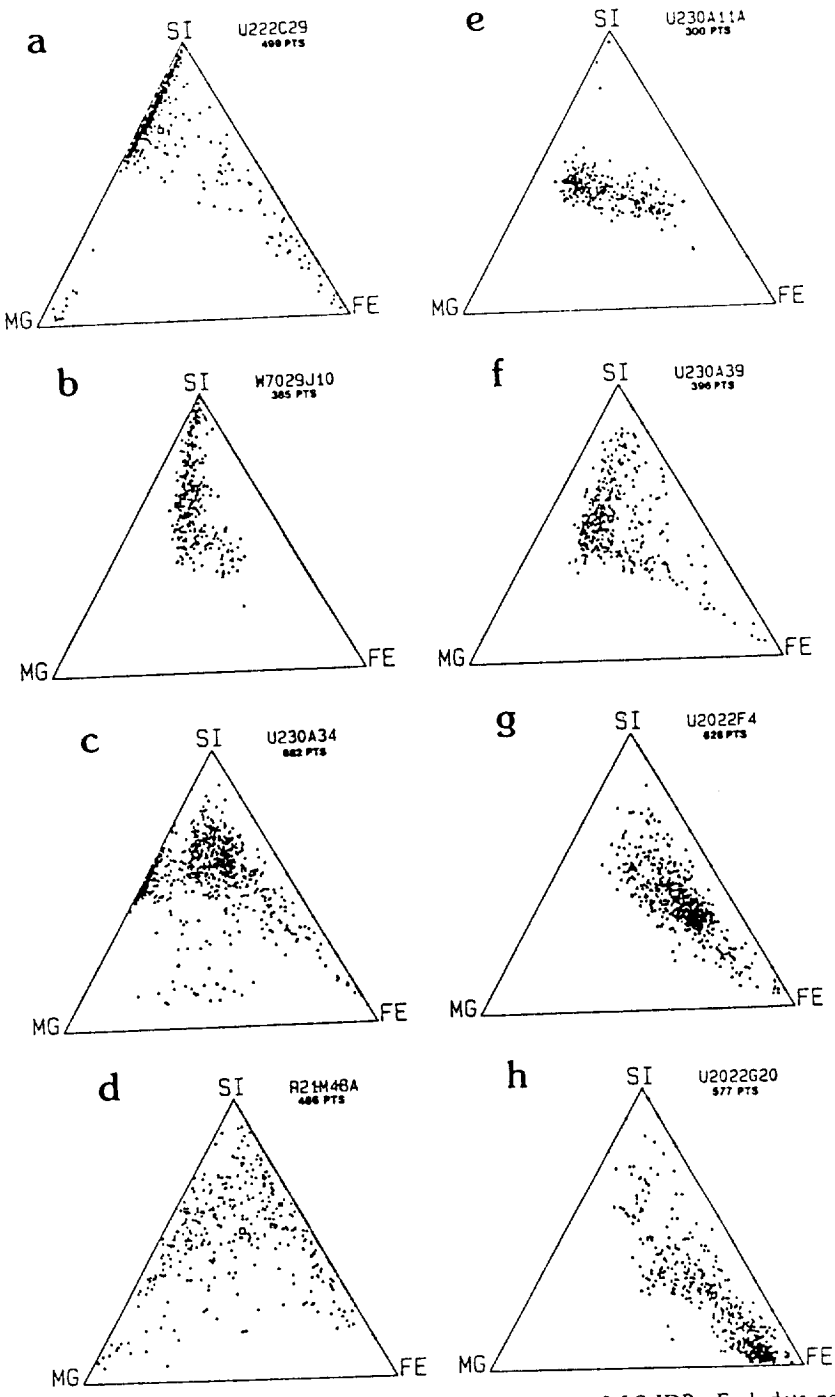

Fig. 3. Mg-Si-Fe ternary plots of quantitative point count analyses collected from 8 LS IDPs. Each data point was collected with spatial resolution estimated to be better than 50 nm.

of minor phases were found in this IDP, including diopside, pyrrhotite, magnetite, enstatite, troilite, and graphitized carbon. This is only the second chondritic IDP in which carbon with measurable 0.34 nm interplanar spacings has been identified, since carbon in chondritic IDPs is usually structurally featureless [2]. Magnetite is apparently a secondary phase because it forms a polycrystalline decoration on sulfide grains. A total of 499 data points were measured by automated analyses; 43% were assigned to saponite, 42% to silica-rich glass (intermixed with saponite), 12% to sulfides, 2% to Mg carbonates and $< 1\%$ to diopside.

3.2. W7029J10

This was a 12×17 μm IDP whose major element composition was approximately chondritic except for low sulfur. The ternary plot (Fig. 3b) indicated that the matrix contains no low-Fe silicates, the Mg/Fe ratio is nearly constant throughout much of the particle, and there are no low-Fe or low-Mg silicates present. In thin section, it exhibited low porosity typical of LS IDPs and the distribution of data points (Fig. 3b) shows a relatively tight clustering characteristic of some LS IDPs. The matrix was almost exclusively noncrystalline, and ranged from a Si-rich material to a ferromagnesium silicate with a serpentine composition. Weak lattice fringes with a spacing of 0.7 nm were observed within one region whose composition was consistent with serpentine. Crystalline phases were dispersed throughout the poorly crystallised matrix. Most of these grains were sub-

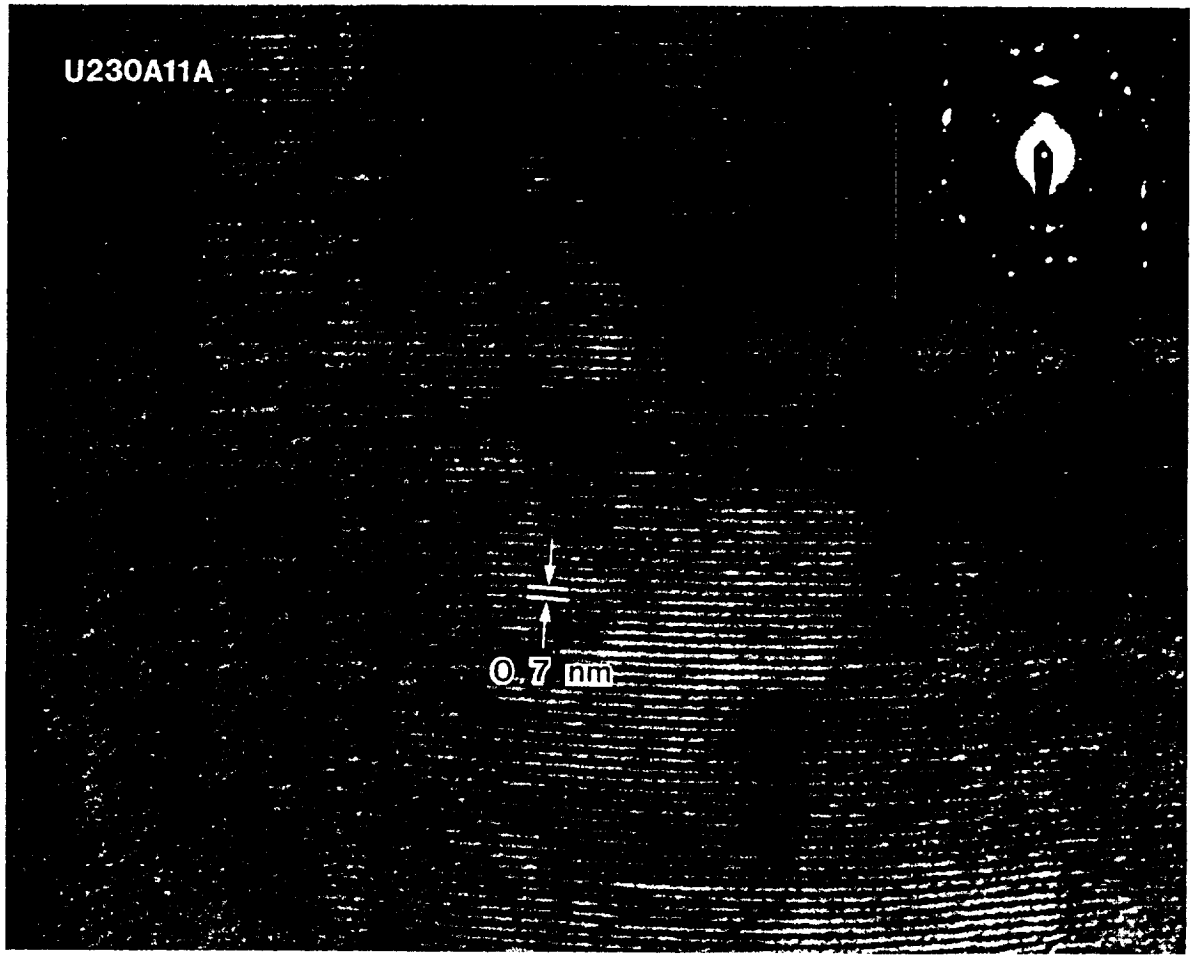

Fig. 4. Lattice fringe image of serpentine within the matrix of U230A11A. The inset, upper right, is an SAED pattern characteristic of serpentines.

micrometer in size, although a large (≈ 1 μm) fassaite grain containing prominent solar flare tracks was found. Other crystalline phases included magnetite, Ni sulfide, and diopside. A total of 385 data points were collected by automated analysis. Most of these data points were assigned to one of three clusters, an Fe-Mg silicate with a serpentine composition (24%), a silica-rich glassy phase (29%) and a cluster arising from a mixture of the two preceeding phases (45%). The remaining data points (2%) were assigned to the minor phases described above.

3.3. U230A34

This IDP (Figs. 3c and 5) is unique among the eight studied and LS IDPs in general because almost half of it was a single crystal of pyroxene. The particle was 20×10 μm, with the pyroxene segment of the polished thick flat making up an area approximately 10×10 μm (Fig. 6). In thin section the pyroxene was found to contain solar flare tracks (Fig 6, inset). The second half of the IDP, which had a bulk chondritic composition, was a mixture of Fe-rich silicate glass and a smectite with a basal spacing between 1.0 and 1.2 nanometers. Fe-sulfide and chromite grains were found embedded in the glass, and the smectite appeared to have formed primarily by aqueous alteration of the glass. Several large (≈ 1 μm) Fe carbonate crystals were found within the layer silicate matrix. The intimate assemblage of an Fe-rich glass and Fe-rich smectite (Fig. 7) implies

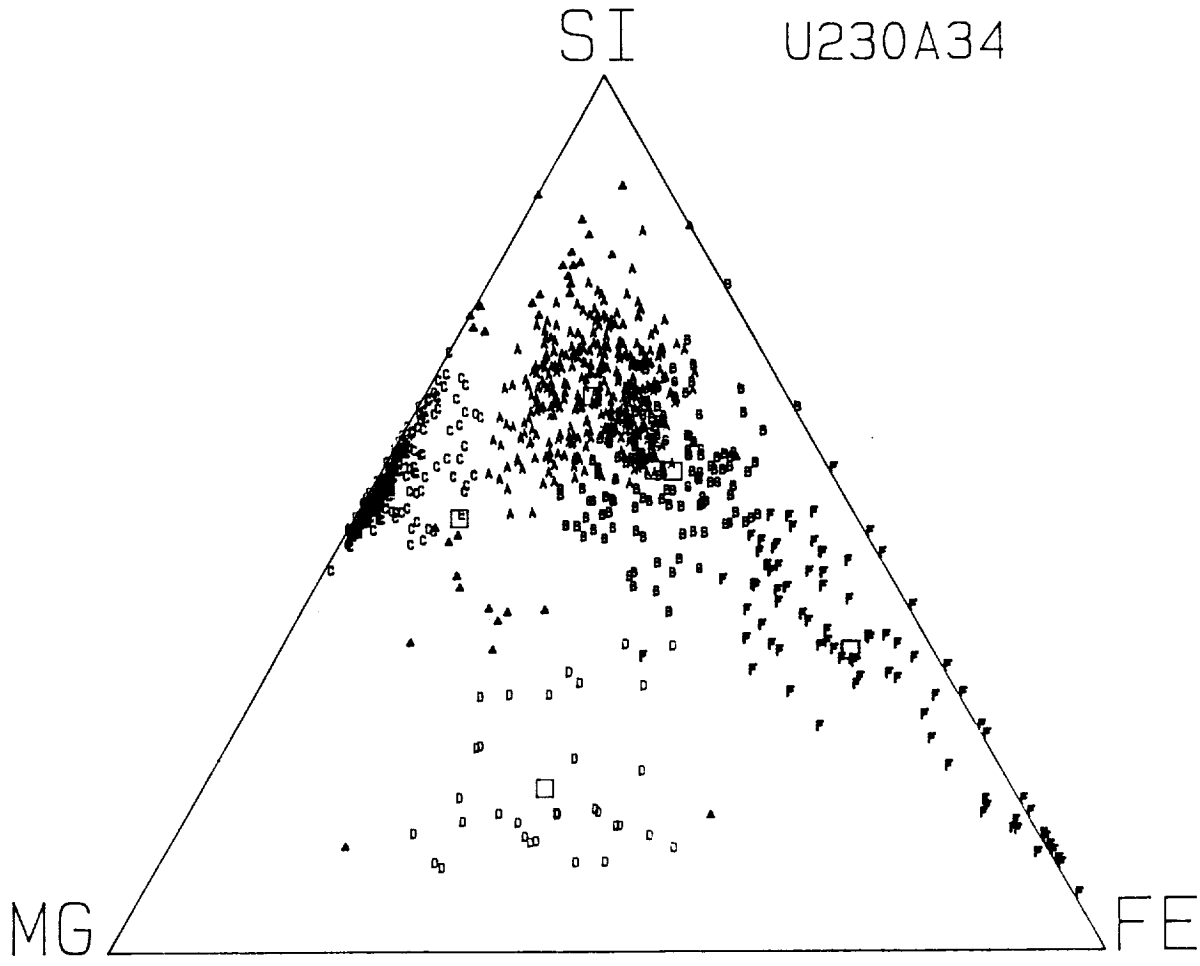

Fig. 5. Ternary Mg-Si-Fe diagram of U230A34 following nine-element cluster analysis. Alphabetical letters and colors are used to assign each data point to its respective cluster. Data points represented by a "Δ" are unassigned. Squares represent the centroids of each cluster. The centroid compositions, phase identifications, and population of each cluster are listed in Table 2.

TABLE 2

Cluster analysis centroid compositions of U230A34

Cluster	No. of data points	Composition (element wt.% normalized) [a]									Cluster significance	Phase(s)
		Mg	Al	Si	S	Ca	Mn	Cr	Fe	Ni		
A	327	14±5	1±1	52±6	4±4	< 0.5	< 0.5	0.7±0.8	27±7	1±2	primary	smectite
B	131	10±5	1±1	35±5	16±5	< 0.5	< 0.5	< 0.5	34±4	4±2	secondary	glass/sulfide
C	263	40±5	< 0.5	53±5	< 0.5	2±1	0.7±0.6	1.0±0.6	3±3	< 0.5	primary	pyroxene
D	32	30±7	< 0.5	15±7	2±3	2±1	< 0.5	< 0.5	49±9	1±1	primary	carbonate
E	1	21	25	30	1	< 0.5	2	10	12	< 0.5	primary	spinel
F	81	3±3	< 0.5	14±7	30±5	< 0.5	< 0.5	< 0.5	47±6	5±3	primary	pyrrhotite
G	13	7±2	1±1	27±5	20±4	< 0.5	< 0.5	< 0.5	29±5	16±6	secondary	glass/pentlandite
Total	848											
Unassigned	34											

[a] Errors reflect analytical error (see Table 1) as well as size shape, and degree of overlap of individual clusters.

that the layer silicate formed during *in situ* aqueous alteration of the glass.

Figure 5 shows a nine-element cluster-analyzed ternary plot for U230A34. Table 2 shows the elemental compositions of the eight cluster centroids. There are 882 points in the data set. Twenty-six of them are unassigned as they did not fall within the compositional envelopes of any of the eight identified clusters. Clusters A, B, C, D, E and F are primary clusters since they represent single mineral phases, while clusters G and H are secondary clusters representing the mixing of two or more phases (see Table 2). Cluster A is smectite and contains 31% of the data points, cluster B is glass (14%), cluster C is pyroxene (29%), cluster D is carbonates (4%) and cluster E is a single data point representing an alumino-silicate grain. Cluster F represents Fe-rich sulfides plus smectite and glass, and cluster G is derived from a mixing of sulfides and glass. Cluster H is most likely a mixture of pyroxene, glass and smectite. The Fe-carbonate and chromite were found during manual examination of a thin section of U230A34.

3.4. *Butterfly (R21-M4-84)*

This is the most fine-grained and mineralogically heterogeneous of the eight IDPs studied, and the distribution of data points in the ternary plot (Fig. 3d) is correspondingly diffuse. It is also perhaps the most enigmatic in that it yielded

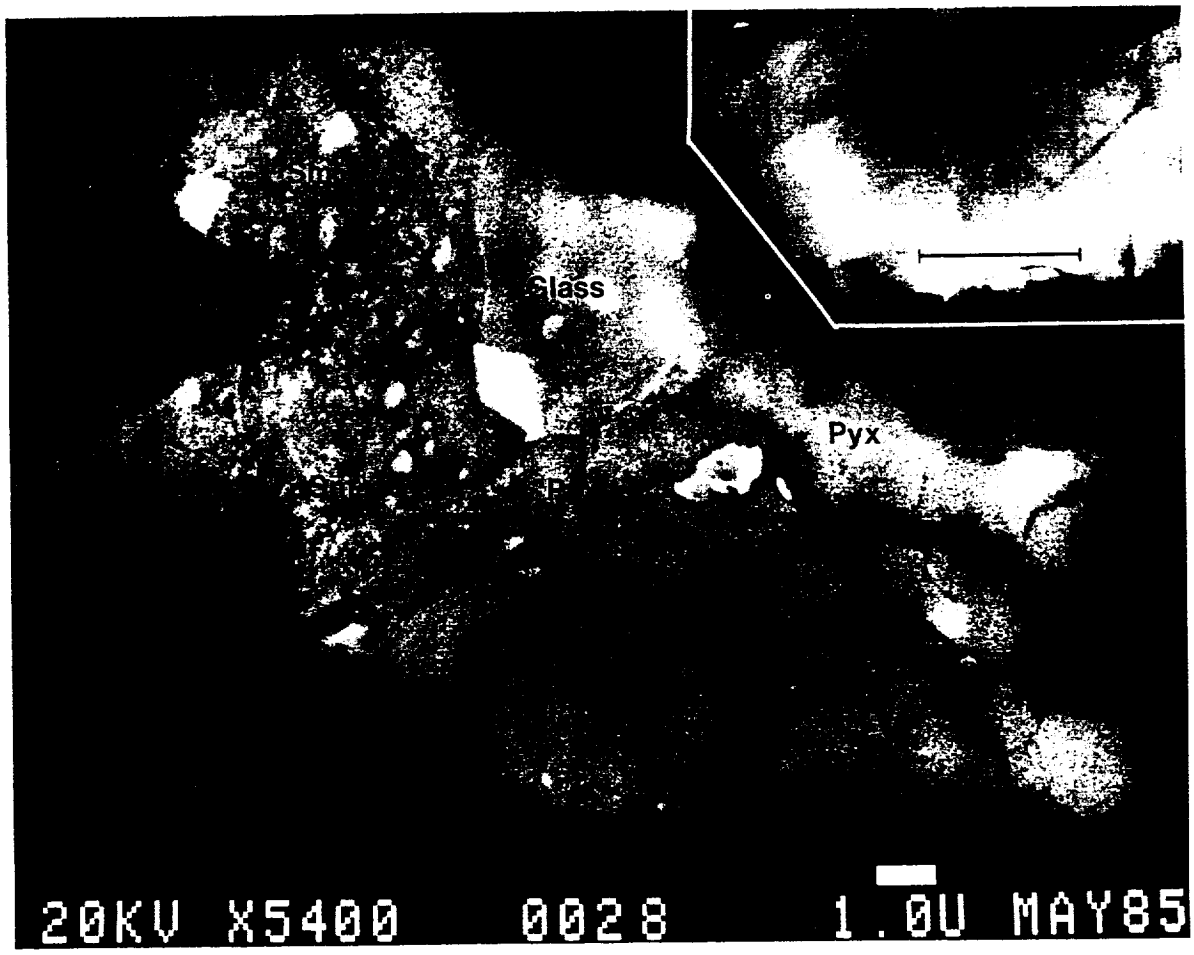

Fig. 6. Backscattered electron micrograph of a polished thick-flat section of U230A34. Approximately half of this IDP is a (fractured) pyroxene crystal (*Pyx*). The inset, upper right, is a darkfield image of part of the pyroxene showing solar flare tracks (dark linear features). Scale bar equals 100 nm. The other half of the IDP has a bulk chondritic composition and contains glass and smectite intermixed with a variety of minerals [principally Fe-sulfides (bright regions)], see also Fig. 7.

several novel analytical results. The original particle was 10×12 μm in size, and it was subdivided and subjected to several types of measurement. Infrared (IR) spectral measurements suggested that it belonged to the anhydrous "pyroxene" class but the IR spectrum also contained $-OH$ and $-CO_3^{2-}$ absorption bands previously identified only in "layer silicate" IDPs. It was therefore suggested that Butterfly is a "pyroxene" IDP altering to an LS IDP [15]. Ion microprobe isotopic measurements showed D/H enrichments as high as 9000 per mil, which is the highest measured for any solar system object (IDP or meteorite) [16]. In thin section Butterfly was a low-porosity object composed largely of < 100 nm crystals embedded in Fe-rich glassy silicate or carbonaceous material. Aggregates of crystals $>$ 100 nm were also observed. Mg-Fe pyroxenes, FeNi grains (metal and/or carbide), Ca-Mg and Ca-Mg-Fe carbonates were found. No evidence of basal spacings characteristic of layer silicates were observed within the matrices. Despite the presence of many suitable crystals, solar flare tracks were not observed. Cd-rich crystals were also found in thin sections (these are discussed further in section 4.1). A total of 457 data points were collected by automated analysis; 28% were assigned to a Fe-rich silicate (glass-like matrix), 21% to Mg-Fe pyrox-

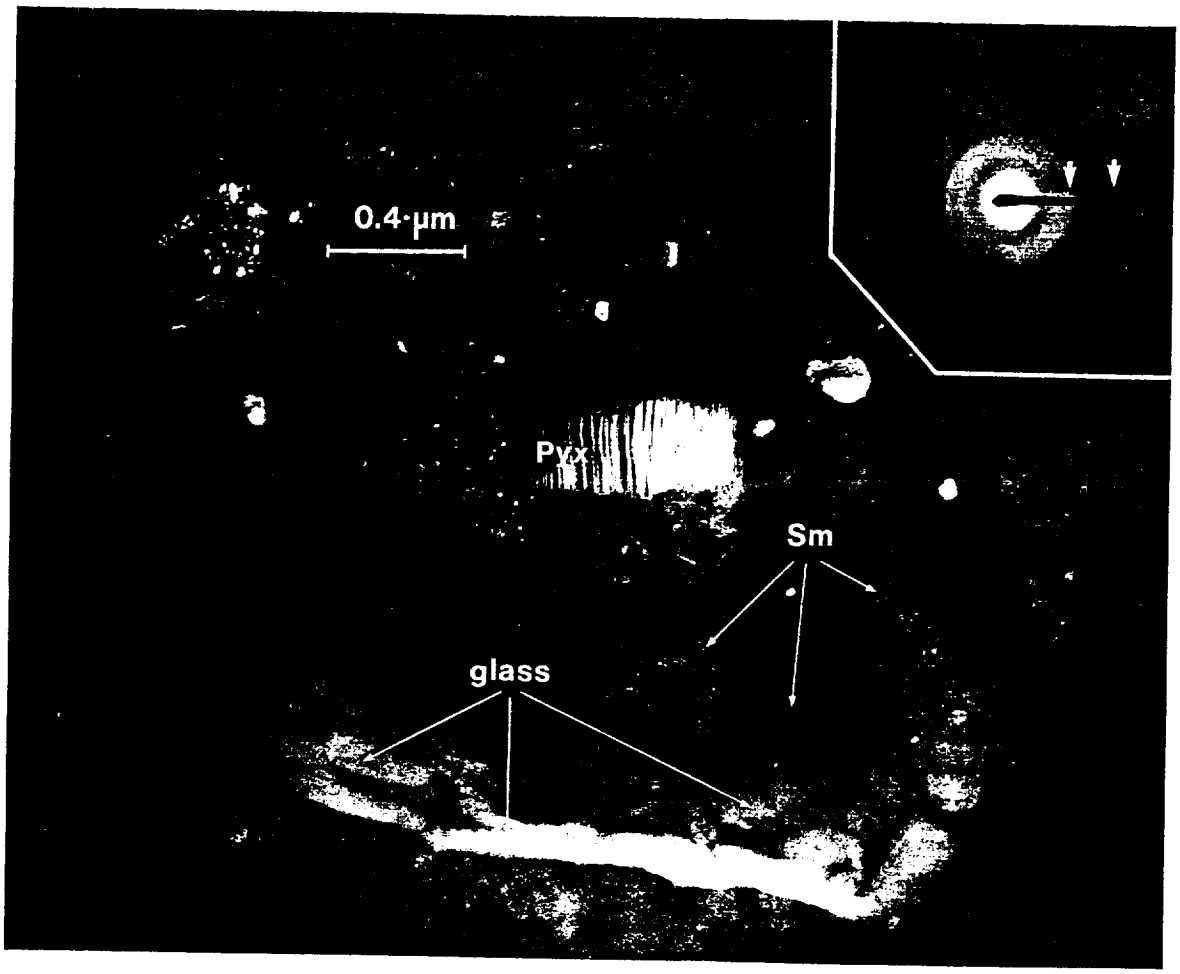

Fig. 7. Darkfield electron micrograph of a thin section of the chondritic portion of U230A34 (see Fig. 6). Smectite (*Sm*) and glass are the major matrix components, and the smectite appears to have formed *in situ* by aqueous alteration of the glass (the compositions of these two phases are listed elsewhere [6]). The inset, upper right, is an SAED pattern that shows an inner diffuse halo plus two superimposed rings (arrowed) at 0.26 and 0.16 nm, respectively. This SAED pattern is typical of silicate glasses that have begun to alter to smectite [24]. An unaltered pyroxene (enstatite) platelet (*Pyx*) is also indicated.

enes, 19% to FeNi alloy (or carbides), 3% to carbonates, 4% to Fe-sulfides (pyrrhotite) and the remaining 25% to clusters whose compositions reflect mixing of two or more of the above phases.

3.5. U230A11A

This was a low-porosity ≈ 30 μm IDP composed of a mixture of non-crystalline Fe-Mg silicate and well-ordered serpentine. The ternary plot (Fig. 3e) indicates that there are no high-Mg silicates, and the distribution of data points shows that this IDP is the most homogeneous of the eight. Lattice fringe imaging and electron diffraction indicated a layer silicate with a 0.7 nm basal spacing (Fig. 4), and quantitative thin-film analysis confirmed that the phase was serpentine. No evidence for the presence of olivine or pyroxene was found in U230A11A so it was not possible to search for solar flare tracks. Two minor constituents, pentlandite and magnetite, are widespread throughout the matrix. Pentlandite occurs as single crystals between 10 and 250 nm in diameter, while magnetite is distributed as crystals smaller than 20 nm. The only other phases that were observed were a chromium oxide grain (≈ 100 nm), a large magnetite platelet (≈ 250 nm) and a single grain of calcium carbonate (≈ 200 nm). U230A11A is the only stratospheric IDP reported so far whose matrix contains abundant, well crystallized serpentine. Three hundred data points were obtained using automation; 38.5% were assigned to Fe-Mg serpentine, 58.5% to (silica-rich) Fe-Mg silicate, 1.4% to pentlandite, $< 1\%$ to pyrrhotite and 1% to an alumino-silicate phase.

3.6. U230A39

This was a low-porosity IDP, 8×14 μm in diameter. Its matrix was composed of glassy Fe-Mg silicate that displayed little textural variation in thin section. Figure 3f demonstrates that this matrix contains no low-Fe silicates, and the Mg/Si does not fall below 0.35. Some darker (less electron transparent) regions of this matrix were found to be enriched in Fe. The matrix was predominantly disordered but layer silicates with basal spacings of 1.2 to 1.4 nm were observed. The bulk compositions of all the thin sections were chondritic except that S was anomalously low. Magnetite was the major crystalline component. It was pervasive throughout the glassy matrix both as large (micrometer-sized) grains as well as crystals as small as a few tens of nanometers. The outer surfaces of the IDP were decorated with a continuous skin of magnetite reminiscent of a fusion crust. The only other crystalline phases found in U230A39 were sulfides. Pyrrhotite grains as large as 0.5 μm were observed, and also pentlandite grains that were generally smaller (20–100 nm). The depletion of sulfur and abundance of magnetite, particularly on the outer surfaces of this IDP, suggest that U230A39 is a strongly heated particle.

A total of 396 quantitative point count analyses were collected; 76% were assigned to a mixture of magnetite and Fe-Mg silicate matrix, 10% to magnetite, 9% to Fe-sulfide (pyrrhotite) and 5% to FeNi sulfide (pentlandite).

3.7. U2022F4

This was a 20×12 μm particle with smooth plate-like surfaces typical of LS IDPs. Its bulk chemical composition was chondritic, although the Fe content was high. Like U230A39, there are no low Fe-silicates in U2022F4, and the Mg/Si ratio in the particle never falls below 0.35 (Fig. 3g). In thin section it contained a homogeneous silicate matrix with a vesicular texture. Finely divided magnetite was dispersed throughout the matrix, and the outer surfaces of the thin sections were heavily decorated with magnetite (Fig. 8). (Surface enrichment of magnetite probably explains the anomalously high bulk Fe content of the whole particle, since during electron beam analysis X-ray production is confined primarily to the outer two micrometers of a particle surface [25].) This magnetite rim is similar to rims on large (> 100 μm), unmelted but strongly heated fusion crusts on micrometeorites from polar ice and unmelted deep-sea particles [26,27]. Therefore, it is likely that U2022F4 was also strongly heated during atmospheric entry. The silicate matrix was glass like and devoid of lattice spacings compatible with layer silicates. A total of 628 data points were measured by automated analysis; 25% of them were assigned to an Fe-Mg silicate matrix, 74% as a mixture of magnetite and silicate matrix, 0.3% as Fe-sulfide (pyrrhotite) and 0.6% as FeNi sulfide (pentlandite).

3.8 U2022G20

This was a 12 × 5 μm particle that was morphologically and compositionally similar to U2022F4. Like U2022F4 it exhibited smooth, plate-like surfaces and a bulk chondritic composition with high iron. Figure 3h indicates the predominance of an Fe-rich phase throughout the particle. In thin section this phase was identified as polycrystalline magnetite dispersed throughout a glassy silicate matrix. Magnetite was also present along the outer surfaces of the thin sections, but not as a well-developed rim like that observed on U2022F4. A total of 577 analyses were collected from U2022G20; 28% were assigned to the silicate matrix, 53% to an FeS/Fe_3O_4 phase (partially oxidized sulfides formed presumably by strong heating), 7% to magnetite, 10.5% to Fe-sulfide and 0.7% to an alumino-silicate phase (presumably glass).

Figures 9 and 10 show ternary plots for thin-sectioned specimens of the Murchison (CM) and Orgueil (CI) carbonaceous chondrites. Each ternary plot represents data sets obtained from different regions of the meteorite matrices. A total of 2826 analyses were collected from Murchison and 1532 from Orgueil. The large number of analyses (4358) were accumulated in order to evaluate the degree of mineralogical heterogeneity (on a 5–10 μm scale) within the meteorite matrices. These data were then compared with the eight LS IDPs shown in Fig. 3. Note that only one of the IDPs, U230A11A (Fig. 3e), bears any resemblance to one of the meteorites (Murchison). The meteorite data are discussed further in section 4.2.

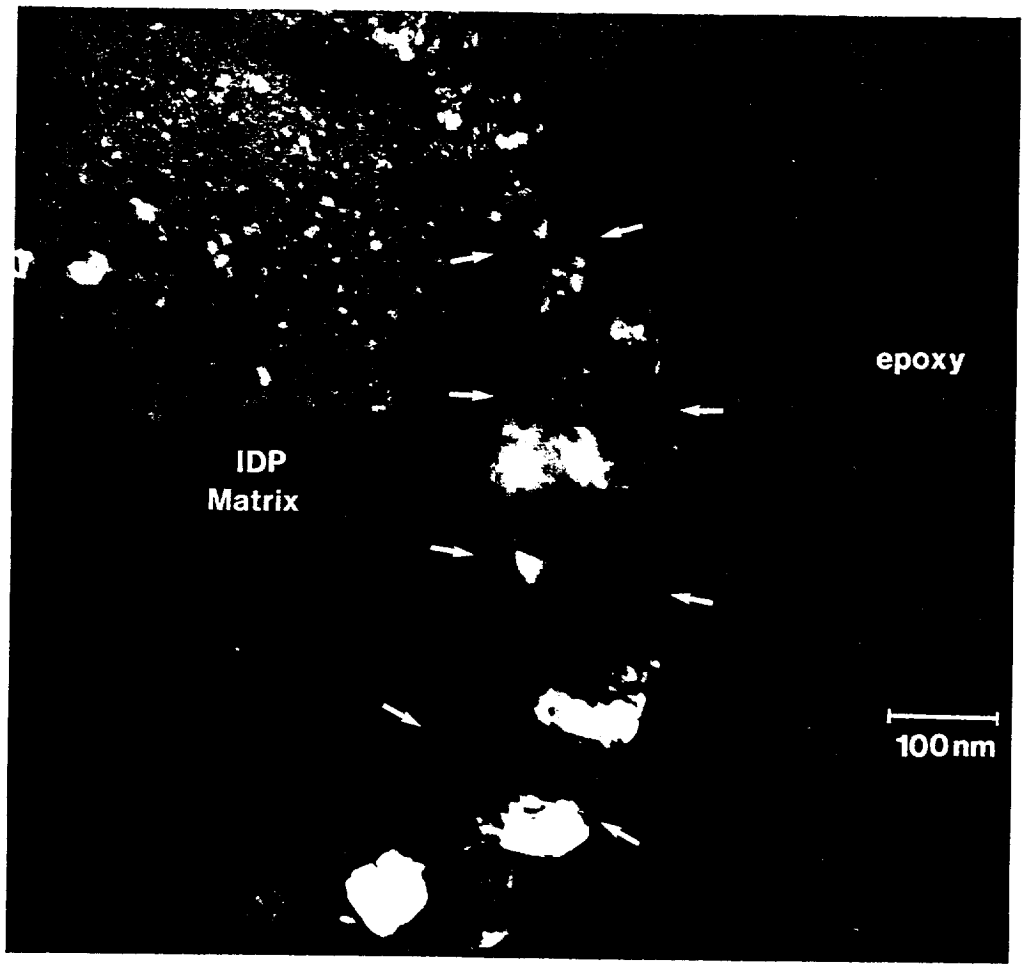

Fig. 8. Darkfield electron micrograph of the outer surface of a thin section of U2022F4. The polycrystalline magnetite rim (delineated by arrows) was probably formed by strong heating during atmospheric entry. Such rims may provide a reliable means of identifying strongly heated IDPs in thin section. Similar rims were observed on U230A39 (Fig. 3f) and U2022G20 (Fig. 3h).

4. Discussion

4.1. General

All of the thin sections were dominated by material with an average grain size less than the section thickness. Therefore, many of the individual point count analyses are not phase specific; i.e., they do not measure the composition of a single phase. Spatial resolution could have been improved by producing even thinner (< 50 nm) sections and using finer electron probes, but both options would have yielded unacceptably low X-

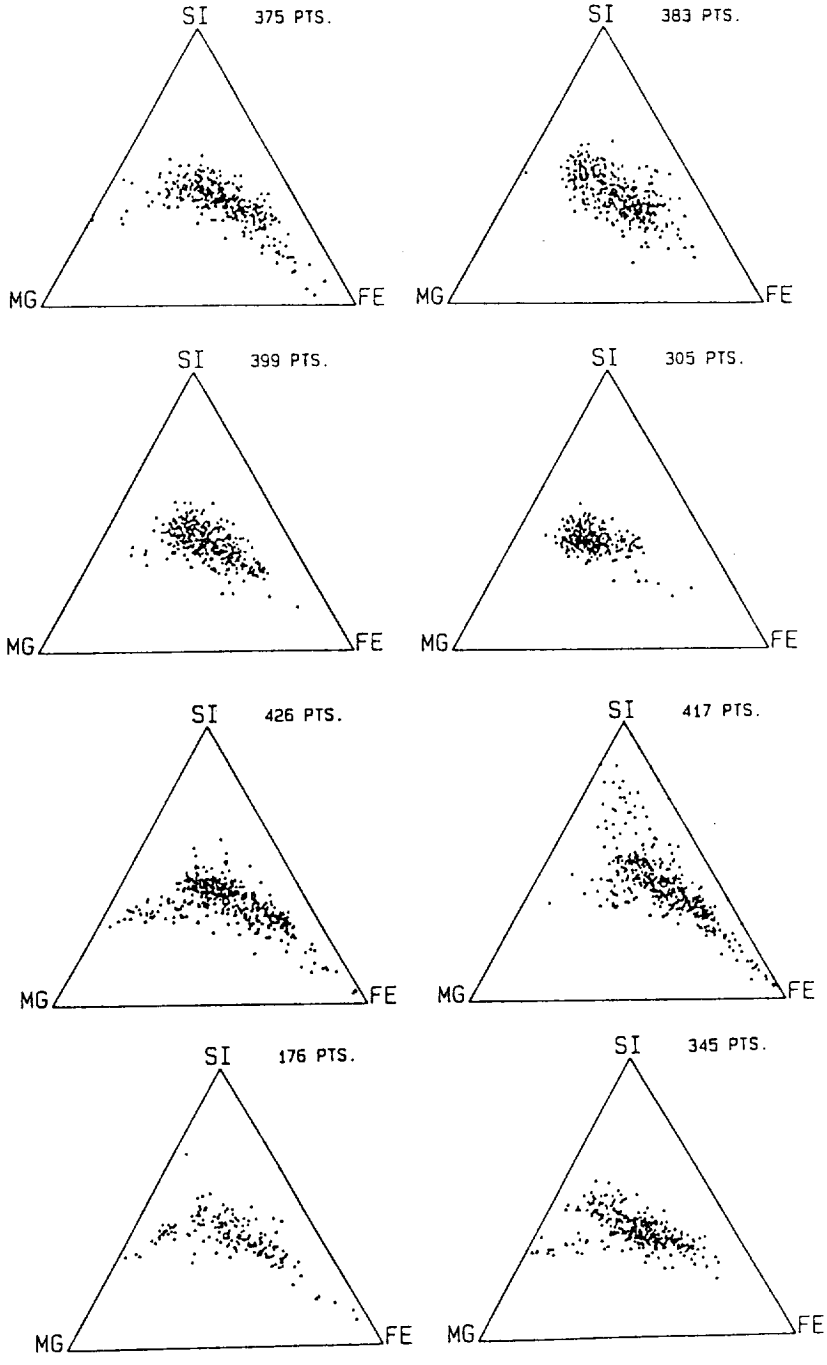

Fig. 9. Ternary Mg-Si-Fe plots (atom fraction) of eight different regions of thin-sectioned Murchison matrix (2826 points total).

ray count rates. In the absence of optimum analytical resolution, cluster analyses of large data sets can identify phases that would otherwise remain undetected. Automated data acquisition and cluster analyses provide a unique overview of the fine-scale mineralogy of IDPs, but they should not be considered a complete substitute for conventional (manual) AEM analysis. Any one of the LS IDPs studied here would benefit from a more extensive manual examination, since it has been demonstrated that conventional AEM studies are uniquely capable of providing fundamental insight into IDP origins and growth modes [11,14,28,29].

The data sets collected from the eight LS IDPs (Fig. 3) provide insight into two important aspects of stratospheric IDP collections, contamination and atmospheric entry heating. The effects of terrestrial contamination on collection substrates (flags) has not previously received much attention, and R21-M4-8A may be the first reported case of an IDP that was contaminated with terrestrial debris. Solar flare tracks were not found in R21-M4-8A but D/H isotopic measurements clearly established it as an extraterrestrial-particle. Our observation of Cd-rich material within thin sections of R21-M4-8A suggest that it was contaminated. Cd-rich particles are common within the JSC Cosmic Dust catalogues, where they are classified as terrestrial contaminants. It has been suggested that they are plating materials used on components of the (U-2) collection airplane [30].

The distribution of data points for particles

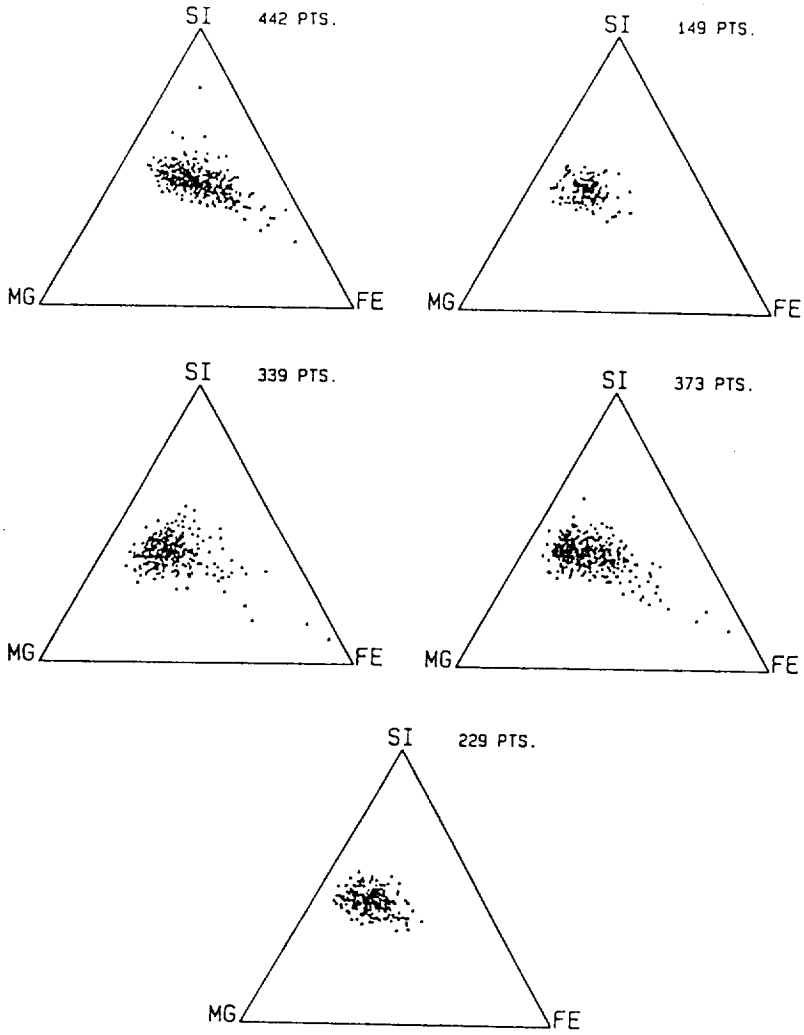

Fig. 10. Ternary Mg-Si-Fe (atom fraction) of five different regions of thin-sectioned Orgueil matrix (1532 points total).

U230A39, U2022F4, and U2022G20 indicates the presence of an Fe-rich phase (Fig. 2, f–h). This trend is due to finely divided magnetite within the IDP matrices and also as a rim along the outer surfaces of the thin sections (Fig. 8). In addition to the rim, which presumably formed during atmospheric entry, the matrices of each IDP have a vesicular structure. These features are most likely a result of strong heating during atmospheric entry. Therefore, it is possible that the progressive clustering of data points towards an Fe-rich composition in Fig. 2, f–h, reflect the effects of heating to progressively higher temperatures.

4.2. Sources of LS IDPs

Evidence in support of asteroidal origin for LS IDPs has been derived from laboratory pulse heating experiments, solar flare track measurements and mineralogical considerations. The heating and track studies showed that most LS IDPs collected from the stratosphere are not heated above 600 °C during atmospheric entry [8]. Such particles would have to have arrived at the top of the atmosphere with low geocentric encounter velocities. Sources that satisfy these orbital constraints include main-belt asteroids and comets with perihelia outside of 1.2 AU and low inclinations [8].

The mineralogical evidence concerns parent-body aqueous alteration. Layer silicates in the IDPs appear to have formed *in situ* during aqueous alteration of anhydrous silicates in a manner similar to the fine-grained matrices of CI and CM carbonaceous chondrites. However, glass appears to be the silicate precursor of the layer silicates in the IDPs studied here (Fig. 7), but in CI/CM chondrites the precursors are believed to be olivine and pyroxene as well as glass [13,31–34]. In U230A34 smectite is intimately intergrown with its glass precursor on a submicrometer scale (Fig. 7), demonstrating that alteration occurred over a very limited (spatial) range. In U222C29 aqueous alteration is more advanced. Euhedral carbonate grains, the largest so far reported in an IDP, are prominent constituents (Fig. 1a), and most of the sulfides were heavily decorated with (secondary) magnetite.

The mineralogical diversity among the IDPs implies that they may have been derived from a variety of parent bodies that typically experienced less aqueous alteration than the parent bodies of CI and CM chondrites. Such conditions are likely to be found on smaller asteroidal bodies and among the outer asteroids that have never been strongly heated [35–37]. The same mineralogical diversity would not show up among conventional meteorites for two reasons. First, meteorites achieve Earth-crossing orbits only after a rare and highly selective series of gravitational perturbations [12], whereas orbital transfer via Poynting–Robertson drag ensures that the orbits of all IDPs decay towards Earth-crossing orbits [7]. Second, atmospheric entry favors survival of strong objects; i.e., only the more highly altered, compacted rocks (e.g., CI and CM chondrites) are strong enough to survive atmospheric entry as large objects. Small particles are not subject to these same strength selection effects during atmospheric entry, so the more fragile asteroidal materials that cannot survive atmospheric entry as large meteorites can survive as micrometer-sized particles.

5. Summary and conclusions

A combination of automated and conventional AEM analyses were applied to study thin sections of eight LS IDPs and the fine-grained matrices of two carbonaceous chondrites. The automated analyses provided large data sets of quantitative chemical data collected with spatial resolution better than 50 nm. These data enable direct mineralogical comparison of the IDPs and meteorites on a scale of less than 50 nm. Like CI and CM chondrites, the IDPs appear to have been derived from parent bodies in which aqueous alteration has occurred. Asteroids are clearly the strongest candidates for the sources of LS IDPs, since the case for aqueous alteration having occurred on many asteroids is now well established [32,34,37,38]. Unlike CI and CM chondrites, the IDPs have retained much of their primitive chondritic mineralogy, as illustrated by their compositional heterogeneity on a submicrometer scale and a lack of secondary mineral phases (e.g., tochilinite and sulfates [31,34,39]) associated with advanced aqueous alteration. The matrices of Murchison and Orgueil appear to have been homogenized as a result of more extensive aqueous alteration.

This study suggests that LS IDPs encompass a wide variety of particulate chondritic materials, so any attempt to derive a classification scheme may require thin sectioning and AEM analyses of a large number of particles (a population of 200 particles was required to discern bulk chemical trends in chondritic IDPs [1]). A study of a large population of LS IDPs is planned because we expect it can provide new information about geochemical conditions on different-sized parent bodies as well as those from regions of the asteroid complex that are not sampled by conventional meteorites.

Thin sectioning and instrument automation techniques have been refined to the point where they can be applied to almost any fine-grained meteoritic material. Detailed mineralogical and petrographic studies are possible, despite the small sizes and fine-scale mineralogical heterogeneity of some specimens (e.g., IDPs). The techniques will play an increasingly important role in extraterrestrial materials characterization, where they will not only improve our understanding of the nature of fine-grained materials, but also establish a data base for evaluation of new types of materials from present and future activities like the Long Duration Exposure Facility (LDEF) [40], the space station Freedom, and the Comet Rendezvous Asteroid Flyby (CRAF) mission [41].

Acknowledgments

This research was supported by NASA contract NAS-9-17749 and McCrone Associates Inc. Constructive reviews were provided by P.R. Buseck and S.A. Sandford.

References

1 L.S. Schramm, D.E. Brownlee and M. M. Wheelock, Major element composition of stratospheric micrometeorites, Meteoritics, 24, 99–112, 1989.
2 J.P. Bradley, S.A. Sandford and R.M. Walker, Interplanetary dust particles, in: Meteorites and the Early Solar System, J. Kerridge and M.S. Mathews, eds., pp. 861–895, Univ. of Arizona Press, 1988.
3 S.A. Sandford and R.M. Walker, Laboratory infrared transmission spectra of individual interplanetary dust particles from 2.5 to 25 microns, Astrophys. J. 291, 838–851, 1985.
4 J.P. Bradley, M.S. Germani and D.E. Brownlee, Automated thin-film analyses of anhydrous interplanetary dust particles in the analytical electron microscope, Earth Planet. Sci. Lett. 93, 1–13, 1989.
5 J.P. Bradley, Analysis of chondritic interplanetary dust thin-sections, Geochim. Cosmochim. Acta 52, 889–900, 1988.
6 K.L. Thomas, M.E. Zolensky, W. Klock and D.S. McKay, Mineralogical descriptions of eight hydrated interplanetary dust particles and their relationship to chondrite matrix, Lunar Planet. Sci. XXI, 1250–1251, 1990.
7 S.A. Sandford, The collection and analysis of extraterrestrial dust particles, Fundam. Cosmic Phys. 12, 1–73, 1987.
8 S.A. Sandford and J.P. Bradley, Interplanetary dust particles collected in the stratosphere: observations of atmospheric heating and constraints on their interrelationships and sources, Icarus 82, 146–166, 1989.
9 J.P. Bradley and D.E. Brownlee, Cometary particles: thin-sectioning and electron beam analysis, Science 231, 1542–1544, 1986.
10 K. Tomeoka and P.R. Buseck, Transmission electron microscopy of the "LOW-CA" hydrated interplanetary dust particle, Earth Planet. Sci. Lett. 69, 243–254, 1984.
11 K. Tomeoka and P.R. Buseck, Hydrated interplanetary dust particle linked with carbonaceous chondrites?, Nature 314, 338–340, 1985.
12 G.W. Wetherill and C.R. Chapman, Asteroids and meteorites, in: Meteorites and the Early Solar System, J.F. Kerridge and M.S. Mathews, eds., pp 35–67, Univ. of Arizona Press, 1988.
13 H.Y. McSween and S.M. Richardson, The composition of carbonaceous chondrite matrix, Geochim. Cosmochim. Acta 41, 1145–1161, 1977.
14 K. Tomeoka and P.R. Buseck, A carbonate-rich, hydrated, interplanetary dust particle: possible residue from protostellar clouds, Science 231, 1544–1546, 1986.
15 K.D. McKeegan, Ion microprobe measurements of H, C, O, Mg, and Si isotopic abundances in individual interplanetary dust particles, PhD Thesis, Washington Univ., 1987.
16 K.D. McKeegan, P. Swan, R.M. Walker, B. Wopenka and E. Zinner, Hydrogen isotopic variations in interplanetary dust particles, Lunar Planet. Sci. XVIII, 627–628, 1987.
17 J.I. Goldstein, Principles of thin-film X-ray microanalysis, in: Introduction to Analytical Electron Microscopy, J.J. Hren, J.I. Goldstein and D.C. Joy, eds., pp. 83–120, Plenum Press, New York, NY, 1987.
18 J.I. Goldstein, J.L. Costley, G.W. Lorimer and S.J.B. Reed, Quantitative x-ray analysis in the electron microscope, Scanning Electron Microsc. 1, 315–324, 1977.
19 D.E. Newbury and R.L. Myklebust, Calculations of electron beam spreading in composite thin foil targets, in: Microbeam Analysis-1980, D.B. Wittry, ed., pp.173–175, San Francisco Press, 1980.
20 G. Cliff and G.W. Lorimer, The quantitative analysis of thin-sections, J. Microsc. 103, 203–207, 1975.
21 P. Sheridan, Determination of experimental and theoretical KASi factors for a 200 keV analytical electron microscope: J. Electron Microsc. Tech. 11, 41–61, 1989.
22 B. Mason and R.O. Allen, Minor and trace elements in augite, hornblende, and pyrope megacrysts from Kakanui, New Zealand, N. Z. J. Geol. Geophys. 16(4), 935–947, 1973.

23 T.W. Shattuck, M.S. Germani and P.R. Buseck, Cluster analysis of chemical compositions of individual atmospheric particles data, in: Experimental Applications of Chemometrics, J.J. Breen and P.E. Robinson, eds., pp. 118–129, Am. Chem. Soc., Series 292, Washington DC, 1985.
24 T.A. Abrajano, J.K. Bates, A.B. Woodland, J.P. Bradley and W.L. Bourcier, Secondary phase formation during nuclear waste glass dissolution, Clays Clay Miner. 38, 537–548, 1990.
25 K.F.J. Heinrich, Electron-beam X-ray Microanalysis, 578 pp., Van Nostrand Reinhold, 1981.
26 M.M. Maurette, D.E. Brownlee and L.S. Schramm, Giant micrometeorites from Antarctic blue ice, Lunar Planet. Sci. XX, 636–637, 1988.
27 D.E. Brownlee, B. Bates, L.B. Pilachowski, E. Olszewski and W. Seigmund, Unmelted cosmic materials in deep sea sediments, Lunar. Planet. Sci. XI, 109–111, 1980.
28 J.P. Bradley, D.E. Brownlee and D.R. Veblen, Pyroxene whiskers and platelets in interplanetary dust: evidence of vapor phase growth, Nature 301, 473–477, 1983.
29 W. Klöck, K.L. Thomas, D.S. McKay and H. Palme, Unusual olivine and pyroxene compositions in interplanetary dust and unequilibrated ordinary chondrites, Nature 339, 126–128, 1989.
30 D.E. Brownlee, D.A. Tomandl, M.B. Blanchard, G.V. Ferry and F. Kyte, An atlas of extraterrestrial particles collected from the stratosphere with NASA U-2 aircraft, NASA Tech. Mem. X-73, 152, 1976.
31 D.J. Barber, Matrix phyllosilicates and associated minerals in C2M carbonaceous chondrites, Geochim. Cosmochim. Acta 45, 945–970, 1981.
32 M.E. Zolensky, W.L. Bourcier and J.L. Gooding, Aqueous alteration on the hydrous asteroids: results of EQ3/6 computer simulations, Icarus, 78, 411–425, 1989.
33 C.M.O'D. Alexander, D.J. Barber and R. Hutchison, The microstructure of Semarkona and Bishunpur, Geochim. Cosmochim. Acta 53, 3045–3057, 1989.
34 K. Tomeoka and P.R. Buseck, Indicators of aqueous alteration in CM carbonaceous chondrites: microtextures of a layered mineral containing Fe, S, O, and Ni, Geochim. Cosmochim. Acta 49, 2149–2163, 1985.
35 L.A. Lebofsky, T.D. Jones, P.D. Owensby, M.A. Feierberg and G.J. Consolmagno, The nature of low albedo asteroids from 3-μm multi-color photometry, Icarus 83, 16–26, 1990.
36 T.D. Jones, L.A. Lebofsky, J.S. Lewis and M.S. Marley, The composition and origin of the, C, P, and D asteroids: water as a tracer of thermal evolution in the outer belt, Icarus, in press.
37 F. Vilas and M.J. Gaffy, Phyllosilicate absorption features in main-belt and outer-belt asteroid reflectance spectra, Science 246, 790–792, 1989.
38 R.E. Grimm and H.Y. McSween, Water and the thermal evolution of carbonaceous chondrite parent bodies, Icarus 82, 244–280, 1989.
39 M.E. Zolensky, Hydrothermal alteration in CM carbonaceous chondrites: implications of the identification of tochilinite as one type of meteoritic PCP, Meteoritics 19, 346–347, 1984.
40 The long duration exposure facility, W.H. Kinard, D.J. Carter, and J.L. Johns, eds., 189 pp., NASA SP-473, 1984.
41 M. Neugebauer and P. Weissman, CRAF mission, EOS 24, 633–646, 1989.

Appendix II, Paper 2

COVER A 10 by 10 micrometer "layer silicate" interplanetary dust particle collected from the stratosphere by the NASA Johnson Space Center Cosmic Dust Collection Program. Data from analytical electron microscopic studies establish that some (and potentially all) interplanetary dust particles of the "layer silicate" subset are derived from asteroids. See page 549. [Scanning electron micrograph by J. P. Bradley; image processing by J. Barabe and S. Kilbourne]

An Interplanetary Dust Particle Linked Directly to Type CM Meteorites and an Asteroidal Origin

J. P. BRADLEY AND D. E. BROWNLEE

Tochilinite, an ordered mixed-layer mineral containing Mg, Al, Fe, Ni, S, and O, has been identified in an interplanetary dust particle (IDP). This mineral is found in only one other class of meteoritic materials, type CM carbonaceous chondrites. The presence of tochilinite in an IDP provides a direct petrogenetic link between a member of the layer-silicate subset of IDPs and a specific class of meteorites and thus establishes that some IDPs collected in the stratosphere have an asteroidal origin. The scarcity of this IDP type suggests that materials with CM mineralogy are not abundant among the dust-producing asteroids.

EXTRATERRESTRIAL MATERIALS CAPtured by Earth include both conventional meteorites and micrometer-sized interplanetary dust particles (IDPs). Meteorites have been intensively studied because laboratory specimens have been available for many decades and most are large (>1 cm) objects that can be examined by multiple analytical techniques. The IDPs have been studied in less detail because most have been collected only during the past decade (*1*) and because techniques sensitive enough for analysis of nanogram quantities of material are required. Meteorites are believed to be derived primarily from asteroids (*2, 3*), but because only a few asteroids have spectral reflectances similar to those of the major meteorite classes (*4*), it appears that meteorites are a highly biased sampling. This bias is believed to result from two processes. First, for bodies larger than about 1 cm^3, only strong objects can survive atmospheric entry, and fragile objects, like cometary meteors and weaker asteroidal materials, fragment into dust (*5*). Second, the

J. P. Bradley, McCrone Associates, Westmont, IL 60559–1275.
D. E. Brownlee, Department of Astronomy, University of Washington, Seattle, WA 98195.

sources of conventional meteorites appear to be largely restricted to regions of the asteroid belt where orbital resonance with Jupiter initiates gravitational transfer to Earth-crossing orbits (*2*). Both comets and asteroids generate IDPs (*1*, *6–8*), and IDPs include both strong objects as well as extremely fragile meteoritic materials that can survive atmospheric entry because of the greatly reduced ram pressure exerted on meteors less than about 1 mm^3 in size (*9*). Because the orbits of small particles decay to Earth-crossing under the influence of Poynting-Robertson drag (*1*, *10*, *11*), asteroidal IDPs can be derived from virtually any dust-producing region of the asteroid belt. One of the fundamental goals of interplanetary dust research is to identify IDPs that have an asteroidal origin, because they may provide a broader and less biased sampling of the asteroid belt than is provided by meteorites.

Among the collected IDPs are a group referred to as chondritic because their bulk elemental compositions generally agree with those of chondritic meteorites (*7*). One particular subset of chondritic IDPs are strong candidates for asteroidal materials because, like CI and CM meteorites, they contain abundant fine-grained layer silicates, carbonates, and related phases (*7*, *12*, *13*). The presence of these phases is indicative of an episode of aqueous alteration, which is believed to have occurred within moderately heated asteroids during the early history of the solar system (*14*). However, it has not been possible to link these "layer-silicate" IDPs directly to chondritic meteorites because no IDP has been found with a mineralogy characteristic of a specific class of meteorites. In this report, we describe a layer-silicate IDP that contains tochilinite, an ordered mixed-layer mineral containing Mg, Al, Fe, Ni, S, and O, that has been found within only one other class of meteoritic materials, the type CM carbonaceous chondrites. The finding of tochilinite establishes a direct petrogenetic link between an IDP and a class of meteorites, implies a common asteroidal provenance for this IDP, and focuses attention on the entire subset of layer-silicate IDPs as a diverse sampling of the hydrous asteroids.

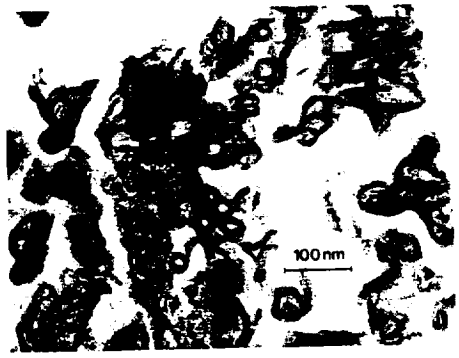

Fig. 2. Bright-field electron micrograph of a tochilinite-rich region of a thin section (~50 nm thick) of RB12A44. The concentric structures are tochilinite tubes (viewed in cross section). [See also Fig. 3D and compare with figures 13 and 14 of (*22*).] Many of the tochilinite tubes contain (noncrystalline) silicate cores.

The tochilinite and serpentine-bearing IDP, RB12A44, was collected from the stratosphere at an altitude of 18 to 20 km with the use of a NASA U-2 aircraft (*1*). It was found as a grouping of five 10- to 12-μm fragments of a larger (~30 μm) IDP that broke up when it impacted onto the collection substrate. We used the scanning electron microscope (SEM) to examine the bulk compositions, surface textures, and morphologies of the fragments and the analytical electron microscope (AEM) to investigate compositions and crystal structures of specific mineral phases (*15*). Particle

Table 1. Compositions (normalized to that of Si) of matrix phases in RB12A44 and a type CM carbonaceous chondrite. (Column 1, bulk composition of the fragment of RB12A44 shown in Fig. 1A; column 2, average and standard deviations (parentheses) for ten individual thin sections of RB12A44; column 3, tochilinite-cronstedtite intergrowth in RB12A44; column 4, cronstedtite, $Mg_{0.61}Al_{0.39}Ca_{0.01}Fe^{2+}_{3.83}Fe^{3+}_{1.09}[Si_{2.63}Al_{0.39}Fe^{3+}_{0.98}]O_{10}(OH)_8$, in RB12A44; column 5, Mg-rich serpentine, $Mg_{3.94}Al_{0.21}Ca_{0.002}Mn_{0.02}Fe^{2+}_{1.65}[Si_{4.0}]O_{10}(OH)_8$, in RB12A44; column 6, tochilinite-cronstedtite intergrowth in Murray (CM) matrix (*22*); column 7, cronstedtite in Murray (CM) matrix (*22*); column 8, Mg-rich serpentine in Murray (CM) matrix (*22*).

Element	1	2	3	4	5	6	7	8
Mg	0.718	0.427 (0.089)	0.770	0.204	0.844	0.922	0.461	1.030
Al	0.113	0.195 (0.032)	0.361	0.281	0.049	0.332	0.118	0.036
S	0.503	0.348 (0.064)	2.980	0.012	0.003	3.052	0.197	0.172
Ca	0.033	0.010 (0.005)	0.016	0.006	0.008			0.003
Cr	0.023	0.023 (0.007)	0.065			0.015		
Mn	0.010	0.014 (0.004)	0.082	0.024	0.008			
Fe	2.433	2.677 (0.438)	10.672	4.462	0.814	10.759	4.261	0.801
Ni	0.100	0.074 (0.015)	0.442			0.339	0.016	0.053

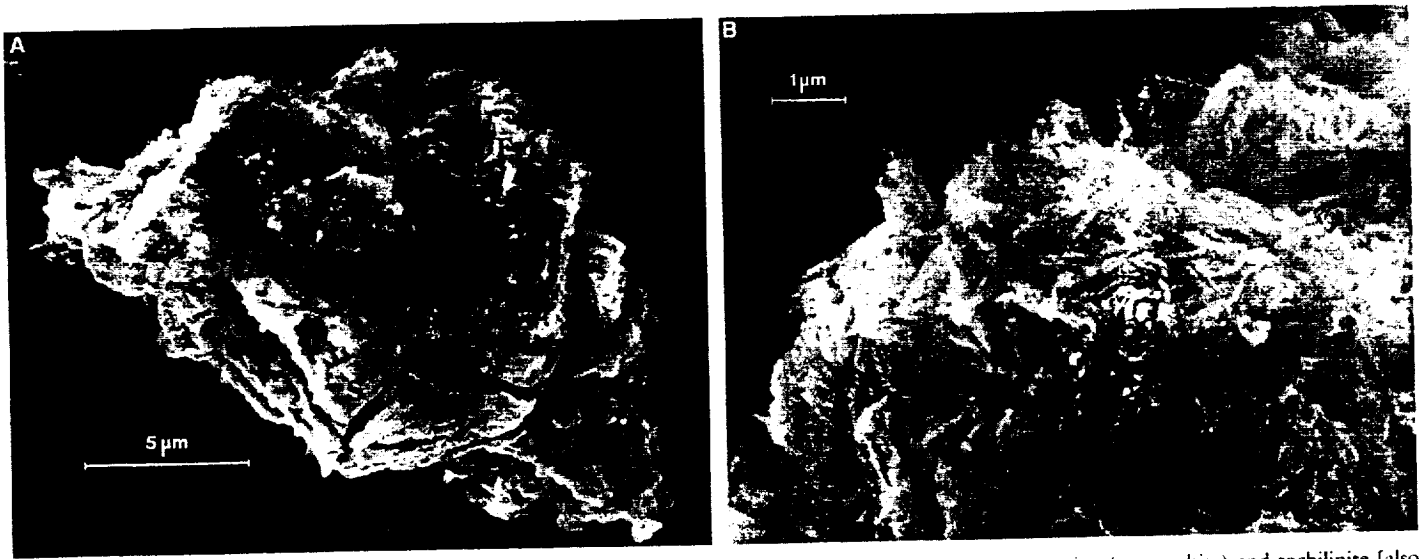

Fig. 1. Scanning electron micrographs of a fragment of RB12A44. (**A**) Low-magnification image showing both fibrous (F) and smooth (S) plate-like surface structures. The smooth regions are serpentine and the fibrous regions are finely intergrown serpentine (cronstedtite) and tochilinite [also known as PCP (*20–26*)]. (**B**) High-magnification image showing the distinctive fibrous morphology of the serpentine-tochilinite intergrowth.

RB12A44 exhibits both smooth, plate-like surfaces and fibrous regions (Fig. 1). The smooth surface structures are typical of layer-silicate IDPs (Fig. 1) (*7*), but the fibrous structures are unusual (Fig. 1B). We produced several ultramicrotomed thin sections (~50 nm thick) of the particle shown in Fig. 1 in order to examine its indigenous microstructures, mineralogy, and petrography (*13*). Solar flare tracks (with a density of $\sim 10^{11}$ cm^{-2}) were observed in several mineral grains (*16*), and the edges of some thin sections contained amorphous rims (10 to 20 nm thick), which are believed to result from direct exposure to the solar wind (*8, 17*).

Two principal mineral phases, serpentine and tochilinite (Figs. 2 and 3), were identified in thin section by lattice-fringe imaging, electron diffraction, and x-ray energy-dispersive spectrometry. Together, these minerals account for >95% of the volume of the IDP. Both Mg-rich and Fe-rich varieties of serpentine are present (Table 1). The serpentine exhibits characteristic basal lattice spacings of 7.0 to 7.3 Å, and the tochilinite exhibits both 5.4 and 10.8 Å spacings (Fig. 3). Most of the Fe-rich serpentine (cronstedtite) is intergrown with tochilinite on a unit-cell scale (Fig. 3). No crystals of pure (cronstedtite-free) tochilinite were identified. The most tochilinite-rich regions of the thin sections exhibit characteristic tubular microstructures (Figs. 2 and 3D). Pentlandite [$(FeNi)_9S_8$], kamacite (FeNi alloy), troilite (FeS), magnetite (Fe_3O_4), and diopside [$(Ca,Mg)Si_2O_6$] are minor constituents in the matrices of RB12A44; single grains of schreibersite [Fe-Ni-(Cr)phosphide], (Fo_{84}) olivine, and an Mg-Fe-S-O phase (presumably sulfate) are also present. The schreibersite and olivine grains are almost 1 μm across, as are some of the pentlandite crystals, but the other mineral grains seldom exceed 200 nm in diameter.

The composition of the particle shown in Fig. 1 and the compositions of the major mineral phases identified in thin sections (Table 1) were determined by quantitative x-ray energy-dispersive spectrometry. We measured the bulk particle composition in the SEM using a correction procedure developed for analyses of small particles (Table 1, column 1) (*18*), and we analyzed thin sections in the AEM using a thin-film correction procedure (column 2) (*19*). Compositions were also determined for the tochilinite-cronstedtite intergrowths, cronstedtite, and Mg-rich serpentine (columns 3 to 6).

Tochilinite is an abundant (4 to 15% by weight) and ubiquitous constituent of the fine-grained matrices of type CM carbonaceous chondrites (*20–26*). It has not been found in any other meteorite (*20, 22, 25*). The presence of tochilinite thus implies that IDP RB12A44 is linked to CM chondrites. Its presence also suggests that RB12A44 was not strongly heated during atmospheric entry, because tochilinite is thermally unstable and converts rapidly to troilite at 245°C (*26*). Tochilinite is texturally distinct from any other minerals found in meteorites (Fig. 2). It is seldom found as crystals >100 nm, and as illustrated in Figs. 2 and 3, it is usually intergrown with cronstedtite on a unit-cell scale (*22, 23*). Although the crystal structure of tochilinite has yet to be verified by single crystal x-ray diffraction, it is believed to consist (ideally) of alternating sheets of Mg, Fe hydroxide, and Fe, Ni, (Cu) sulfide (*27*). The texture and composition of tochilinite provide key information for understanding the mechanism of aqueous alteration in the parent bodies of CM chondrites (*21–25*). Tomeoka and Buseck (*22*), for example, proposed that tochilinite and tochilinite-cronstedtite intergrowths (referred to as FESON and PCP, respectively) formed in the parent body regolith during a three-stage process of aqueous alteration. Their proposed sequence of mineralogical reactions is consistent with bulk compositional changes that have been observed to occur in the matrices of some CM chondrites that preserve differing degrees of aqueous alteration (*20, 25*).

The compositions and microtextures of tochilinite-cronstedtite intergrowths in RB12A44 are similar to those observed in the matrices of CM chondrites (compare Table 1, columns 3 to 8) (*22*), and most of the minor phases found in association with tochilinite in CM chondrites [for example, troilite, magnetite, pentlandite, and Fe-Ni-(Cr)-phosphide (*22*)] are also found in RB12A44. The link to CMs is significant because there is evidence that this rare chondrite class [<2% of meteorite falls (*4*)] is abundant in space. The CM chondrites have the lowest albedo of all chondrites, and they show the best spectral and albedo match to the C asteroids that dominate the mid-region of the asteroid belt (*4, 28*). Fragments of CM material are the most common type of xenolith inclusions found inside other meteorites (*28*), and the ratio of siderophile elements to Ir of the meteoritic component of lunar soils suggests that CM-like material has provided a large amount of the material accreted to the moon over the past 3.7 billion years (*29*). The average oxygen isotopic composition of cosmic deep-sea spheres (melted 0.1- to 1.0-mm IDPs) is consistent with that of CM chondrites and distinct from that of CI and ordinary chondrites (*30*).

The apparent rarity of IDPs with CM-type mineralogy is also significant. Of almost 100 layer-silicate IDPs that have been

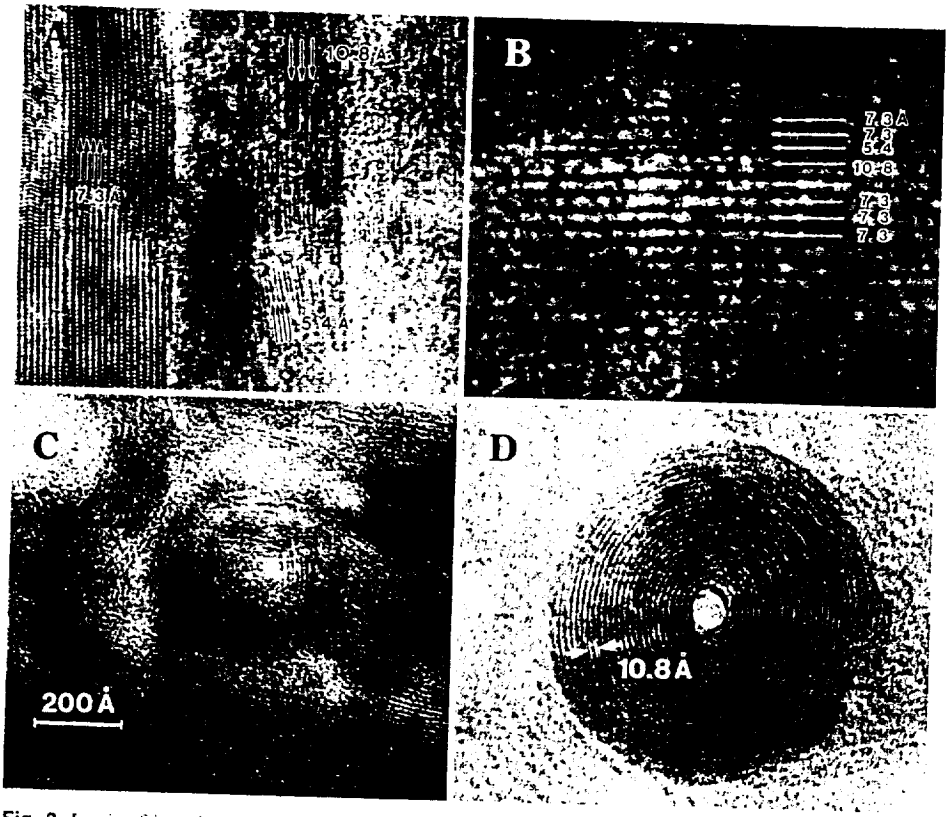

Fig. 3. Lattice-fringe images of cronstedtite and tochilinite in RB12A44. (**A**) Mixture of cronstedtite (7.3 Å spacing) and tochilinite (5.4 and 10.8 Å spacings). (**B**) Unit cell intergrowth of cronstedtite and tochilinite. (**C**) Psuedo-rectangular tochilinite "prototube" (*22*) nucleated in a cronstedtite plate. (**D**) Tochilinite tube.

studied by electron microscopy (*7, 12, 13, 31*), RB12A44 is the only one in which tochilinite and cronstedtite have been found. A specific search for these phases might reveal a higher abundance, but it is unlikely to exceed 10% of these IDPs. Therefore, if layer-silicate IDPs are a representative sampling of the asteroid belt, then CM chondrites cannot dominate the main belt, despite their similarity to the C reflectance class of asteroids (*28*). Both layer-silicate IDPs and C class asteroids could be samples of a broad spectrum of CM-like materials sharing common physical properties (for example, reflectance), but having significant mineralogical differences. For example, most layer silicate IDPs contain smectite rather than serpentine, and although the degree of aqueous alteration is variable from one IDP to another, it is often less than the matrices of CM chondrites (*13, 31*).

The identification of a CM-type IDP confirms predictions, based on calculations of particle orbital dynamics, that asteroidal material should be present among stratospheric IDPs (*6, 11*); most likely, materials from a variety of asteroidal parent bodies are present. However, only a subset of the IDPs have been studied. Most research has been focused on fine-grained IDPs because study of the variety of minerals they contain provides the best means for understanding their origins; coarser-grained IDPs have not yet been studied in detail. (Because of their coarse grain size, most meteorites could not be linked to a specific class of parent body on the basis of analysis of a 10-μm fragment.) In this study, we were able to make a strong link between RB12A44 and CM chondrites only because CMs are very fine grained and can be mineralogically distinct on a micrometer scale. If all layer-silicate IDPs are indeed of asteroidal origin, future sample studies combined with studies of dust dynamics should provide new information about geochemical conditions among the asteroids.

REFERENCES AND NOTES

1. S. A. Sandford, *Fundam. Cosmic Phys.* **12**, 1 (1987).
2. E. Anders, *Icarus* **24**, 363 (1975); G. W. Wetherill and C. R. Chapman, in *Meteorites and the Early Solar System*, J. F. Kerridge and M. S. Mathews, Eds. (Univ. of Arizona Press, Tucson, AZ, 1988), pp. 35–67.
3. E. Anders, in *Asteroids: An Exploration Assessment*, D. Morrison and W. C. Wells, Eds. (*NASA Publ. CP2053*, National Aeronautics and Space Administration, Houston, TX, 1978), pp. 316–335.
4. M. E. Lipschutz, M. J. Gaffey, P. Pellas, in *Asteroids II*, R. P. Binzel, T. Gehrels, M. S. Mathews, Eds. (Univ. of Arizona Press, Tucson, AZ, 1989), pp. 740–777.
5. Z. Sekanina, *Astron. J.* **90**, 827 (1985).
6. S. A. Sandford, *Icarus* **68**, 377 (1986); G. J. Flynn, *ibid.* **77**, 287 (1989); S. A. Sandford and J. P. Bradley, *ibid.* **82**, 146 (1989).
7. L. S. Schramm *et al.*, *Meteoritics* **24**, 99 (1989).
8. J. P. Bradley and D. E. Brownlee, *Science* **231**, 1542 (1986).
9. F. Verniani, *Space Sci. Rev.* **10**, 230 (1960).
10. J. S. Dohnanyi, in *Cosmic Dust*, J. A. M. McDonnell, Ed. (Wiley-Interscience, New York, 1978), pp. 527–605.
11. G. J. Flynn, *Proc. Lunar Planet. Sci. Conf.* **20**, 363 (1990).
12. K. Tomeoka and P. R. Buseck, *Earth Planet. Sci. Lett.* **69**, 243 (1984); I. D. R. MacKinnon and F. J. M. Rietmeijer, *Rev. Geophys.* **25**, 1527 (1987); K. L. Thomas, M. E. Zolensky, W. Klock, D. S. McKay, *Lunar Planet. Sci.* XXI, 1250 (1990); K. Tomeoka and P. R. Buseck, *Nature* **314**, 338 (1985).
13. J. P. Bradley, *Geochim. Cosmochim. Acta* **52**, 889 (1989).
14. R. E. Grimm and H. Y. McSween, Jr., *Icarus* **82**, 244 (1989).
15. Instruments used for this study were JEOL JSM-35C, 840, and 6400F SEMs, a 200-keV 2000FX AEM, and a 400-keV 4000FX AEM. All instruments were equipped with solid-state x-ray energy-dispersive spectrometers.
16. J. P. Bradley, D. E. Brownlee, P. Fraundorf, *Science* **226**, 1432 (1984).
17. K. Thiel, J. P. Bradley, R. Spohr, *Nucl. Tracks Rad. Meas.* **15**, 685 (1988); *ibid.*, in press.
18. J. T. Armstrong and P. R. Buseck, *Anal. Chem.* **47**, 2178 (1975).
19. G. Cliff and G. W. Lorimer, *J. Microsc.* **103**, 302 (1975); P. Sheridan, *J. Electron Microsc. Tech.* **11**, 41 (1989).
20. H. Y. McSween, Jr., *Geochim. Cosmochim. Acta* **51**, 2469 (1987).
21. K. Tomeoka and P. R. Buseck, *Nature* **306**, 354 (1983).
22. ———, *Geochim. Cosmochim. Acta* **49**, 2149 (1985).
23. K. Tomeoka, H. Y. McSween, Jr., P. R. Buseck, in *Proceedings of the Second National Institute for Polar Research Symposium on Antarctic Meteorites* (1989), p. 221.
24. M. E. Zolensky, *Meteoritics* **19**, 346 (1984).
25. E. Zolensky and H. Y. McSween, Jr., in *Meteorites and the Early Solar System*, J. Kerridge and M. S. Mathews, Eds. (Univ. of Arizona Press, Tucson, AZ, 1988), pp. 114–143.
26. L. Fuchs, E. Olsen, K. H. Jensen, *Smithson. Contrib. Earth Sci.* **10** (1973).
27. N. I. Organova, V. A. Drits, A. L. Dmitrik, *Am. Mineral.* **59**, 190 (1974); D. J. Barber, A. Bourdillon, L. A. Freeman, *Nature* **305**, 295 (1980); I. D. R. MacKinnon and M. E. Zolensky, *ibid.* **309**, 240 (1984).
28. J. Gradie, C. Chapman, E. Tedesco, in *Asteroids II*, R. P. Binzel, T. Gehrels, M. S. Mathews, Eds. (Univ. of Arizona Press, Tucson, AZ, 1989), pp. 316–335.
29. J. Wasson, W. V. Boynton, C. Chou, *Moon* **13**, 121 (1975).
30. R. N. Clayton, T. K. Mayeda, D. E. Brownlee, *Earth Planet. Sci. Lett.* **79**, 235 (1986).
31. M. S. Germani, J. P. Bradley, D. E. Brownlee, *ibid.* **101**, 162 (1990).

32. This research was supported by NASA grants NAS-9-17749 (J.P.B.), NSG 9052 (D.E.B.), and McCrone Associates. The Curatorial Facility at NASA Johnson Space Center provided IDP RB12A44. We thank L. Schramm, K. Tomeoka, A. Woodland, and M. Zolensky for constructive advice and J. Kerridge for detailed reviews.

27 September 1990; accepted 7 January 1991

Appendix II, Paper 3

ELECTRON MICROSCOPE STUDIES OF CARBON-RICH GRAINS IN A NEW COLLECTION OF ANTARCTICA MICROMETEORITES.

M.Maurette[1], C.Jouret[2], Ph.Bonny[1], J.P.Bradley[3], M.S.Germany[3], Y.Kihn[2]; [1]CSNSM, 91406 Campus-Orsay; [2]Laboratoire d'Optique Electronique, 31855 Toulouse; [3]McCrone Associates, Inc., Westmont, IL 68559.

The 50um-200um size fraction of a new collection of micrometeorites collected near Cap-Prudhomme in Antarctica (1,2), contains a high proportion of friable unmelted chondritic micrometeorites. They are very much enriched in a family of fragments that we preselect with a binocular, relying on simple criteria such as being dark, "fluffy", weakly magnetic and colorless . Each one of a set of 20 such fragments with sizes ~200um was divided into at least 3 chunks, upon a gentle crushing between two glass slides. A first chunk was run with a SEM equiped with an energy dispersive X Ray spectrometer, to identify a subset of 13 unmelted micrometeorites with a characteristic chondritic composition (i.e. high Si, Mg and Fe concentrations, and measureable amounts of Al, Ni, Ca, Cr and S). Most of the other grains were either some forms of iron hydroxide, or fly-ashes, rich in S and Fe. For each one of these micrometeorites a second chunk was further crushed in micron size grains, and analyzed with 2 high voltage transmission electron microscopes (HVEM). The grains were first run with a microscope equiped with an electron spectrometer (HVES), yielding the characteristic electron energy loss spectra of the grains from ~100eV to ~2500eV. Grains showing high carbon content were next run in the reaction chamber of another microscope, where their dynamical transformations upon pyrolisis up to 1000°C (at 10^{-6} Torr) was constantly monitored with a video camera on line with the microscope. For the 3 micrometeorites simultaneously investigated at McCrone Associates, a third chunk was imbedded into epoxy resin, and ultramicrotomed. The resulting sections were run with a 200 keV analytical electron microscope, already used (3) to characterize interplanetary dust particles (IDPs).

Our greatest challenge was to successfully tackle the severe problem of carbon contamination. The use of high voltage electron microscope already minimizes the build up of contamination layers on micron-size grains, because the total rate of ionization energy losses deposited by $\geq$ 1MeV electron is about 20 time smaller than in a conventional electron microscope, where much higher beam current have to be used. Moreover the search for carbon exclude the use of ordinary and/or holley carbon membranes for supporting the grains. We tried silica membranes from different origins (glass blowing; oxidation of a silicon wafer), at the expense of loosing the O and Si peaks of micrometeorites. Unfortunately all types of silica membranes showed some residual carbon contamination. We finally decided to crush directly chunks of micrometeorite on a gold electron microscope grid (without membrane), held between two glass slides. This technique works beautifully: a test sample made by crushing a single crystal of olivine do not show any measurable carbon peak after several hours of exposure in the electron beam (fig.1A). Moreover the grains can be heated up to 1000°C without being lost.

Our method of determining C concentrations from "point count HVES analysis" has to be oulined for any meaningful comparison with other methods, involving for example bulk analysis of large grains. Indeed the problem of relating a set of high resolution chemical analyses (scale ~ $\sim 10^{-3}um^2$) to bulk analysis (scale $>10^4um^3$) has still to be correctly tackled. For each micrometeorite we first select 10 grains with a size of a few um, stuck to the electron microscope grid, that appear as aggregates of tiny grains, showing some type of amorphous material. We thus exclude from our selection any large single crystal. We further select on each one of the grains a "favorable" zone, where the oxygen peak shows a double peak structure, indicating that the grain is thin enought as to allow a good determination of its C/O and C/Fe atomic ratios, with a procedure outlined elsewhere (4). Each one of the analyzed spot has a cross sectional area of about $0.3um^2$ and a thickness $\leq$ 0.5um, corresponding to a scale of analyzed volume of $\leq 0.2um^3$.

In figure 1A to 1D we report electron energy loss spectra for the 3 micrometeorites with sizes ~200um that are currently analyzed at McCrone (see below), namely: (a) micrometeorite G20, containing the highest concentration of carbon. In this type of micrometeorites all 10 zones show a high C peak with C/O ratios, ranging from 1.1 (fig.1C) to 0.5; (b) micrometeorite G10, which is somewhat less enriched in carbon than the previous one. Again, all 10 zones show a detectable C peak, but now the highest C concentration reaches a lower value of 0.7 (fig.1B); (c) micrometeorite G21, belonging to a major class (relative abundance ~40%), where the C content is much lower: only 2 of the the 10 zones show a detectable C peak corresponding to C/O ratios of 0.3 (fig.2D) and 0.2; (d) the other micrometeorites (relative abundance ~40%) did not show up a C peak. For

calibration purposes we have run one chunk of the Orgueil meteorite, and the "10-zones" point count analysis reveals a behavior very similar to that of micrometeorite 621, defined as containing a "low" C content. The constituent fine grained material of about 20% of the unmelted Antarctica micrometeorites contain carbon concentrations that would be much higher than the value (~5%) quoted from bulk analysis of Orgueil (6). In this preliminary set of 13 micrometeorites the concentrations of S and C show no correlation.

HVEM pyrolysis runs show a marked difference between IDPs and Antarctica micrometeorites. In 1976 we investigated a "porous" IDP, only quoting results obtained for temperatures in excess of 500°C (5). A reexamination of electron micrographs taken at lower temperatures shows that the constituent amorphous material of this grain suffers a drastic "shrinking" that reduces its apparent thickness by up a factor 2 at a very low temperature of ~200°C. Then no further transformation did occur up to ~1000°C. In sharp contrast Antarctica micrometeorites do not show any low temperature transformation. Textural transformations start around 700°C, when the least refractory components of some grains sufficiantly soften as to induce the formation of some rounded habits. A complete spherulization is observed for some micrometeorites at temperatures (~1000°C), lower than "melting" temperatures quoted for carbonaceous chondrites (about 1300°C).

Analytical electron microscope studies of ultramicrotomed sections of G20 and G21, allow the following comparison with the 3 major types of IPDs investigated with the same instrument (3): (a) oddly enought G20, which contains the highest carbon concentration appears much more coarse-grained (2A) than G21 (2B). We have a puzzle here because HVEM observation of crushed fragments from the same grains show rather similar aggregates of submicron size grains, imbedded in some amorphous material. In contrast observations of "porous" IDPs with both microscopes reveal very similar textural features; (b) sharp amorphous rings typical of some disordered graphite have been observed in G20 and G21; (c) Cluster analysis of Si/Mg/Fe ternary diagrams, plotted from at least 150 point count EDX analyses of G20 and G21 at a scale of 10^{-3}um^3 (see fig.2A and 2B, respectively) illustrate that both types of Antarctica micrometeorites look again different from IDPs: they show a tighter clustering of data points, that also indicates higher Fe concentrations and/or higher abundance of Fe-rich olivine.

Figure 1: HVES Point Count Analysis of Carbon

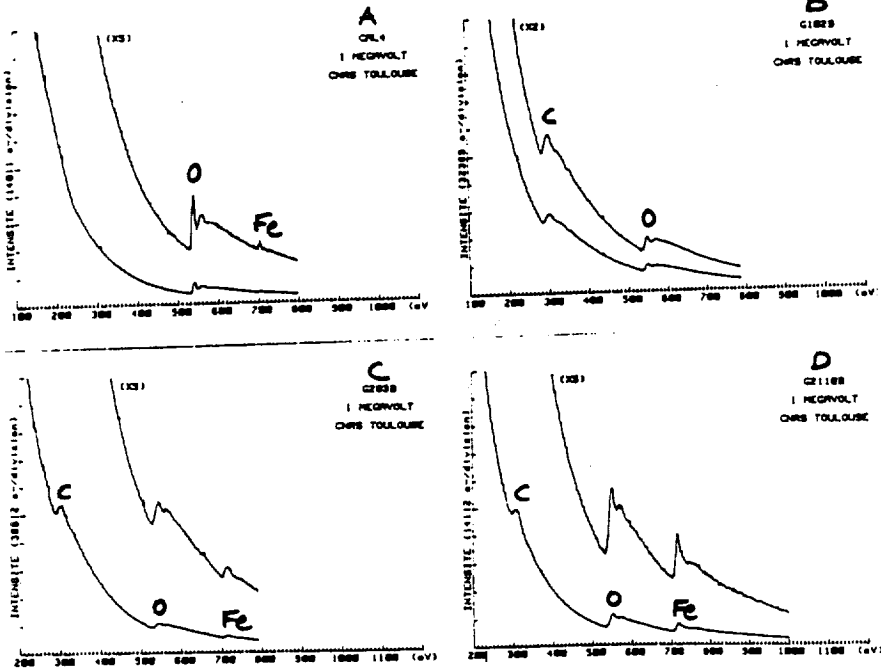

Figure 2

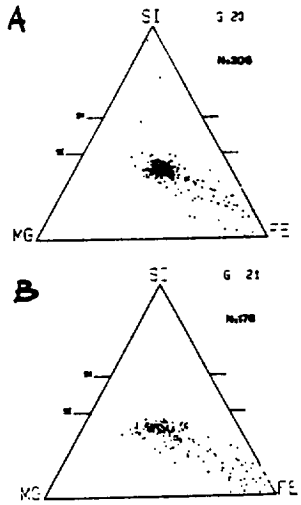

REFERENCES: (1) Maurette, M, Pourchet M., et al (1988) Abstract, this volume; (2) Maurette M., Brownlee D.E., Schramm P. (1988) Abstract, this volume; (3) Bradley J., Germany M. (1988) LPSC XIX, 126; (4) Egerton R.S. (1975) Phil.Mag.31, 1990; (5) Bibring J.P. et al (1977) LPSC IX, 79.

Appendix II, Paper 4

ELECTRON ENERGY LOSS SPECTROSCOPY OF THE FINE GRAINED MATRICES OF INTERPLANETARY DUST PARTICLES

J. P. Bradley, McCrone Associates, Wesstmont, IL 60559-1275

Meteoritics, 26, 322-323, 1991.

The fine-grained matrices of some anhydrous IDPs are dominated by 1-20 nm diameter mineral grains. Such small grains have hindered mineralogical and petrographic studies, which are critical for understanding the origins and growth/aggregation modes of IDPs. Matrix compositions have been measured using x-ray spectroscopy with spatial resolution ≈50 nm, but compositional analyses at the individual 1-20 nm mineral grains within these matrices is not possible [1]. In the absence of the necessary (x-ray) spatial resolution, electron energy loss spectroscopy (EELS) offers an alternative means of probing the compositional, crystallographic, and electronic environment of elements on an atomic scale [2]. EELS in the electron microscope is particularly suitable for fine grained materials analysis, because it is inherently more sensitive than x-ray spectroscopy, and therefore lower beam currents and smaller electron probes can be used for data acquisition.

Figure 1 shows EELS edges for iron and oxygen obtained from minerals in thin sections of IDPs. Fe and O were selected because they are major components of chondritic materials, they reside in several phases, and their core scattering edges are relatively well understood [2,3]. In IDPs, Fe is present in alloys, silicates, sulfides, and oxides, while O is present in silicates and oxides. Comparison of the core scattering edges in Figures 1a and 1b demonstrates that reduced iron (Fe^{O}) can be distinguished from oxidized iron (Fe^{2+} or Fe^{3+}). In principle, it is also possible to distinguish between Fe^{2+} and Fe^{3+} by measuring a chemical shift (≈2 eV) of the edge position [4], and possibly determine the ratio of total oxidized to total reduced iron (Fe^{2+} + Fe^{3+}/Fe^{O}) in an IDP thin section. Figures 1c and 1d suggest that it is possible to distinguish oxygen in a silicate network from oxygen in oxides. Core scattering edges from other important chondritic elements (e.g. C, Mg, Si, S, Mg, Ni) may also be exploited to probe their local solid state environments in the matrices of IDPs.

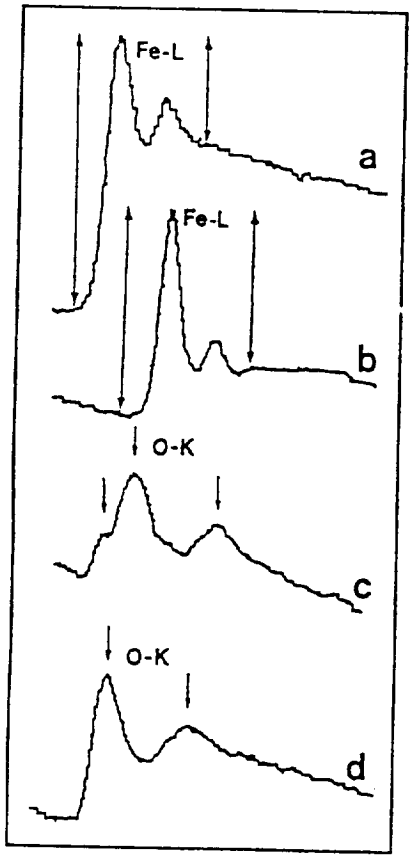

REFERENCES [1] M.S. Germani, J.P. Bradley, D.E. Brownlee, Earth Planet. Sci. Lett., 101, 162-179, 1990. [2] R.F. Egerton, Electron Energy Loss Spectroscopy in the Electron Microscope, Plenum, New York, 1986, 410 pp. [3] J. Tafto and J. Zhu, Ultramicroscopy, 9, 349-354, 1982. [4] J. Tafto and O.L. Krivanek, Phys. Rev. Lett., 48, 560-563, 1982.

FIGURE 1 Electron energy loss core scattering edges. (a) Fe-$L_{2,3}$ (≈708 eV) for Fe^{O} in kamacite [FeNi], (b) Fe-$L_{2,3}$ edge (≈708 eV) for Fe^{n+} in magnetite [$(Fe^{2+}Fe^{3+})_3O_4$], (c) O-K edge (≈532 eV) for oxygen in magnetite, (d) O-K edge (≈532 eV) for oxygen in enstatite ($MgSiO_3$).

Appendix II, Paper 5

COMBINED INFRARED AND ANALYTICAL ELECTRON MICROSCOPE STUDIES OF INTERPLANETARY DUST PARTICLES

J. P. Bradley, H. J. Humecki, and M. S. Germani

McCrone Associates, Westmont, Il 60559-1275, USA

The **Astrophysical Journal**, in press,

Publication date August 1, 1992

ABSTRACT

Silicate grains in thin sections of eight chondritic interplanetary dust particles (IDPs) were studied using analytical electron microscopy (AEM) and infrared (IR) microspectroscopy. Relative abundances of olivine, pyroxene, layer silicates, and glass were determined by collecting 200-700 quantitative point count analyses, each with (x-ray) spatial resolution <0.05 μm, from each thin section. Three of the IDPs are pyroxene-rich, two are olivine-rich, one is layer silicate-rich, and two are glass-rich. IR transmission spectra were obtained within the spectral range 2.5-16.0 μm (625-4000 cm^{-1}) from the thin sections. The 10 μm "silicate feature" of the pyroxene-rich IDPs (U222B42, W7027H14, U230A3) consists of two principal bands at 9.1 - 9.4 μm (1064-1099 cm^{-1}) and 10.5 - 10.75 μm (930 - 953 cm^{-1}). The bands are consistent with monoclinic clinopyroxene whose presence in the thin sections was confirmed using electron diffraction. The olivine-rich IDPs, U220A14 and U230A4, each produce an intense silicate band at 11.2-11.3 μm (885-893 cm^{-1}), with less intense bands at 10.1 and 10.75 μm (930, 991 cm^{-1}), while the layer silicate-rich IDP (U230A43) produces a ~~single~~ principal silicate band at ≈9.8 μm (1031 cm^{-1}). (An additional band at 6.8 μm (1471 cm^{-1}) indicates the presence of carbonates in U230A43). The glass-rich IDPs, W7027A11 and U219C11, produce broad silicate band structure between 8 and 12 μm, with a prominent peak at 11.3 μm. The 10 μm silicate features of the olivine, pyroxene, and layer silicate-rich IDPs are unlike those of comets, but those of W7027A11 and U219C11 are similar to comets Halley and Bradfield in terms of overall band width and shape, as well as the 11.3 μm "olivine" feature. The mineralogy and petrography of U219C11 and W7027A11

resemble those of comet grains analyzed by the PIA and PUMA instruments during the Halley encounters. Chondritic IDPs dominated by glass and submicrometer silicate crystals are strong candidates for the dust grains responsible for silicate IR emission from comets.

INTRODUCTION

The 10-micrometer infrared (IR) feature observed in astronomical spectra of comets (and other astrophysical objects) is believed to represent the Si-O stretching mode in silicate grains (Ney, 1977). The compositions, degree of crystallinity, and sizes of the grains responsible for this silicate emission have been the subjects of numerous investigations (Ney, 1974; Woolf, 1975; Stephens and Russel, 1979; Mukai and Koike, 1990). During the past decade laboratory IR studies of interplanetary dust particles (IDPs) have provided a new approach to studying the 10-μm silicate feature in astronomical spectra. IDPs are particles of cosmic dust that have survived atmospheric entry without melting (i.e. micrometeorites). Cosmic dust is a ubiquitous component of the inner solar system and, since comets and asteroids are known sources of dust, some IDPs are likely to be derived from comets (Whipple, 1982; Sykes et al., 1986; Sandford, 1986; Flynn, 1990).

IDPs are collected from the stratosphere (at 20-25 km altitude) using U-2 aircraft (Sandford, 1987). They are typically between 5 and 50 μm in diameter (Fig. 1), and their bulk compositions for the rock-forming elements are approximately chondritic (solar) (Schramm et al, 1989). Many contain prominent solar flare tracks (with densities $>10^{10}$ cm^{-2}), indicating exposure ages of $\approx 10^4$ years within the inner solar system, and confirming that they were not modified by pulse heating during atmospheric entry (Thiel et al., 1991; Sandford and Bradley, 1989). Chondritic IDPs include some of the most primitive materials available for laboratory investigation; one subset consists of unequilibrated aggregates of mineral grains, silicate glass, and carbonaceous material, in which chemical and crystallographic evidence of primordial grain-forming reactions have been observed (Fraundorf, 1981a; Bradley et al., 1983; Klöck et al., 1989). D/H isotopic

anomolies measured in some IDPs suggest the survival of presolar interstellar components (McKeegan et al., 1985).

Laboratory IR studies have established that most IDPs exhibit a dominant 10-μm "silicate feature" (Sandford and Walker, 1985). The shape of this feature has been used to classify chondritic IDPs. Three classes of chondritic particles are recognized, referred to as "olivine", "pyroxene", and "layer silicate", after the minerals that provide the best match for the observed 10-μm silicate feature (Sandford and Walker, 1985). Electron microscopic studies have confirmed that olivine, pyroxene, and layer silicates are major constituents of IDPs belonging to the respective IR classes (Tomeoka and Buseck, 1984; Christoffersen and Buseck, 1986). Although no specific IR class of IDPs provides a match for either a cometary (or interstellar) 10-μm silicate feature, a reasonable comet match can be obtained simply by combining spectra from each of the the three classes (Sandford and Walker, 1985).

Since these earlier IR studies, new data have been collected from both comets and IDPs. Detailed chemical, physical, and mineralogical data from a large number of stratospheric IDPs are now available. These data support the thesis that IDPs are derived from diverse parent body environments, with the "layer silicate" class most likely from asteroids, the "olivine" class from comets, and the "pyroxene" class derived from either comets or asteroids (Tomeoka and Buseck, 1985; Sandford and Bradley, 1989; Bradley and Brownlee, 1991; Keller et al., 1992). High quality IR data (collected using ground-based and airborne telescopes) are now available for several comets (Campins and Ryan, 1989; Hanner et al., 1990; Bregman et al., 1987). The Giotto and Vega spacecraft missions to comet Halley provided the first in-situ IR measurements and compositional analyses of comet grains at their source (Kissel et al., 1986; Jessberger et

al., 1988). Finally, it is now possible to obtain both AEM and IR data from thin (<100nm thick) sections of IDPs (Bradley et al., 1991). In light of these developments, it is appropriate to further explore the relationship between comets and IDPs.

In this paper, we apply analytical electron microscopy (AEM) and IR microspectroscopy to study ultramicrotomed thin sections (<100 nm thick) of eight IDPs. The purpose of this study is to identify IDPs, or specific components of IDPs, with IR spectral transmission characteristics at 10 μm similar to those of comets. The mineralogy and petrography of these IDPs may then provide insight into the nature of comet dust. The thin sections studied include IDPs from each of the three IR classes as well as silicate mineral standards. Silicate spectral transmission between 8 and 12 μm from each thin section is evaluated in terms of silicate mineralogy (as determined from AEM studies) and then compared with IR data from comets Halley and Bradfield. Most of the IDPs do not provide a good match to comets, in accordance with earlier findings of Sandford and Walker (1985). However, two IDPs provide a match to comets in terms of overall band width and shape between 8 and 12 μm, and the presence of a prominent 11.3 μm peak. In addition, these IDPs appear to be mineralogically and petrographically similar to dust grains analyzed by the PIA and PUMA instruments during the comet Halley encounters. This study suggests that chondritic materials dominated by glass and submicrometer silicate crystals are the best analogs for silicate grains in comets.

EXPERIMENTAL PROCEDURES

Individual (10-30 μm diameter) IDPs and selected mineral grains were embedded in epoxy and thin-sectioned using an ultramicrotome equipped with a diamond knife. Details of the thin sectioning precedure are described elswhere (Bradley, 1989). The

sections < 100 nm thick (Fig. 2) were mounted on thin (<20 nm thick) carbon films supported on 3mm slotted copper TEM grids. Sections were also mounted on polished KBr and diamond plates so that the influence of epoxy, carbon films, and TEM grids on IR spectral features could be evaluated. The sections on diamond were oxygen plasma ashed to remove the epoxy (and carbonaceous phases indigenous to the IDPs).

The IR spectrophotometer is an IRμS (Spectra-Tech), equipped with a thermal emission source and 15X and 32X objectives (numerical aperture 0.58 & 0.65) for operation in the range 4000 - 625 cm^{-1} (2.5 - 16 μm). Spectral resolution was determined to be 8 cm^{-1}. The TEM grids were positioned over a 2mm diameter hole in an aluminum plate mounted on the specimen stage of the spectrophotometer. Adjustable slits in the beam path are used to select the analysis region. Spectra were acquired by co-addition of successive interferograms until an acceptable signal-to-noise level was achieved within a reasonable collection time (typically 4000 within ≈30 minutes). An open area (with no sample and no carbon substrate) served as a reference. Background spectra were collected from a region (of epoxy plus carbon substrate) alongside the section of the IDP. A final baseline corrected (and smoothed) spectrum was obtained by subtracting the background from the sample spectrum.

IR spectra were collected from mineral standards and chondritic IDPs. The standards included two enstatite ($MgSiO_3$) polymorphs, orthorhombic orthoenstatite and monoclinic clinoenstatite, forsteritic olivine (Mg_2SiO_4), and a layer silicate (smectite) (Fig. 3). These minerals are responsible for the 10-μm feature in IDP spectra (Sandford and Walker, 1985) and some or all of them contribute to the same feature in comet spectra [Stephens and Russel, 1979; Campins and Ryan, 1989; Hanner et al., 1990]. IR spectra

were also collected from thin sections of each of the three IR classes of chondritic IDPs (Figs. 4-6).

The compositions and abundances of silicates in the IDP sections were determined using an automated 200 keV analytical electron microscope (AEM) equipped with digital beam control and a solid state energy-dispersive x-ray spectrometer. Several hundred quantitative x-ray point count analyses (for Mg, Al, Si, S, Ca, Cr, Mn, Fe, and Ni) were acquired on a two dimensional grid from each section. The spatial resolution of each data point is estimated to be better than 50 nm [Bradley et al. 1989, Germani et al. 1990]. The resulting data sets are plotted on Mg-Si-Fe ternary plots because these elements are major constituents of chondritic IDPs and the distribution of data points reflects the relative abundances of the pyroxene, olivine, layer silicates, and glass in thin sections (Figs. 4-7).

At least two sources of sources of error can result from IR microspectroscopy of thin sections on TEM grids. The first is spectral interference due to diffraction effects, which arise when attempting to collect IR data from areas with dimensions of the order of the wavelength of the incident radiation (McMillian and Hofmeister 1988). The second is the background subtraction step, which is a software based manual procedure. Accurate background subtraction is critical because spectral transmission through sections <100 nm thick is on the order of 95-98 %. Carbon substrates and epoxy contribute strongly to the background band structure between 2.0 and 8.5 μm but do not contribute significantly within the spectral range of the 10-μm silicate feature.

The influence of diffraction effects, background subtraction, and other interferences can be assessed by evaluating the shape of the 10-μm silicate feature in terms of the relative abundances of silicates derived from automated AEM analyses. For example,

the silicate feature for U220A14 in Figure 5A suggests that the thin section contains abundant olivine and significantly less pyroxene. Multi-element cluster analysis was performed on the compositional data set shown in Figure 5B using procedures described by Bradley et al. (1989 and Germani et al. (1990). Out of the total 706 data points, 367 were assigned to olivine ($[Mg_{1.26}Fe_{0.74}]SiO_4$) and 160 to pyroxene ($[Mg_{0.67}Fe_{0.33}]SiO_4$), i.e. olivine/pyroxene volume ratio ≈2.3. Figure 5A indicates that there is qualitative if not semi-quantitative aggreement on the relative abundances of olivine and pyroxene determined by IR and AEM measurements.

RESULTS

Figure 3 shows IR spectra (between 7.5 and 13.5 μm) obtained from crystalline mineral standards: A, B, and C were collected from ultramicrotomed sections (<100 nm thick) on TEM grids, and spectra D and E were collected from crushed micrometer-sized fragments mounted on KBr discs. The 10-μm silicate feature of (orthorhombic) orthoenstatite exhibits a single intense band at 9.78 μm (1022 cm^{-1}) with shoulder structures at 9.35 and 10.25 (1584,976 cm^{-1}); weaker bands occur at 8.00 and 11.41 μm (1250, 876 cm^{-1}) (Fig. 2a). Monoclinic clinoenstatite exhibits bands at 9.35, 9.83, 10.62, 11.05, and 11.57 μm (1070, 1018, 942, 905, 864 cm^{-1}) (Fig. 2b). Forsteritic olivine (Mg_2SiO_4) exhibits prominent bands at 11.20 μm (893 cm^{-1}) and at 10.1 μm (990 cm^{-1}) (Fig. 2c). Weaker bands occur at 10.50, 11.81, and 12.42 μm (962, 847, 806 cm^{-1}). (In olivines, the intensity of the 10.1 μm band decreases relative to that of the 11.2 μm band with increasing Fe content (Mukai and Koike, 1989)). Smectites typically exhibit a narrow, relatively structureless silicate feature which peaks at ≈ 9.8 μm (1020 cm^{-1}) (Fig. 2e). The spectra in Figure 2 are comparable with published IR data for these silicates

(Bilton et al., 1972; van der Marel and Beutelspacher, 1976; Sandford and Walker, 1985; Hofmeister, 1987; Madon and Price, 1989; Mukai and Koike, 1990), thereby confirming that useful IR data can be obtained from thin (< 100nm) sections on TEM grids.

Figures 4 through 6 show IR and AEM data collected from "pyroxene", "olivine", and "layer silicate" classes of chondritic IDPs. Data from three pyroxene-rich IDPs U222B42, W7027H14, and U230A3 are presented in Figure 4. The 10-μm silicate feature in each of the IR spectra (Fig. 4 A-C) exhibit prominent bands at 9.1-9.4 μm (1064-1099 cm^{-1}) and 10.4-10.75 μm (930-952 cm^{-1}). The intensity ratio of the two bands varies from one IDP to another. The 9.1-9.4 μm band for W7027H14 and U230A3 exhibits a pronounced doublet structure (Figs. 4 B & C). Weaker bands are present (in some cases) at 8.4-8.6 μm (1163-1176 cm^{-1}) and 11.2-11.4 μm (877-893 cm^{-1}). (Significant variations in band structure were observed among the "pyroxene" IDPs studied by Sandford and Walker, 1985). Comparison of Figures 3A, 3B, and 4(A-C) suggests that monoclinic clinoenstatite is the most likely polymorph. The Mg-Si-Fe ternary plots in Figure 4 D-F show that enstatite ($MgSiO_3$) is the dominant silicate in all three IDPs, and electron diffraction analyses confirmed that clinoenstatite is the dominant polymorph. Studies of other "pyroxene" IDPs have shown that clinoenstatite is the most common polymorph in chondritic IDPs (Fraundorf, 1981b; Bradley et al. 1983).

AEM and IR data for the "olivine" and "layer silicate" IDPs are presented in Figures 5 and 6. The "olivine" IDPs are U220A14 and U230A3 (Fig. 5). The major silicate phases in U220A14 are olivine ($[Mg_{1.26}Fe_{0.74}]SiO_4$) and pyroxene ($[Mg_{0.63}Fe_{0.37}]SiO_3$). Silicate glass is present as a minor component. Olivine is 2.3 times more abundant than pyroxene and the 10-μm silicate feature in Figure 5A reflects these relative abundances. U230A4 contains olivines whose compositions range from Mg_2SiO_4 to

$[Mg_{1.45}Fe_{0.55}]SiO_4$. The silicate feature for U230A4 (Fig. 5C) is similar to those of Fe-bearing olivines (see Mukai and Koike, 1990).

Data for the "layer silicate" IDP U230A43 are presented in Figure 6. Most layer silicates (e.g. serpentine, smectite, micas) exhibit a 10-μm feature with an absorption maximum at $\approx$9.8 μm (1020 cm^{-1}), although the band width is typically narrower than that of U230A43 (cf Figs. 3D & 6A). In addition to the silicate feature, this IDP exhibits a prominent band at 6.8 μm corresponding to the asymmetric stretching vibration of carbonates (Sandford and Walker, 1985). AEM data indicate that U230A43 contains Mg-rich smectites, Mg-Fe carbonates, and Fe-rich sulfides. The distribution of data points in Figure 6B reflects the mixing of these three major phases.

Figure 7 shows IR and AEM data from thin sections of two glass-rich IDPs W7027F11 and U219C11. Both of these IDPs were originally highly porous, fragile objects (e.g. Fig. 1) consisting almost exclusively of a loosely aggregated matrix of carbonaceous material, glass, and submicrometer crystals (Fig. 2). Similar matrix material is found in "pyroxene" IDPs (Fig. 8), where it is typically mixed with much larger (up to 5 μm) silicate and sulfide grains. The IR spectrum for W7027A11 (Fig. 7A) was obtained from a thin section that contains abundant glass and small (<100 nm) crystals. A significant number of larger (0.1-1.0 μm) olivine crystals are also present, and these crystals are responsible for the prominent band at 11.3 μm. The spectrum for U219C11 (Fig. 7B) was obtained from the thin section labelled A in Figure 2. Brightfield and darkfield images show that this section consists almost exclusively of glass and small crystals (< 100nm in diameter). No silicate grains >150 nm were observed. The silicate features from both IDPs exhibit broad band widths and rounded profiles similar to those of silicate glasses (cf. Figs. 7A,

7B, and 9). In Figures 7C and 7D, the wide distribution of data points and lack of pronounced clustering result from the abundance of glass and small mineral grains (<100 nm).

Iron-magnesium-silicon distributions for an olivine-rich, a pyroxene-rich, and a glass-rich IDP are shown in Figure 10(A-C). The data are presented in terms of Fe/Si versus Mg/Si so they can be compared with compositional data from comet Halley dust grains (Fig. 10D) (from Lawler et al., 1989). This direct comparison is valid because the volume of material analyzed for each of the IDP data points (in Fig. 10 A-C) is similar to the volumes of the comet grains analyzed in Figure 10D (Brownlee et al., 1987; Lawler et al., 1989). In Figure 10A, the data points for the olivine-rich IDP are tightly clustered because the average grain size in the analyzed thin section is large (relative to the volume of material analyzed at each data point). The pyroxene-rich IDP (Fig. 10B) also contains large grains but, since fine grained material and glass are also present, many data points are well dispersed. The glass-rich IDP (Fig. 10C) is dominated by fine grained material and glass, producing a wide dispersion of data points. Comet Halley's grains exhibit a dispersion similar to that of the glass-rich IDPs U219C11 and W7027A11 (cf, Fig. 10 C & D).

DISCUSSION

The shape of the 10-μm silicate feature obtained from thin sections of IDPs correlates well with the relative abundances of pyroxenes, olivine, and silicate glass measured using an automated AEM. Assuming this feature can be directly compared to the 10-μm feature in astronomical spectra, it should be possible to evaluate silicate emission from

comets in terms of the mineralogy of IDP thin sections. This comparison is valid only if the (silicate) grains responsible for the cometary emission are less than ≈5 μm in diameter (Hanner et al., 1987; Swamy et al., 1988; Mukai and Koike, 1990). (For grains > 5 μm the strength of the silicate emission at 10 μm decreases with increasing grain size). Comets Bradfield and Halley exhibit a distinctive twin-peaked structure (Fig. 11), which has been interpreted as evidence for a predominance of submicrometer grains (Bregman et al., 1987; Mukai and Koike, 1990). Grain sizes between 0.1 and 1.0 μm were indicated by instruments on board the Giotto and Vega spacecraft during the Halley encounters (Kissel and Kreuger, 1987; McDonnell et al., 1987; Simpson et al., 1987).

Most of the eight IDPs studied here do not exhibit a comet-like silicate feature (cf, Figs.4-6, 11), in accordance with earlier findings of Sandford and Walker (1985). The IDPs exhibit narrow and complex band structure between 8 and 12 μm, which is related to silicate mineralogy, degree of crystallinity, and grain size. Comets, on the other hand, exhibit relatively broad band structure between 8 and 12 μm, suggesting the presence of significant components of ultra fine-grained crystals and silicate glass (cf, Figs. 7, 9, and 11). The peaks at ≈11.3 μm for comets Halley and Bradfield (Fig. 11A) are believed to be due to olivine crystals (Bregman et al, 1987; Campins and Ryan, 1989; Combes et al. 1988; Hanner et al., 1990). Most (olivine-rich) "olivine" IDPs are aggregates of 0.1-1.0 μm grains (Christoffersen and Buseck, 1986; Rietmeijer, 1989; Bradley et al., 1989), but comparison of Figures 5 and 11 suggests that they are too coarse grained and contain too little glass to be cometary. "Pyroxene" IDP's contain minor olivine but, since they typically contain large (0.5-5.0 μm) silicate grains, they also exhibit a 10-μm silicate feature incompatible with comets (Figs. 4 and 11). "Layer silicate" IDPs are dominated

by poorly crystallised layer silicates but olivine is usually rare or absent (Rietmeijer and MacKinnon, 1985; Germani et al., 1991; Zolensky and Lindstrom, 1991; Keller et al., 1992). They exhibit a relatively sharp, narrow 10-μm feature typical of layer lattice silicates but unlike those of comets (Figs. 6 & 11) (see also Sandford and Walker, 1985). Only IDPs U219C11 and W7027A11 that are dominated by glass and submicrometer crystals provide a reasonable match to comets. Specifically, the overall band width and lack of complex band structure between 8 and 12 μm, together with the presence of a distinct 11.3 μm feature, are common to IDPs U219C11, W7027A11, and comets Halley and Bradfield (Fig. 11).

Data from the PIA and PUMA instruments on board the Giotto and Vega spacecraft suggest a compositional/ mineralogical link between comet (Halley) and IDPs like U219C11, W7027A11, and "pyroxene" IDPs (Fig. 10). These same data suggest incompatibility with both olivine-rich and layer silicate-rich IDPs. The PIA and PUMA time-of-flight mass spectrometers on board the spacecraft provided the first in situ analyses of comet grains at their source. However, data interpretation has been hampered by a lack of calibration for (impact ionization induced) ion yields, non linear instrument performance, and constraints on telemetry (Jessberger et al., 1988; Lawler et al., 1989). Out of a total of ≈10,000 spectra ≈500 have been determined to be of sufficient quality for compositional/mineralogical evaluation of Halley particles (Brownlee et al., 1987; Jessberger et al., 1988; Lawler et al., 1989). The following conclusions have been drawn from analyses of these spectra. 1) The bulk composition (for the forming elements) of Halley grains is approximately chondritic. 2) Few if any of the detected (0.1 to 1.0 μm) particles were single mineral grains. 3) Most of the particles are composed either of aggregates of even smaller mineral grains or they contain abundant glass. 4)

Most of the Mg is contained in silicates, as suggested by a relatively uniform Mg/Si atom ratio, while Fe is contained in a range of mineral phases (e.g. metal, oxides, sulfides, and silicates) as indicated by a wide range in the Fe/Si atom ratio (Fig. 11 D).

The mineralogical and petrographic properties of Halley grains listed above are also common to IDPs U219C11, W7027A11, and the glass-rich matrices of "pyroxene" IDPs. Each of these materials exhibit bulk compositions that are approximately chondritic. Single mineral grains > 0.1 μm diameter are uncommon and loosely agglomerated aggregates of glass and crystals between 0.1 and 1.0 μm in diameter are dominant (Fig. 9). Mg-silicates, (principally enstatite ($MgSiO_3$), Mg-silicate glass, and Mg-rich olivine) are common, Fe is present in metal (kamacite), oxides (magnetite), and sulfides.

Particles like U219C11 and W7027A11 composed almost exclusively of aggregates of submicrometer crystals and glass are rare among the collected IDPs. Such particles may be related to pyroxene-rich IDPs, because pyroxene-rich IDPs also contain aggregates of submicrometer crystals and glass. Glass-rich IDPs like W7027A11 and U219C11 are likely to be more fragile than pyroxene-rich IDPs since, unlike pyroxene-rich IDPs, they are not "held together" by larger (0.5-5.0 μm diameter) mineral grains. U219C11 was selected from a "spray" of fragments of a larger ($\approx$50 μm) particle that had disintegrated when it impacted onto the collection substrate. Pyroxene-rich IDPs may belong to a broader class of materials, which includes U219C11 and W7027A11, but they may be disproportionately represented among the collected IDPs because they were strong enough to survive ejection from their parent body and deceleration in the atmosphere. Measurements of the dust coma of comet Halley suggest that large conglomerates of particles spontaneously disintegrate into smaller particles as they travel outwards from

the nucleus (Simpson et al., 1987). On the other hand, U219C11 and W7027A11 may belong to a hitherto unknown class (or classes) of glass-rich chondritic IDPs. Clearly, the relationship between glass-rich and pyroxene-rich IDPs requires further investigation.

This study has identified IDPs with silicate emission characteristics between 8 and 12 μm that are similar to those of comets Halley and Bradfield. Implanted solar flare tracks and sputtered rims resulting from solar wind damage suggest that the mineralogy and petrography of these IDPs have not been significantly perturbed since ejection from their parent bodies (Bradley and Brownlee, 1986; Thiel et al., 1991). Because the IDPs contain glass and submicrometer silicate grains, phases that are predisposed to aqueous alteration, we conclude that they were derived either from an anhydrous parent body or from a hydrous parent body where conditions suitable for aqueous alteration do not prevail. Comets are the logical parent bodies, but so too are asteroids at heliocentric distances beyond the main belt where temperatures have not exceeded the water-ice solidus (Herbert, 1989; Vilas and Gaffey, 1989). Calculations of IDP orbital dynamics suggest that unmelted (track-rich) IDPs collected at 1 AU are most likely from asteroids (Flynn, 1989), although for some asteroids distinction between a cometary versus asteroidal source may be simply one of orbital parameter (Rietmeijer, 1991). In the absence of unambiguous source attribution, the IDPs studied here provide insight into the nature of the materials responsible for silicate emission from comets. Future IR/AEM studies of IDPs and fine-grained components of conventional meteorites may facilitate identification of cometary and interstellar materials.

REFERENCES

Bilton, M. S., Gilson, T. R., and Webster, M. 1972, *Spectrochim. Acta*, **28A**, 2113.

Bradley, J. P. 1989, *Geochim. Cosmochim. Acta*, **52**, 889.

Bradley, J.P., Brownlee, D.E., and Veblen, D.R. 1983, *Nature*, **301**, 473.

Bradley, J. P. and Brownlee, D. E. 1986, *Science*, **231**, 1542.

Bradley, J. P. and Brownlee, D. E. 1991, *Science*, **251**, 549.

Bradley, J.P., Germani, M.S., and Brownlee, D.E. 1989, *Earth Planet Sci. Lett.*, **93**, 1.

Bradley, J.P., Humecki, H., and Germani, M.S. 1991, *Lunar Planet. Sci.*, **XXII**, 131.

Bregman, J.D., Campins, H., Witteborn, F.C., Woods, D.H., Rank, D.M., Allamandola, L.J., Cohen, M., and Tielens, A.G.G.M. 1987, *Astron. Astrophys.*, **187**, 616-620.

Brownlee, D. E., Wheelock, M. M., Temple, S., Bradley, J. P. and Kissel, J. 1987, *Lunar Planet. Sci.*, **XVIII**, 133.

Campins, H. and Ryan, E. V. 1989, *Astrophys. J.*, **341**, 1059.

Christoffersen, R., and Buseck, P.R. 1986, *Earth Planet. Sci. Lett.*, **78**, 53.

Combes, M., Moroz, V. I., Crovisier, J., Encrenaz, T., Bibring, J.-P., Grigoriev, A. V., Sanko, N. F., Coron, N., Crifo, J. F., Gispert, R., Bockelee-Morvan, D., Nikolsky, Yu. V., Krasnopolsky, V. A., Owen, T., Emerich, C., Lamarre, J. M., and Rocard, F. 1988, *Icarus*, **76**, 404.

Flynn, G. J. 1989, *Icarus*, **77**, 287.

Flynn, G. J. 1990, in *Proc. 20th Lunar Planet Sci. Conf.* (Lunar and Planetary Institute, Houston) p363.

Fraundorf, P. 1981a, *Geochim. Cosmochim. Acta.*, **45**, 915.

Fraundorf, P. 1981b, *Lunar Planet. Sci.*, **12**, 292.

Germani, M.S. Bradley, J.P., Brownlee, D.E., 1990, *Earth Planet Sci. Lett.*, **101**, 162.

Hanner M.S., Tokunaga A.T., Golisch, W.F., Griep, D.M. and Kaminski C.D. 1987, *Astron. Astrophys.*, 187, 653.

Hanner, M.S. Newburn, R.L., Gehrz, R.D., Harrison, T. and Ney, E.P. 1990, *Astrophys. J.*, **348**, 312.

Herbert, F. 1989, *Icarus*, **78**, 402.

Hofmeister, A.M. 1987, *Phys. Chem. Minerals*, **14**, 499.

Keller, L. P., Thomas, K. L. and McKay, D. S. 1992, *Geochim. Cosmochim. Acta*, in press.

Kissel, J. and Kreuger, F. R. 1987, *Nature*, **326**, 755.

Kissel, J., Brownlee, D.E., Büchler, K., Clark, B.C., Fechtig, H., Grun, E., Hornung, K., Igenbergs, E.B., Jessberger, E.K., Krueger, F.R., Kuczera, H., McDonnell, J. A. M., Morfill, G. M., Rahe, J., Schwehm, G. H., Sekanina, Z., Utterback, N. G., Volk, H. J., and Zook, H. A. 1986, *Nature*, **321**, 336.

Klöck, W., Thomas, K.L., McKay, D.S. and Palme, H. 1989, *Nature*, **339**, 126.

Jessberger E.K., Christoforidis, A., and Kissel, J. 1988, *Nature*, **332**, 691.

Lawler, M. E., Brownlee, D. E. and Wheelock, M. M. 1989, *Icarus*, **80**, 225.

Madon, M. and Price, G.D. 1989, *J. Geophys. Res.*, **94(B11)**, 15,687.

McDonnell, J. A. M., Alexander, W. M., Burton, W. M., Bussoletti, E., Evans, G. C., Evans, S. T., Firth, J. G., Grard, R. J. L., Green, S. F., Grun, E., Hanner, M. S., Hughes, D. W., Igenbergs, E., Kissel, J., Kuczera, H.,Lindblad, B. A., Langevin, Y., Mandeville, J.-C., Nappo, S., Pankiewicz, G. S. A., Perry, C. H., Schwehm, G. H., Sekanina, Z., Stevenson, T. J., Turner, R. F., Weishaupt, U., Wallis, M. K. and Zarnecki, J. C. 1987, *Astron. Astrophys.*, **187**, 719.

McKeegan, K.D., Walker, R.M., and Zinner, E. 1985, *Geochim Cosmochim. Acta.*, **49**, 1971.

McMillan, P.F. and Hofmeister, A.M., 1988, in *Reviews in Mineralogy, Vol. 18, Spectroscopic Methods in Mineralogy and Geology*, ed. P.H. Ribbe (Mineralogical Society of America, Washington, DC) p. 99.

Mukai, T. and Koike, C. 1990, *Icarus*, **87**, 180.

Ney, E. P. 1974, *Icarus*, **23**, 551.

Ney, E. P. 1977, *Science*, **195**, 541.

Rietmiejer, F. J. M. 1989, *Proc. Lunar Planet. Sci. Conf.*, **19**, 513.

Rietmeijer, F. J. M. 1991, *Earth Planet. Sci. Lett.*, **102**, 148.

Rietmeijer, F. J. M. and MacKinnon, I. D. R. 1985, *J. Geophys. Res.*, **90**, D149.

Sandford, S. A. 1986, *Icarus*, **68**, 377.

Sandford, S. A. 1987, *Fund. Cosmic Phys.*, **12**, 1.

Sandford, S.A. and Bradley, J.P. 1989, *Icarus*, **82**, 146.

Sandford, S. A. and Walker, R. M. 1985, *Astrophys. J.*, **291**, 838.

Schramm, L.S., Brownlee, D.G., and Wheelock, M.M., 1989, *Meteoritics*, 24, 99.

Simpson, J. A., Rabinowitz, D., Tuzzolino, A. J., Ksanfomality, L. V. and Sagdeev, R. Z. 1987, *Astron. Astrophys.*, **187**, 742.

Stephens, J. R. and Russel R. W. 1979, *Astrophys. J.*, **228**, 780.

Swamy, K.K.S., Sandford, S.A., Allamandola, L.J., Witteburn, F.C., and Bregman, J.D., 1988, *Icarus*, **75**, 351.

Sykes, M. V., Lebovsky, L. A., Hunten, D. M. and Low, F. 1986, *Science*, **232**, 1115.

Thiel, K., Bradley, J. P. and Sphor, R. 1991, *Nucl. Tracks Radiat. Meas.*, **19**, 709.

Tomeoka, K. and Buseck, P. R., 1984, *Earth Planet. Sci. Lett.*, **69**, 243.

Tomeoka, K. and Buseck, P. R., 1985, *Nature*, **314**, 338.

Van der Marel, H. W. and Beutelspacher, *Atlas of Infared Spectroscopy of Clay Minerals and Their Admixtures* (Elsevier, New York, 1976) pp 396.

Vilas, F. and Gaffey, M. J. 1989, *Science*, **246**, 790.

Whipple, F. L. 1982, in *Cosmic Dust*, ed. J. A. M. McDonnell (Wiley, New York) p 1.

Woolf, N. J. 1975, in *The Dusty Universe*, ed. G. B. Field and A. G. W. Cameron (New York: Neale), p. 59.

Zolensky, M.E. and Lindstrom, D.J. 1991, *Proc. Lunar Planet Sci. Conf. 22*, in press.

ACKNOWLEDGMENT

This research was funded by NASA Contract NAS-9-17749 and McCrone Associates. We thank H. Bales, A Teetsov for assistance with particle manipulation and ultramicrotomy.

FIGURE CAPTIONS

Figure 1. Scanning electron micrograph of glass-rich chondritic IDP W7027A11. Note the high porosity and fragile, aggregated microstucture of this particle.

Figure 2. Brightfield electron micrograph of an ultramicrotomed thin section of three fragments (labelled A, B, & C) of a glass-rich chondritic IDP U219C11 (section thickness 50 - 80 nm). An inclusion of silicate glass is arrowed in A, and silicate glass (containing predominantly <100 nm diameter) Fe sulfide crystals is arrowed in C.

Figure 3. Infrared (IR) spectra showing the 10-μm "silicate features" of A) orthoenstatite ($MgSiO_3$), B) clinoenstatite ($MgSiO_3$), C) forsteritic olivine (Mg_2SiO_4), D) layer lattice silicate (smectite). The positions of the strongest bands are indicated in wavenumbers. (Vertical scale - transmittance).

Figure 4. (**A - C**) Infrared (IR) spectra from thin sections of IDPs U222B42, W7027H14, and U230A3 (vertical scale - transmittance). (**D - F**) Corresponding Mg-Si-Fe ternary plots (atom %) of quantitative x-ray point count analyses, D (U222B42) - 232 points, E (W7027H14) - 332 points, F (U230A3) - 323 points. "PY" and "OL" denote compositional tie lines for pyroxene ($MgSiO_3$ - $FeSiO_3$) and olivine (Mg_2SiO_4 - Fe_2SiO_4) respectively. Clustering of data points about an Mg-rich pyroxene (enstatite) composition indicates that all three IDPs are pyroxene-rich.

Figure 5. **(A - B)** Infrared (IR) spectra from thin sections of IDPs U220A14 and U230A4 (vertical scale - transmittance). "Cpx" and "ol" in A indicate clinopyroxene and olivine absorption bands (see also Figs. 3b, 3c, and 7). **(C - D)** Corresponding Mg-Si-Fe ternary plots (atom %) of quantitative x-ray point count analyses, C (U220A14) - 706 points, D (U230A4) - 266 points. "PY" and "Ol" denote compositional tie lines for pyroxene ($MgSiO_3$ - $FeSiO_3$) and olivine (Mg_2SiO_4 - Fe_2SiO_4) respectively. The concentrations of data points on the olivine tie line indicate that olivine is the dominant silicate in both IDPs.

Figure 6. **A** Infrared (IR) spectrum of the layer silicate (smectite) rich IDP U230A43 (vertical scale - transmittance). The strongest band (peaked at ≈9.8 μm) is the silicate feature and the ≈6.8 μm band corresponds to the carbonate asymmetric stretching vibration (see Fig. 6b). Corresponding Mg-Si-Fe ternary plot (atom %) - 458 points. The distribution of data points reflects the mixing of the three major components of this thin section, Mg-rich smectite (solid boxed area), Mg-Fe carbonates (dotted area), and Fe sulfides (dashed area).

Figure 7. **(A - B)** Infrared (IR) spectra from thin sections of the glass-rich chondritic IDPs W7027A11 and U219C11 (vertical scale - transmittance). **(C - D)** Corresponding Mg-Si-Fe ternary plots of quantitative x-ray point count analyses, C (W7027A11) - 497 points, D (U219C11) - 556 points.

Figure 8. (A) Brightfield and (B) corresponding darkfield images of ultra fine-grained, chondritic matrix of a pyroxene-rich IDP (U220A19). This matrix is dominated by mineral grains <100 nm in a glass matrix.

Figure 9. Emissivities of silicate glasses with enstatite and olivine compositions (data from Stephens and Russel, 1979).

Figure 10. Iron-magnesium-silicon distributions in (A) olivine-rich IDP U220A14, (B) pyroxene-rich IDP U222B42, (C) glass-rich IDP W7027A11, (D) comet Halley's dust. A, B, and C each contain 290 data points. The Halley data (D), derived from 433 selected PUMA-1 compressed spectra, have been corrected to peak at chondritic (solar) abundances (Mg/Si=1.08 and Fe/Si=0.90) (from Lawler et al., 1989).

Figure 11 Comparison of the silicate emission characteristics of comets and glass-rich IDPs. (A) Comet Bradfield (1987s) divided by the continuum and normalized at 12.81 μm (from Hanner et al., 1990). Comet Halley (Dec. 1985) divided by a 320K blackbody continuum and normalized at 6.0 μm (from Bregman et al., 1987). (B) IDPs U219C11 and W7027A11.

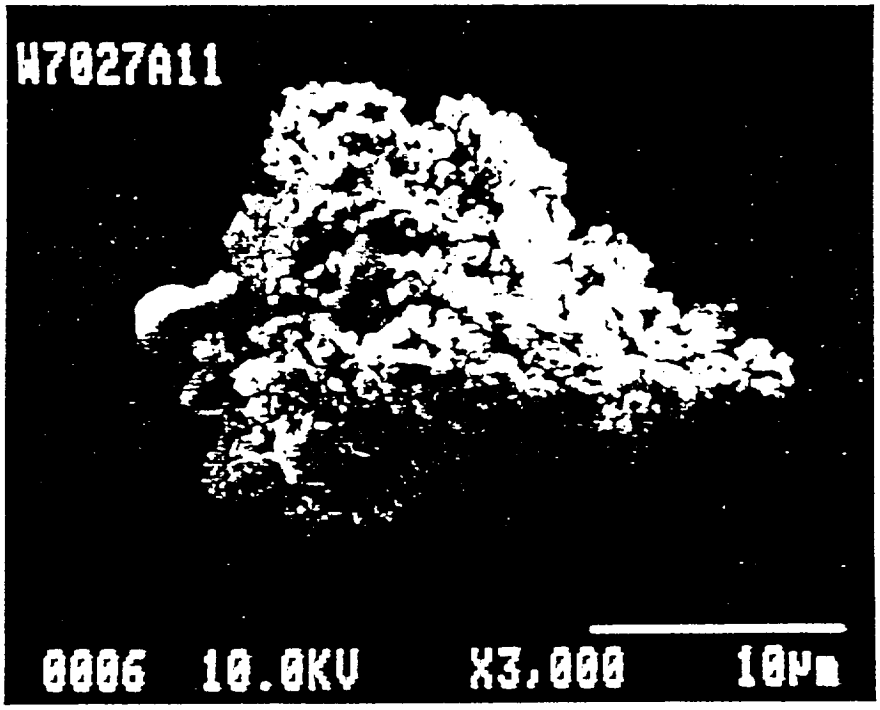

1

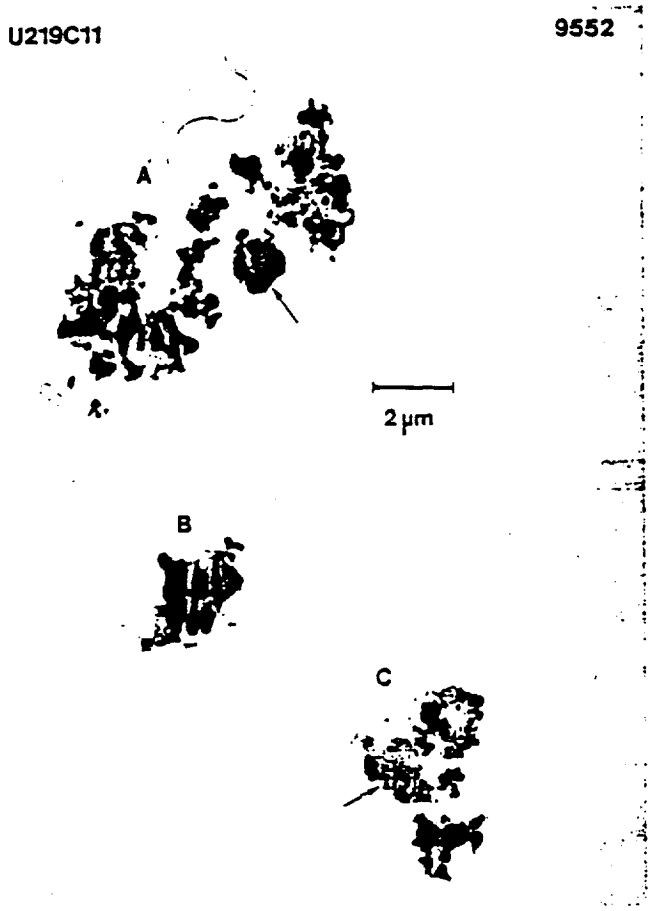
U219C11
9552
A
2 µm
B
C

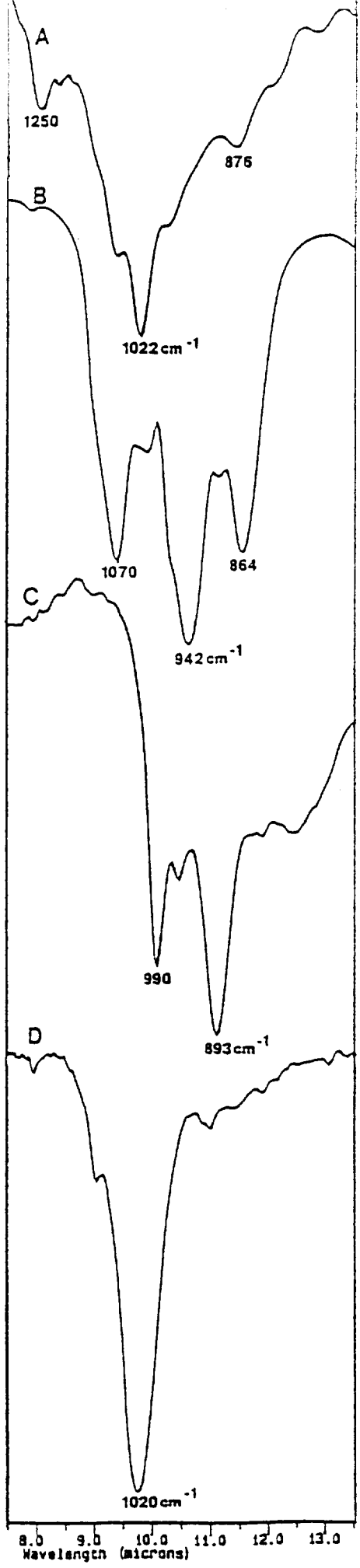
A
1250
876
B
1022cm -1
1070
864
C
942cm -1
990
893cm -1
D
1020cm -1
8.0
9.0
10.0
11.0
12.0
13.0
Wavelength (microns)

3.

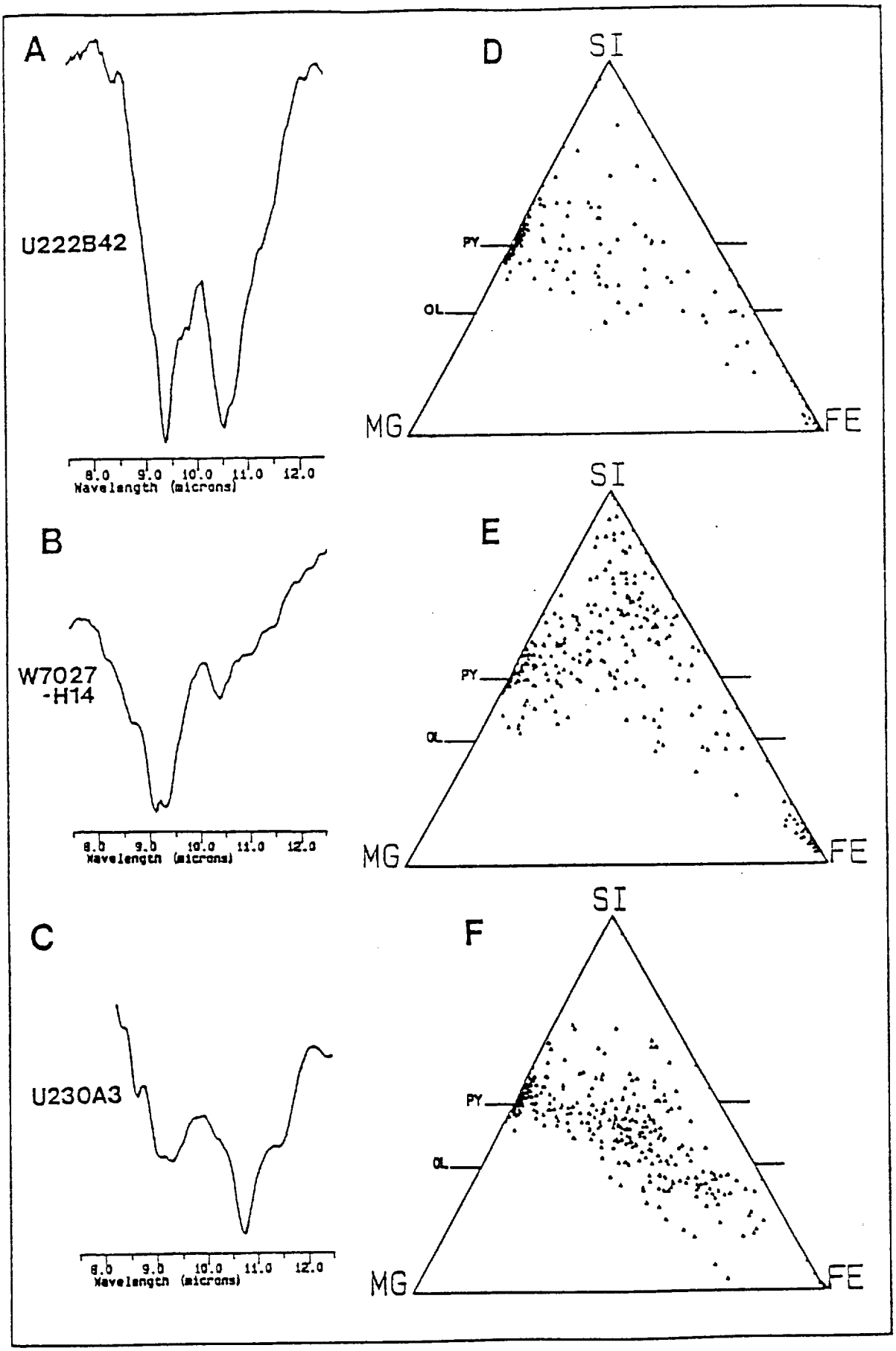
A
U222B42
8.0 9.0 10.0 11.0 12.0
Wavelength (microns)
B
W7027
-H14
8.0 9.0 10.0 11.0 12.0
Wavelength (microns)
C
U230A3
8.0 9.0 10.0 11.0 12.0
Wavelength (microns)
D
SI
PY
OL
MG
FE
E
SI
PY
OL
MG
FE
F
SI
PY
OL
MG
FE

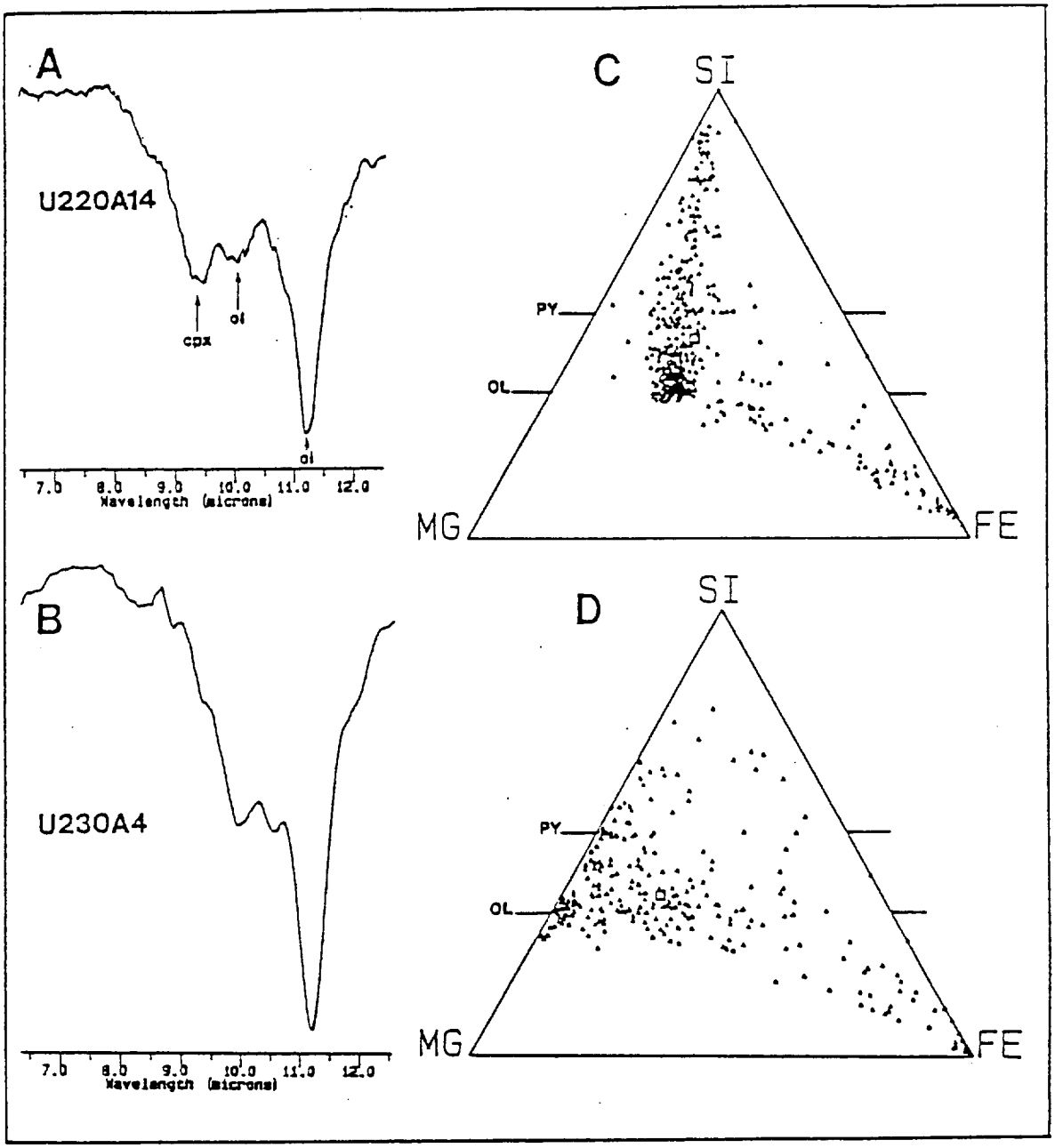
A
U220A14
cpx
ol
ol
7.0
8.0
9.0
10.0
11.0
12.0
Wavelength (microns)
B
U230A4
7.0
8.0
9.0
10.0
11.0
12.0
Wavelength (microns)
C
SI
PY
OL
MG
FE
D
SI
PY
OL
MG
FE

5.

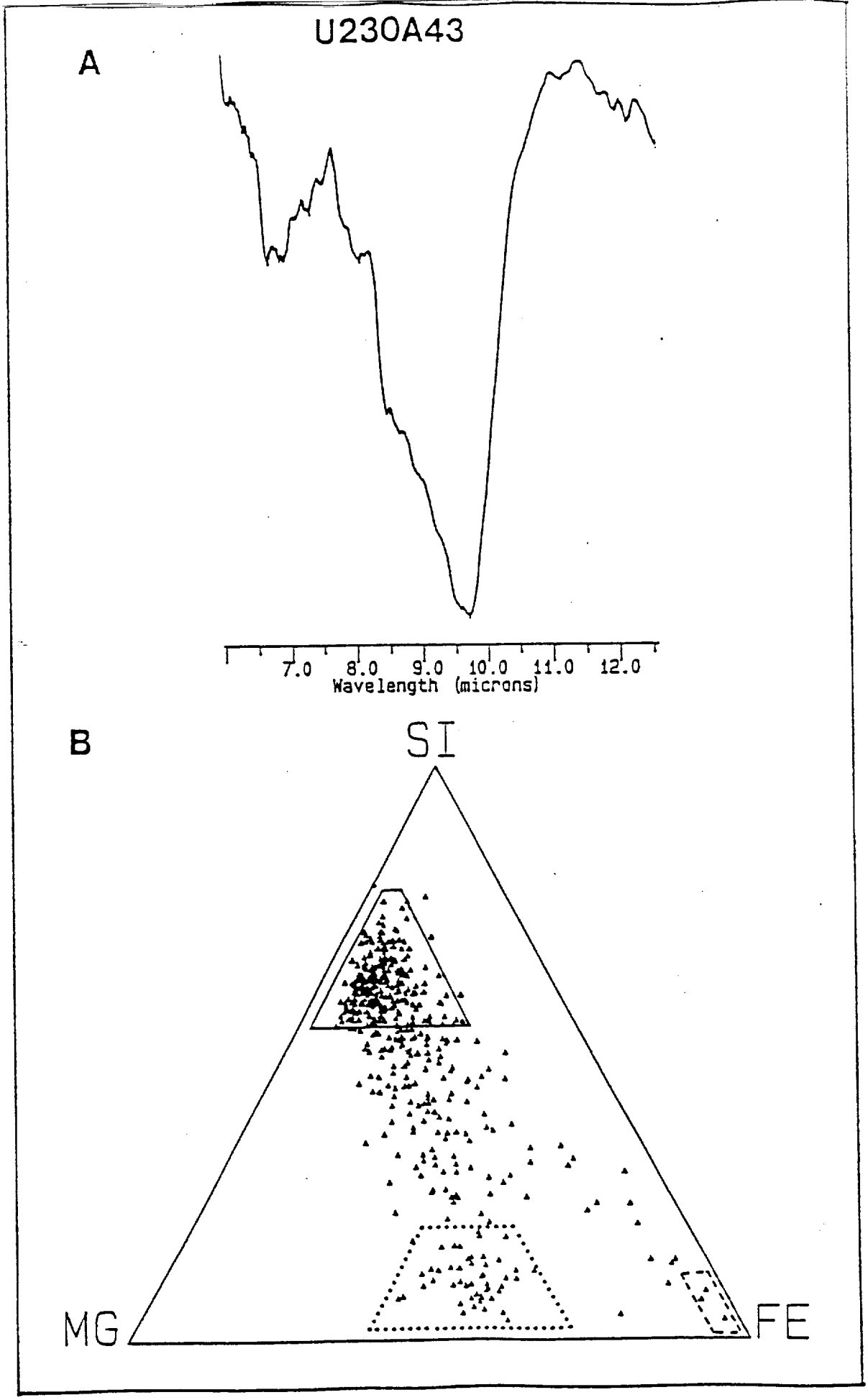
U230A43
A
7.0
8.0
9.0
10.0
11.0
12.0
Wavelength (microns)
B
SI
MG
FE

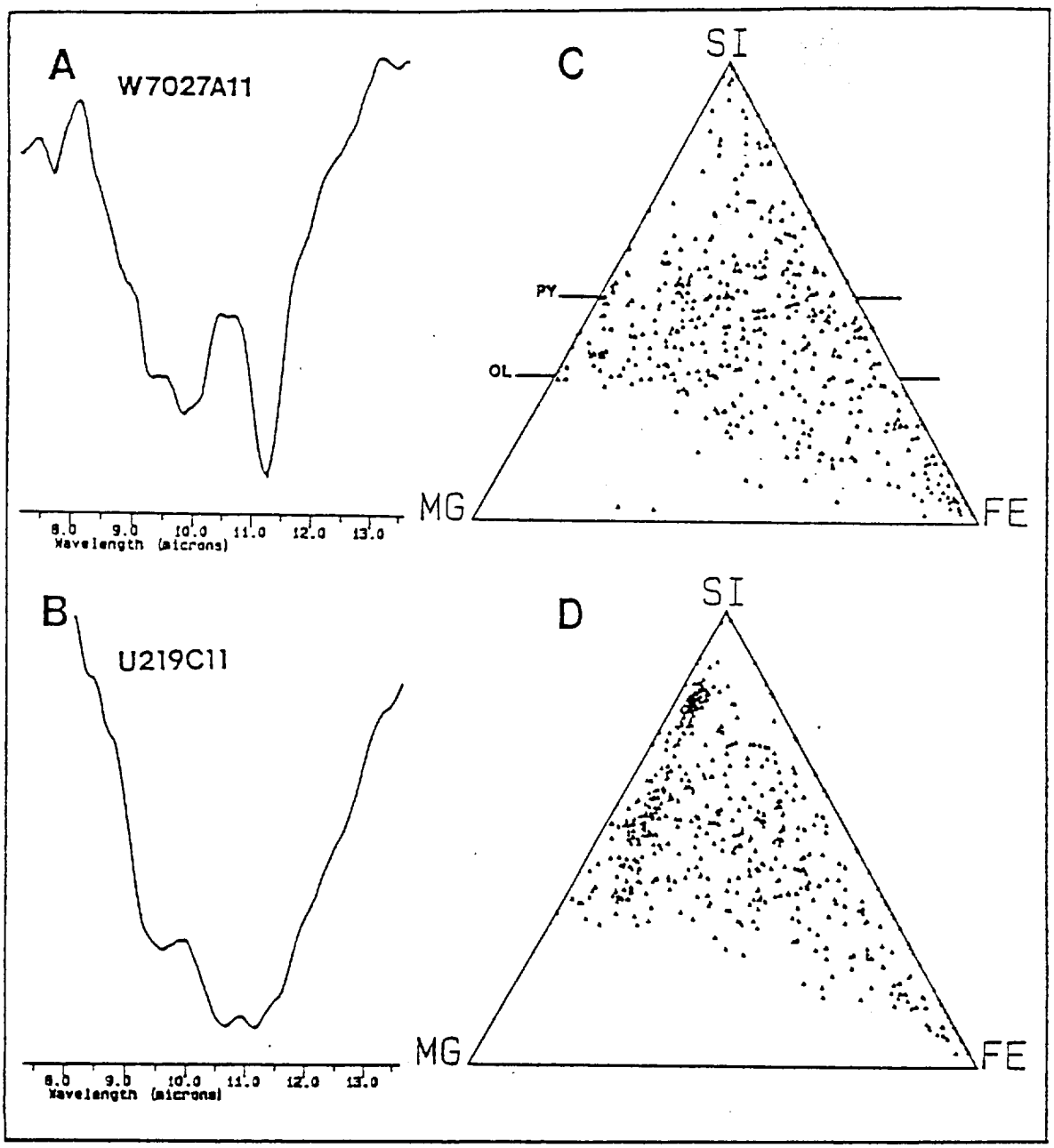
A
W7027A11
8.0 9.0 10.0 11.0 12.0 13.0
Wavelength (microns)
C
SI
PY
OL
MG
FE
B
U219C11
8.0 9.0 10.0 11.0 12.0 13.0
Wavelength (microns)
D
SI
MG
FE

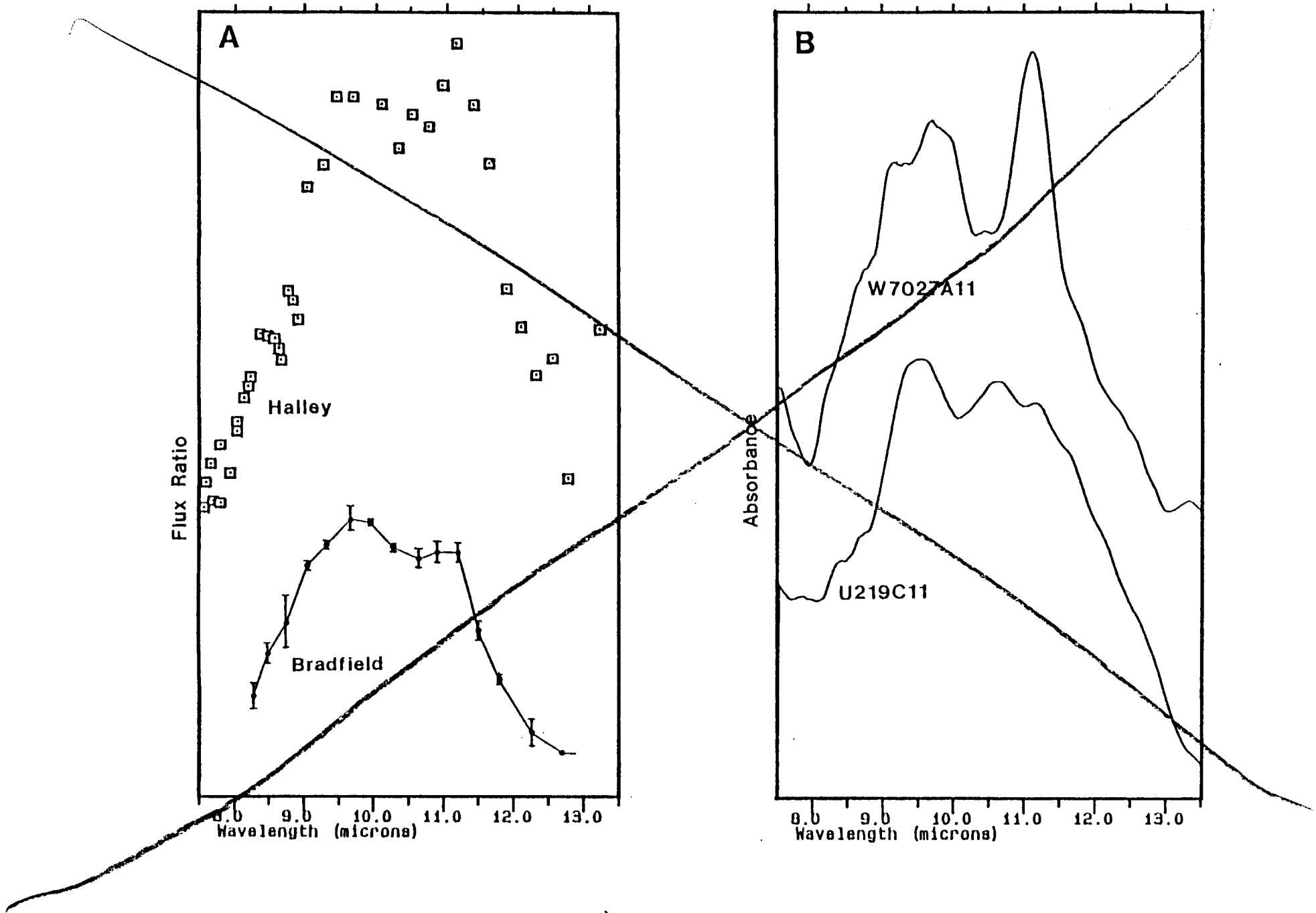
A
B
Flux Ratio
Absorbance
Halley
Bradfield
W7027A11
U219C11
8.0
9.0
10.0
11.0
12.0
13.0
Wavelength (microns)

(a)

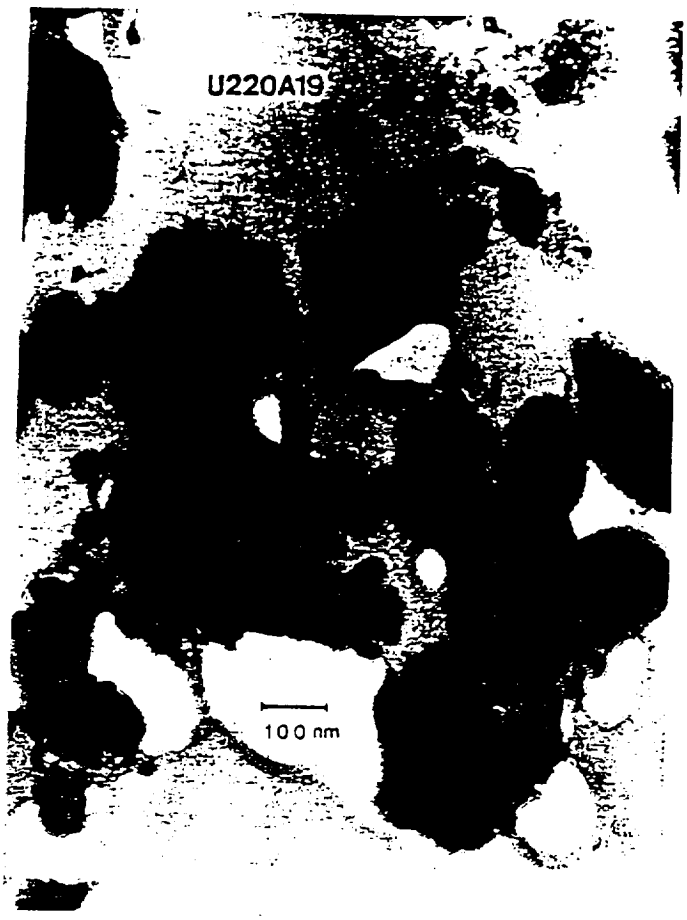

(b)

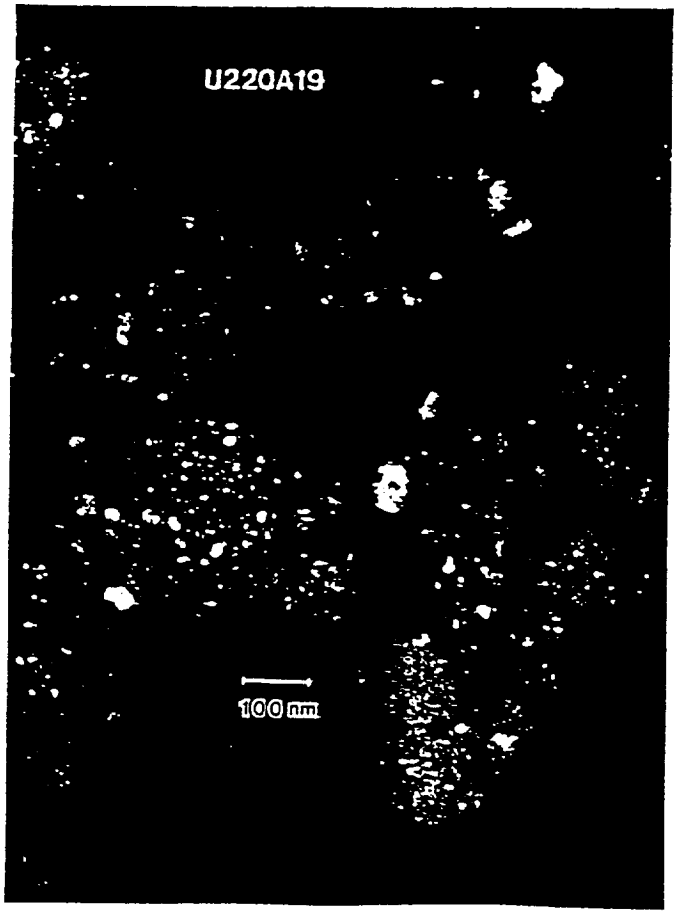

8

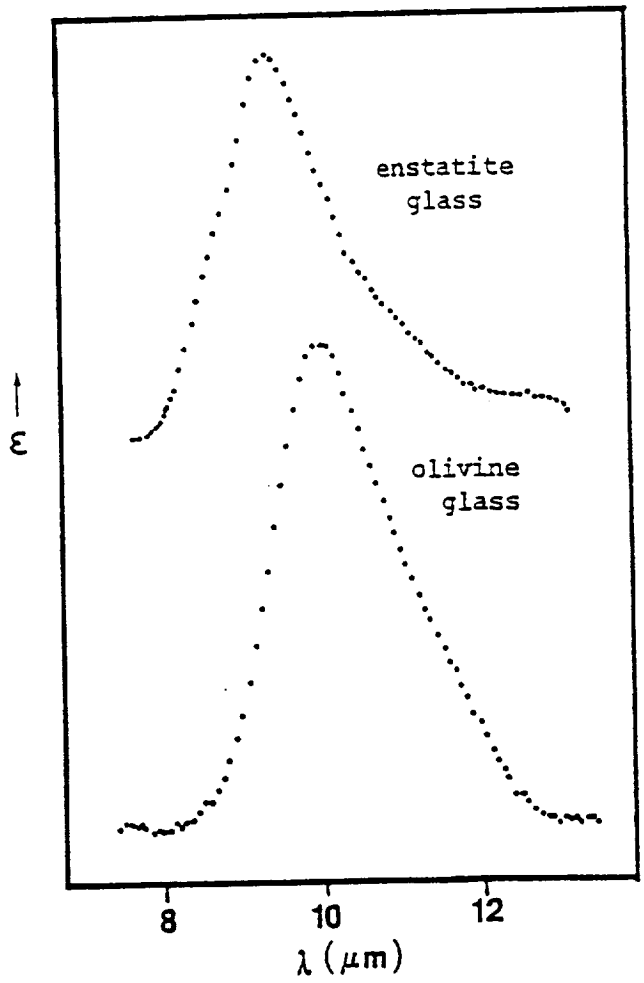
enstatite
glass
olivine
glass
ε
8
10
12
λ (μm)

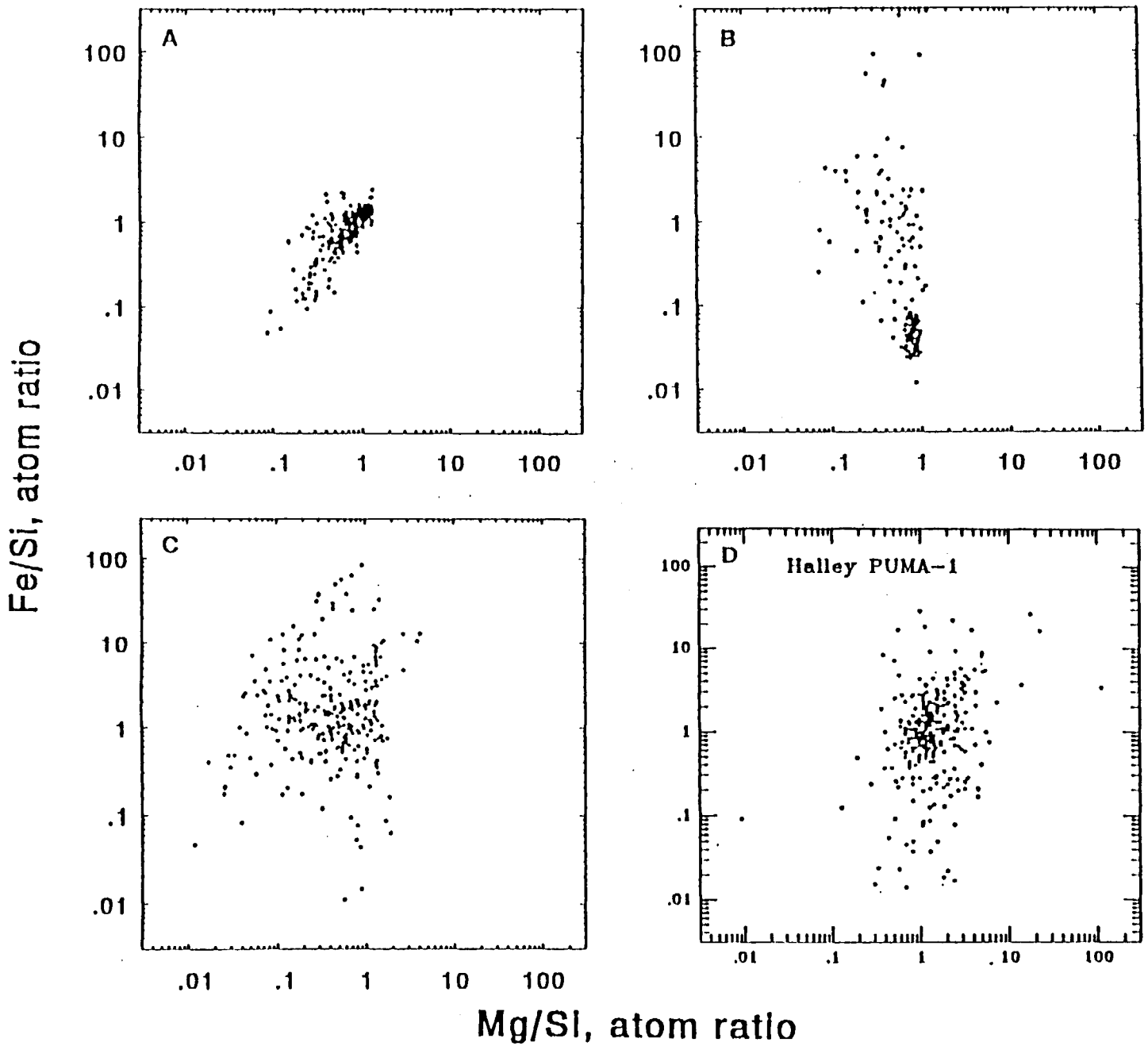
A
B
C
D
Halley PUMA-1
100
10
1
.1
.01
.01
.1
1
10
100
Fe/Si, atom ratio
Mg/Si, atom ratio

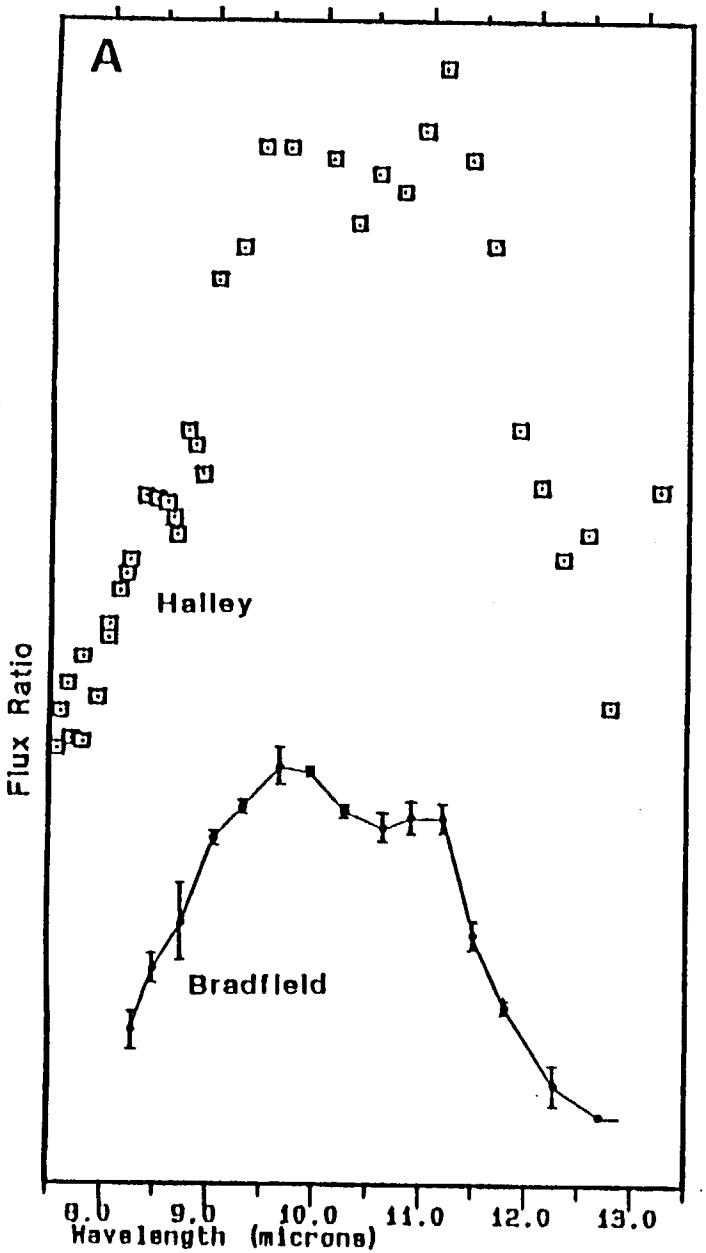
A
Flux Ratio
Halley
Bradfield
8.0
9.0
10.0
11.0
12.0
13.0
Wavelength (microns)

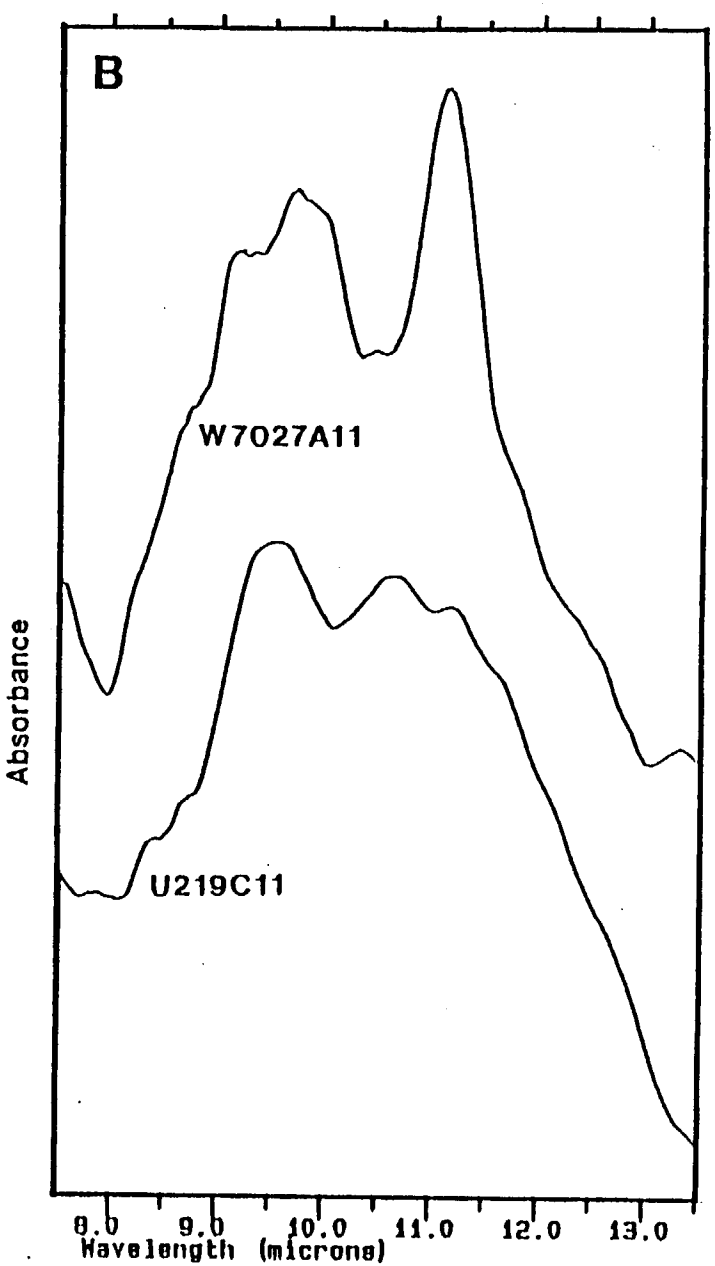
B
Absorbance
W7027A11
U219C11
8.0
9.0
10.0
11.0
12.0
13.0
Wavelength (microns)

11

Appendix II, Paper 6

Nucl. Tracks Radiat. Meas., Vol. 19, Nos 1–4, pp. 709–716, 1991
Int. J. Radiat. Appl. Instrum., Part D
Printed in Great Britain

0735-245X/91 $3.00 + .00
Pergamon Press plc

INVESTIGATION OF SOLAR FLARE TRACKS IN IDPs: SOME RECENT RESULTS

K. THIEL[1], J. P. BRADLEY[2], and R. SPOHR[3]

[1]Nuclear Chemistry Dept., Univ. of Köln, Zülpicher Str. 47, D-5000 Köln 1, FRG
[2]Walter C. McCrone Ass., Inc., 850 Pasquinelli Drive, Westmont, Ill. 60559, USA
[3]GSI/Darmstadt, P.O. Box 11 05 52, D-6100 Darmstadt 11, FRG

ABSTRACT

Latent solar cosmic ray (SCR) tracks were studied in selected olivine and pyroxene crystals of stratospheric dust particles (IDPs) using a transmission electron microscope operating at 200 keV voltage. As a reference, terrestrial and meteoritic olivine and pyroxene single crystals were heavy ion irradiated at GSI with doses of 10^9-10^{10} cm^{-2} of Ar-, Ge-, Zr-, Nb-, and U-ions in the energy range of 3.9 to 18 MeV/amu using additional Al-degrader foils to cover the solar flare energy spectrum. Most of the track containing IDPs show track densities of $\sim 10^{10}$ cm^{-2} which is consistent with interplanetary exposure ages in the order of $\sim 10^4$ years. The highest track density observed so far in an IDP is 5×10^{11} cm^{-2}. Direct lattice images of single latent heavy ion tracks at a resolution of better than 18 Å reveal details of their microstructure that are not accessible to indirect measuring techniques like small-angle scattering or etching of samples containing high density uniform tracks.

KEYWORDS

Solar cosmic ray tracks; interplanetary dust particles; IDPs; latent tracks; heavy ion tracks.

INTRODUCTION

The detection of solar flare tracks in certain stratospheric dust particles recovered by means of high altitude aircraft in the course of the NASA Cosmic Dust Collection Program provided unambiguous proof of the extraterrestrial origin of this type of material (Bradley *et al.*, 1984). The question of the extraterrestrial *source* of these interplanetary dust particles (IDPs), however, is still open. It has been proposed that comets are the main contributors of dust to the interplanetary dust complex in the zodiacal cloud (Whipple, 1967; Delsemme, 1976; Dohnanyi, 1976). Another IDP dust source was identified to be (most likely) the main asteroid belt by measurements performed with the Infrared Astronomical Satellite (IRAS) (Low *et al.*, 1984). Further sources of dust are not expected to contribute substantially to the present-day IDP-flux as was discussed by Sandford (1987).

Theoretical estimates show that dust particles $\sim 10\,\mu$m in size should have lifetimes in the inner solar system in the order of $\sim 10^4$ yr due to Poynting-Robertson effect and particle-particle collisions (Dohnanyi, 1978). On the other hand the investigation of micro-impact craters and solar flare tracks on the surface of lunar rocks indicate that the interplanetary micrometeorite flux was nearly constant within the last 10^6...10^9 yrs (Morrison and Zinner, 1976; Poupeau *et al.*, 1977). To allow for both facts a continuous supply of new dust from the above mentioned sources is required to keep the zodiacal cloud in equilibrium. This injection of dust into interplanetary space takes place via dust release from active cometary nuclei during perihelion passages and via asteroid-asteroid collisions in the main asteroidal belt. The relative contribution of both sources is still uncertain, yet. Estimates based on the observed dust release of comets during perihelion passage indicate, that the dust supply of the interplanetary dust complex may be dominated by the cometary contribution. A more comprehensive discussion of this question and a review of the present situation on IDPs is given by Bradley *et al.* (1988).

The IDP component of cometary origin raises special interest due to the fact that it should represent the most primordial material available in the solar system, having suffered little if any secondary alteration. This type of material should contain information about the solar nebular and presolar history that is not derivable from planetary or lunar samples. Any criteria allowing distinction between cometary and asteroidal IDPs, therefore, would be a valuable step towards this information. It has been proposed to use the shape of the solar flare track density distribution to discriminate between cometary and asteroidal populations of IDPs (Sandford, 1986). The present paper will discuss this approach, report some new observations of solar flare tracks in IDPs and comment on some aspects of the structure of latent heavy ion tracks.

EXPERIMENTAL

Selected olivine and pyroxene crystals from stratospheric dust particles were ultramicrotomed into slices of ~300-500 Å thickness and searched for latent solar flare tracks and amorphous sputter rims caused by high dose solar wind irradiation damage. Imaging was done using transmission electron microscopy at 200 keV high voltage. A more detailed description of the experimental techniques and sample preparation procedure is given by Bradley and Brownlee (1983; 1986).

To calibrate and improve the technique terrestrial and meteoritic olivine and pyroxene single crystals from locations in Mongolia and from the meteorites Murchison and Jilin were used. The crystals were gently crushed to obtain fragments in the size range of ~1 to ~200 μm. Sample holders carrying several thousand crystal fragments were then irradiated at GSI with doses of 10^9-10^{10} cm^{-2} of Ar-, Ge-, Zr-, Nb-, and U-ions in the energy range of 3.9...18 MeV/amu using additional Al-degrader foils to cover the solar flare energy spectrum (see Table 1).

Table 1. Irradiation of various minerals at GSI/Darmstadt to calibrate the TEM technique used for latent track search in cosmic dust.

Target material	Projectile	Energy [MeV/u]	Particle dose [cm^{-2}]
Pyroxene (terr.)	Ar-36	15	$1.0x10^{10}$
Pyroxene (terr.)	Ge-74	13	$1.0x10^{10}$
Olivine (terr.)	Ge-74	13	$1.0x10^{10}$
Olivine (Jilin)	Zr-90	3.9	$1.0x10^{10}$
Olivine (terr.)	Zr-90	3.9	$1.0x10^{10}$
Olivine (Murchison)	Nb-93	18	$1.1x10^{10}$
Olivine (terr.)	Nb-93	18	$1.1x10^{10}$
Olivine (terr.)	U-238	16	$3x10^9$-$1.0x10^{10}$

RESULTS AND DISCUSSION

Latent track structure. - Suitable fragments of the irradiated olivine and pyroxene crystals were selected for imaging calibration and for defining an improved microscope configuration to achieve better performance (Fig. 1). The uniform tracks produced under well defined conditions allowed to better distinguish between contrast modulation (Bragg schlieren) and real changes of the track microstructure (Thiel *et al.*, 1988). For the range of projectile mass and energy that was investigated no indications have been observed for the occurrence of non-overlapping extended defects along the ion path in olivines and pyroxenes.

This could be confirmed for latent tracks produced by solar flare Fe-group ions in olivine and pyroxene crystals of stratospheric IDPs. The only structural change that was observed within a latent track was the gradual thickening of the damage trail due to increasing specific ionization of the decelerated ion near the end of the track. This finding is at variance with the latent track

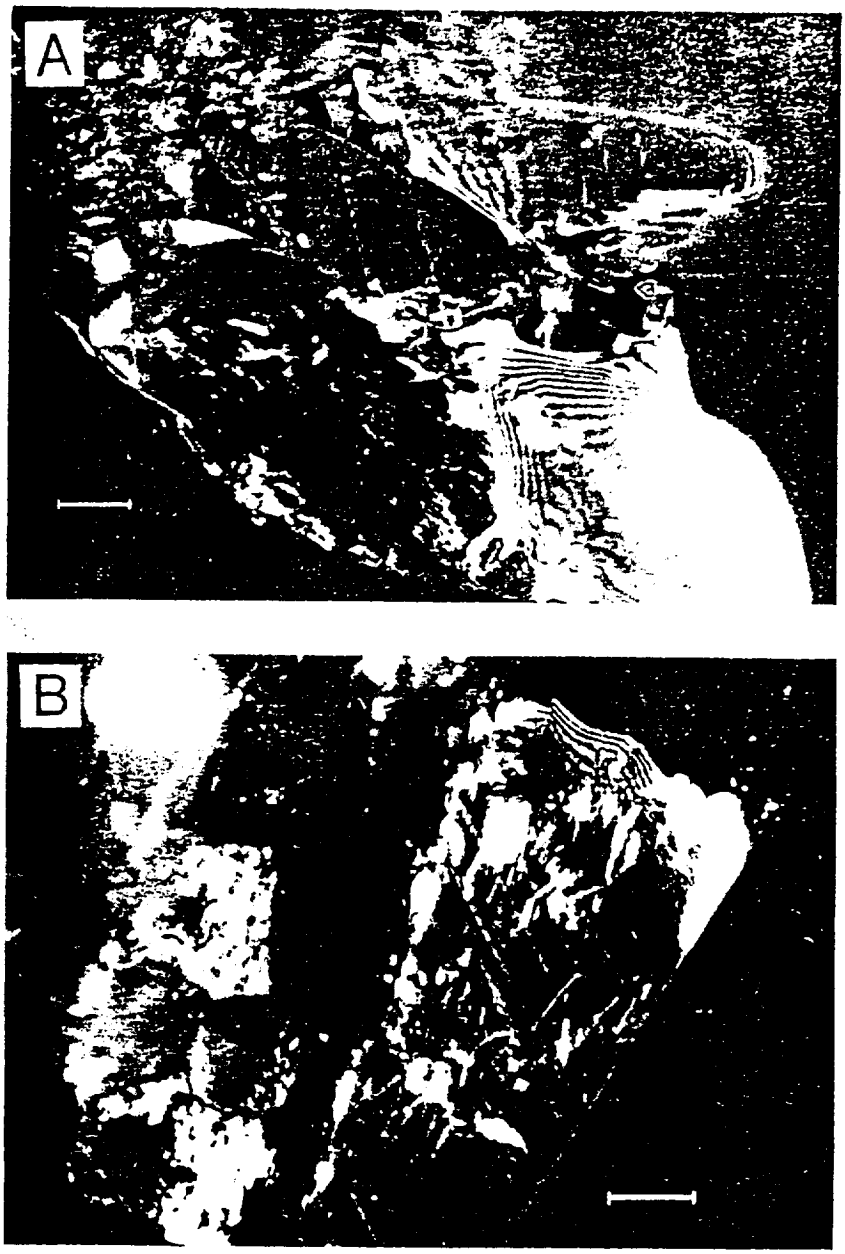

Fig. 1. Latent heavy ion tracks (bright parallel lines) in thin-sectioned olivine crystals of the meteorite Murchison. The samples have been irradiated at arbitrary crystallographic orientation (A-B) with a particle dose of 1.1×10^{10} cm^{-2} Nb-93 ions of an energy of 18 MeV/u at the UNILAC-accelerator of GSI/Darmstadt. The length of the scale bar designates 100 nm.

model proposed by Dartyge *et al.* who claim the existence of non-overlapping extended defects being separated by distinct spaces in Fe-tracks in olivine (Dartyge *et al.*, 1981). To confirm the observed track structure a more careful investigation of the high energy part of latent tracks is planned with improved spatial resolution.

SCR-track record of IDPs.- The presence of amorphous or polycrystalline radiation damage layers of a few 10 nm up to ~200 nm thickness around certain IDPs confirm that these particles have been exposed to low energy solar wind nuclei as small entities without any shielding as was already pointed out by Bradley *et al.* (1988) (see also Fig. 2). The solar flare track density found

Fig. 2. Darkfield transmission electron micrograph of various grains showing solar wind sputtered rims within a thin-sectioned IDP-agglomerate. Note the optically structured layering of the radiation damage zone (white and light grey) around the large grain to the right.

in the interior of these dust particles, therefore, is unbiased by shielding and directly corresponds to the solar flare particle dose and thus to the space exposure age of the respective grain.

Most of the grains containing solar flare tracks that have been investigated so far show track densities around 10^{10} cm^{-2} which corresponds to exposure times in interplanetary space of approximately 10^4 yr. This is consistent with the calculations carried out by Dohnanyi (1978). It has been noted by Sandford (1986) that solar flare track densities in IDPs of a given size and mass should have different frequency distributions depending on whether the IDP particles originate from the region of the asteroid belt or from a comet with high orbital eccentricitiy (see also Fig. 3):

(1) An IDP population of asteroidal origin collected at 1 astronomical unit (1 AU) should exhibit a narrow frequency distribution of solar flare track densities. This is due to the fact that dust grains starting from a nearly circular orbit in the asteroid belt undergo a substantial, almost equal space exposure during Poynting-Robertson deceleration before they reach an Earth crossing orbit. The time interval between the earliest and the latest possible arrival of an asteroidal IDP at 1 AU is comparatively short and the scatter of the recorded track densities is correspondingly small. Due to the relatively long total exposure time the track density values, however, are high.

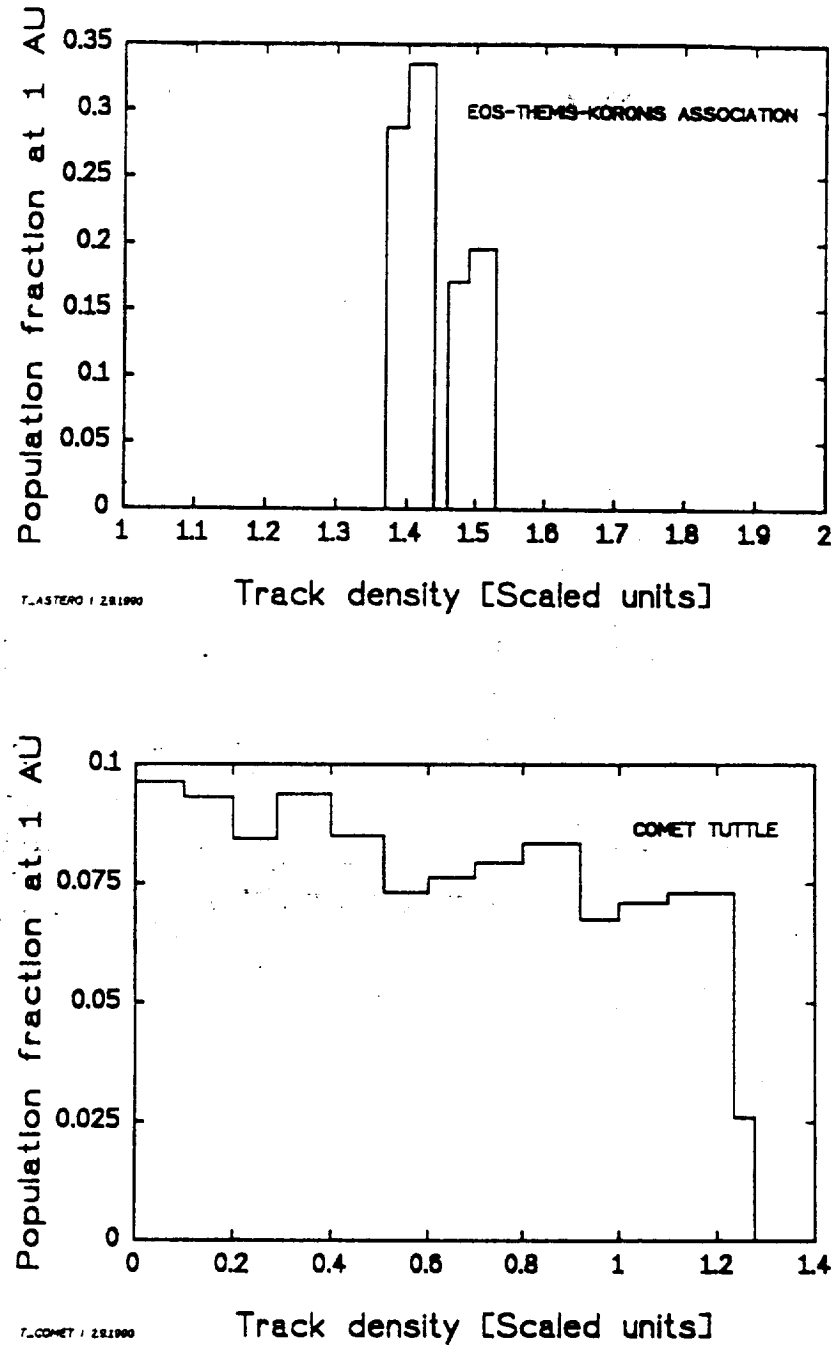

Fig. 3. Calculated track density distributions in IDPs at 1 AU for an asteroidal (top) and cometary origin (bottom) according to Sandford (1986). The track density values given are scaled units taking into account the relevant particle properties and track production rate.

(2) On the other hand, an IDP population originating from a comet of high orbital eccentricity should record a broad range of track densities extending to very low values. This is because particles travelling on highly elliptical orbits have a chance to arrive very early and very late at an Earth crossing orbit due to Poynting-Robertson effect and solar gravitation. The time window of arrival at 1 AU, therefore, and the range of track densities acquired during space exposure will be correspondingly broad, extending to low values.

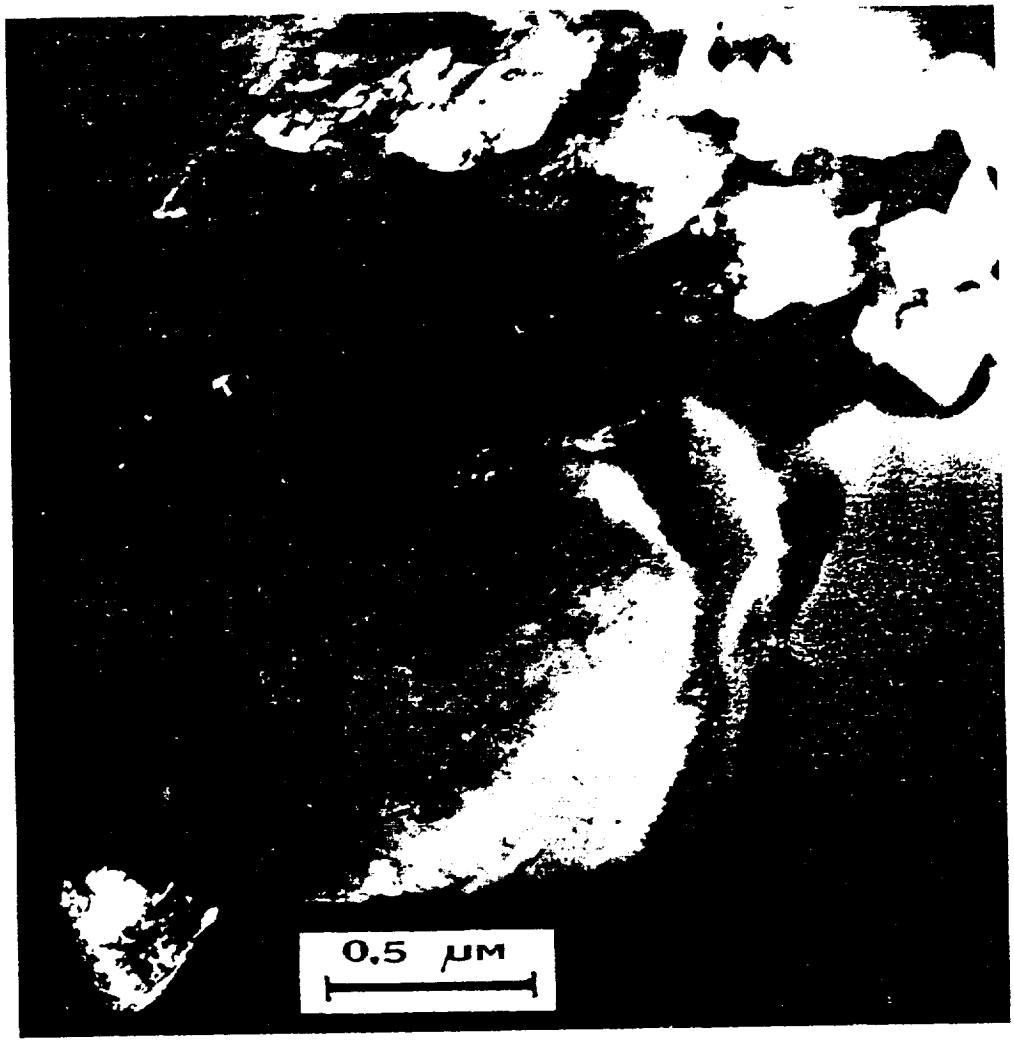

Fig. 4. Darkfield transmission electron micrograph of a stratospheric dust particle (IDP W7027C4) of extremely high solar flare track density ($\sim 5 \times 10^{11}$ cm^{-2}). The light and dark grey structured zone on the right side of the grain represents the solar wind sputtered rim which is of extraordinary thickness in this case.

On the basis of this model of solar flare track production in IDPs it should be possible to discriminate at least in special cases between IDPs of asteroidal and cometary origin. Especially particles of low track density are candidates of a cometary descent. IDPs showing very high track densities on the other hand may occur in both, the asteroidal and the cometary population. However, taking into account that the fraction of particles having a similar high track density in the asteroidal population is higher by a factor ≥30 compared to the cometary population (Sandford, 1986) a high-track-density IDP is likely to be of asteroidal origin rather than of cometary descent. This conclusion has indirectly been supported by the recent work of Flynn (1990) who points out that there exists a near Earth collection bias that considerably enhances the low-velocity (most likely asteroidal) component of the stratospheric IDPs.

In a recent search for solar flare tracks in stratospheric dust particles a large individual grain (IDP W7027C4) could be identified that contains tracks with a density as high as 5×10^{11} cm^{-2} (Figs. 4 and 5). This is the highest track density measured so far in an IDP. The grain also exhibits one of the thickest solar wind sputtered rims encountered so far, exceeding 200 nm. From the discussion of solar flare track densities given in this chapter one may deduce that this particle is

Fig. 5. High resolution TEM-micrograph of the particle shown in fig. 4.

one of the most probable IDP candidates known so far for an asteroidal origin. It is clear that this IDP has experienced a substantially longer exposure interval than other IDPs of comparable dimensions, which implies that it was derived from a different source. Asteroids are the most likely source for a particle with a track density of 5×10^{11} cm^{-2}, although a cometary origin cannot be completely ruled out. A better discrimination of cometary from asteroidal IDPs on the basis of solar flare track densities should be possible when a larger amount of track containing stratospheric dust grains have been identified.

ACKNOWLEDGMENT

This work was financially supported by Deutsche Forschungsgemeinschaft, Bonn-Bad Godesberg, and NASA grant NAS-9-1[illegible]49.

REFERENCES

Bradley, J. P. and D. E. Brownlee (1983). Microanalyses of dispersed interplanetary dust particles. In: *Microbeam Analysis* - Ed. R. Gooley, San Francisco Press, San Francisco, pp. 187-190

Bradley, J. P., D. E. Brownlee, and P. Fraundorf (1984). Discovery of nuclear tracks in interplanetary dust. *Science* 226, 1432-1434

Bradley, J. P. and D. E. Brownlee (1986). Cometary particles: Thin sectioning and electron beam analysis. *Science* 231, 1542-1544

Bradley, J. P., S. A. Sandford, and R. M. Walker (1988). Interplanetary dust particles. In: *Meteorites and the Early Solar System*, Eds. J. F. Kerridge and M. S. Matthews, The University of Arizona Press, Tucson, pp. 861-895

Dartyge, E., J. P. Duraud, Y. Langevin, and M. Maurette (1981). New model of nuclear particle tracks in dielectric minerals. *Phys. Rev.* B 23, 5213-5229

Delsemme, A. H. (1976). The production rate of dust by comets. In: *Interplanetary Dust and the Zodiacal Light. Lecture Notes in Physics* 48, Eds.: H. Elsässer and H. Fechtig, Springer Verlag, Berlin, pp. 314-318

Dohnanyi, J. S. (1976). Sources of interplanetary dust: Asteroids. In: *Interplanetary Dust and the Zodiacal Light. Lecture Notes in Physics* 48, Eds.: H. Elsässer and H. Fechtig, Springer Verlag, Heidelberg, pp. 187-206

Dohnanyi, J. S. (1978). Particle dynamics. In: *Cosmic Dust*, Ed. J. A. M. McDonnell, John Wiley & Sons, New York, pp. 527-605

Flynn, G. J. (1990). The near-Earth enhancement of asteroidal over cometary dust. *Proc. 20th Lunar Planet. Sci. Conf.*, LPI, Houston, pp. 363-371

Low, F. J., D. A. Beintema, T. N. Gautier, F. C. Gillett, C. A. Beichmann, G. Neugebauer, E. Young, H. H. Aumann, N. Boggess, J. P. Emerson,, H. J. Habing, M. G. Hauser, J. R. Houck, M. Rowan-Robinson, B. T. Soifer, R. G. Walker, and P. R. Wesselius (1984). Infrared cirrus: New components of the extended infrared emission. *Astrophys. J.* 278, L19-L22

Morrison D. A. and E. Zinner (1976). Distribution and flux of micrometeoroids. *Phil. Trans. Royal Soc. London* A285, 379-384

Poupeau, G., R. S. Rajan, R. M. Walker, and E. Zinner (1977). The modern and ancient flux of solar wind particles, solar flare particles and micrometeoroids. In: *Space Research XVII*, Eds. M. J. Rycroft and A. C. Strickland. Pergamon Press, New York, pp. 599-604

Sandford, S. A. (1986). Solar flare track densities in interplanetary dust particles: The determination of an asteroidal versus cometary sources of the zodiacal dust cloud. *Icarus* 68, 377-394

Sandford, S. A. (1987). The collection and analysis of extraterrestrial dust particles. *Fund. Cosmic Phys.* 12, 1-73

Thiel, K., J. P. Bradley, and R. Spohr (1988). On the nature of latent nuclear tracks in cosmic dust particles. *Nucl. Tracks Radiat. Meas.* 15, 685-688

Whipple, F. L. (1967). On maintaining the meteoritic complex. In: *The Zodiacal Light and the Interplanetary Medium*, NASA SP-150, p. 409-426